Fracture and DHC Behavior of As-fabricated & Irradiated Indian PHWR Pressure Tubes

By

Priti Kotak Shah

(ENGG01200904026)

Bhabha Atomic Research Centre, Mumbai

A thesis submitted to the

Board of Studies in Engineering Sciences

In partial fulfillment of requirements

For the Degree of

DOCTOR OF PHILOSOPHY

of

HOMI BHABHA NATIONAL INSTITUTE

August, 2016

Dedicated

to

The Universe

Homi Bhabha National Institute

Recommendations of the Viva Voce Board

As members of the Viva Voce Board, we certify that we have read the dissertation prepared by Mrs. Priti Kotak Shah entitled "Fracture and DHC Behaviour of As-fabricated & Irradiated Indian PHWR Pressure Tubes" and recommend that it maybe accepted as fulfilling the dissertation requirement for the Degree of Doctor of Philosophy.

Chairman :(Dr. G. K. Dey) Date :

Guide:(Dr. R. N. Singh) Date :

Tech. Advisor:(Shri J. S. Dubey) Date :

External Examiner : Date:

Member 1 :(Dr. A. P. Tiwari) Date:

Member 2 :(Dr. S. S. Taliyan) Date:

Member 3 :(Dr. M. K. Samal) Date:

Final approval and acceptance of this dissertation is contingent upon the candidate's submission of the final copies of the dissertation to HBNI. I hereby certify that I have read this dissertation prepared under my direction and recommend that it may be accepted as fulfilling the dissertation requirement.

Date:

Place: Guide

STATEMENT BY AUTHOR

This dissertation has been submitted in partial fulfilment of requirements for an advanced degree at Homi Bhabha National Institute (HBNI) and is deposited in the Library to be made available to borrowers under rules of the HBNI. Brief quotations from this dissertation are allowable without special permission, provided that accurate acknowledgement of source is made. Requests for permission for extended quotation from or reproduction of this manuscript in whole or in part may be granted by the Competent Authority of HBNI when in his or her judgement the proposed use of the material is in the interests of scholarship. In all other instances, however, permission must be obtained from the author.

Signature

Priti Kotak Shah

DECLARATION

I, hereby declare that the investigation presented in the thesis has been carried out by me. The work is original and has not been submitted earlier as a whole or in part for a degree/diploma at this or any other Institution/University.

Signature

Priti Kotak Shah

ACKNOWLEDGEMENTS

The work presented in this thesis has been primarily carried out in Post Irradiation Examination Division (PIED) of Bhabha Atomic Research Centre. I would like to express my gratitude to my ex-supervisor, Dr. J.K. Chakravartty for his guidance. I would like to thank my Guide Dr. R.N. Singh for his constant encouraging words and cooperation at each stage of research. I would like to take this opportunity to thank my mentors Shri S. Anantharaman, Ex-Head, PIED & Shri J. S. Dubey, Head, Mechanical Property Evaluation Section, PIED for the endless help rendered by them and for the guidance received from them and their all round support that led to the successful completion of this work.. They have imbibed in me the culture of research and the training received from them has laid the foundation of my research career. Post irradiation examination, involved in the present and any research work, is not only difficult but also impossible to carry out alone. I sincerely thank each & every member of PIED for their direct or indirect invaluable contribution to this work. Working has always been great fun, thanks to the vibrant team of PIED which made complicated problems look simple. I would like to specially thank Shri Ashwini Kumar, Shri H. N. Tripathi, Shri K. B. Gaonkar, Shri Ashish Sushibhine and Shri S. B. Deherkar for helping me in carrying out some of the experiments. Thanks to Shri R. S. Shriwastaw who encouraged me to aim higher. A big big thank you to my Parents-in-law for their blessings. I have been able to concentrate and complete my work because of constant support of my husband Shri Manoj Shah and my two little angels, the joy of my life Meghu & Mishu. Finally, thanks to my Parents Shri Rajani Kanta Kotak & Smt. Usha Ben Kotak and Sisters Smt. Rupa Jobanputra & Smt. Krishna Thacker for always being there for me. No words would be enough to express my sincere gratitude to my Guru & my Master Masay, Shri Manotosh Mallick, who kept teaching me the simplest and the greatest lessons of life which I would cherish for years to come.

Abstract

Pressure tubes, made of Zr-2.5Nb alloy, are the primary pressure boundary material for the Pressurised Heavy Water Reactors (PHWRs). These zirconium alloy components are located in the core region of the reactor and thus are exposed to aggressive environment of high temperature, high stress, corrosive media and neutron radiation. Neutron irradiation is the most important source of damage in zirconium alloys. The damage is manifested in one or more form of (a) dimensional changes (b) changes in mechanical properties and (c) changes in microstructure/chemical composition. One or some of these changes may limit life of these components. The life limiting factor for the pressure tube may be creep or reduction in fracture toughness or crack growth due to delayed hydride cracking (DHC). Information on in-service behaviour and extent of ageing induced degradation of these properties in the zirconium alloy components, are therefore, justifiably useful for un-interrupted safe running of nuclear power plants. Though extensive work has been carried out on unirradiated pressure tube material and is available in open literature, very limited amount of work e.g. mechanical property of irradiated Indian PHWR pressure tube is available. Studies have been carried out in this thesis work on the variation of important mechanical properties of Indian Zr-2.5Nb pressure tube with respect to different parameters such as temperature, hydrogen concentration and irradiation to different fluences . The fracture toughness and delayed hydride cracking behaviour of irradiated Indian irradiated Zr-2.5Nb pressure tubes and rolled joint stub have been evaluated and compared with the data available in open literature. These two parameters are important for Leak before Break (LBB) behaviour in the tube. Inherent variability in the properties has

been evaluated using as-fabricated off-cuts of the pressure tubes. Effect of hydrogen concentration to a higher value than expected in reactor, and strain rate effects on the axial and transverse properties have also been studied on unirradiated alloy.

Tensile properties of several as-fabricated pressure tubes, of two types, fabricated from double and quadruple melted ingot have been evaluated using miniature specimens, along axial and transverse orientation and from both front and back-end to study the variability in properties. Double-melted pressure tubes showed relatively higher strength and lower elongation and larger standard deviation as compared to the quadruple melted pressure tubes. In general the transverse specimens and back end of the tubes showed higher yield strength (YS) and ultimate tensile strength (UTS).

Zr-2.5Nb pressure tube showed near similar impact energy at room temperature in axial and transverse orientation. At higher temperatures crack growth along axial direction absorbs more energy. Ductile-to-brittle-transition at around $180\,^{\circ}C$ was also clearly exhibited by hydrided Zr-2.5Nb pressure tube alloy, when crack growth occurs along axial direction on the radial-axial plane, under dynamic loading.

Fracture toughness of irradiated pressure tubes, after different fluence and hydrogen concentration, was characterized and studied in detail. The experiment was also carried out on portions of the pressure tubes, which form part of the mechanical rolled joints with end fittings. The rolled joint portion of the tube, has significant amount of residual tensile stresses, which in combination with the normal operating hoop stress, lead to varying degree of hydride reorientation in radial-axial plane along the tube length in the rolled portion. Thus effects of a) different neutron fluence b) hydrogen concentration as it occurs in actual service has been studied. The fracture toughness parameters have been evaluated using disk compact tension specimens, at different test temperatures. At nearly all the test temperatures, of the two irradiated pressure tubes studied, one pressure tube (Q10) showed better fracture toughness as compared to other irradiated pressure tube (S7). The fabrication route of both the tubes were same, however Q10 tube had lower amount of carbon, chlorine, phosphorus and initial

hydrogen concentration. Small variation in these trace element impurities had significant effect on the fracture behavior. Fractographic examinations showed presence of large density of fissure like features on the fracture surface of S7 tube having higher trace impurities.

Initiation fracture toughness (J_i) values for the irradiated pressure tubes and irradiated & hydrided pressure tubes have shown that the reduction in fracture toughness due to irradiation & hydriding had almost saturated, during in-reactor service of around 8 years, and further hydriding, even up to 75 $wppm$ H_{eq}, had no significant effect on the fracture toughness. The fracture toughness was found to increase with the increase in test temperature till a temperature of around 150 to 200 $^{\circ}C$. The values of the critical internal pressure have been estimated, based on the J_i values obtained, for the irradiated pressure tube S-7 at different test temperatures.

Delayed hydride cracking is a major sub-critical crack growth mechanism in the Zr-2.5Nb pressure tube alloy. DHC velocity is sensitive to the microstructure, texture and strength of the tube material. Due to irradiation during service, the pressure tube material undergoes significant changes in microstructure and irradiation hardening. The role of these changes have been evaluated for the irradiated material to obtain actual values that can be used for LBB analysis. It also gave an idea of the performance of the tubes made by indigenous fabrication route with respect to international experience. DHCV in irradiated pressure tube was found to be around 2 to 4 times higher than that in as-fabricated pressure tubes at a given test temperature. The relationship between DHCV and temperature has been found to follow Arrhenius dependence with an activation energy of 45 and 60 kJ/mol in irradiated and as-fabricated material, which agrees well with the values reported in the literature. This activation energy or temperature dependence of DHCV is due to the combined effect of temperature on diffusion coefficient of hydrogen in α-Zr and terminal solid solubility of hydrogen in α-Zr. The intermittent propagation of DHC crack and its arrest created ripple like lines on the fracture surface, which lie nearly parallel to the crack front and perpendicular to the direction of crack growth. The striation spacing was observed to decrease with

decrease in test temperature. Also at a given test temperature the striation spacing for as-fabricated pressure tube were larger than that of the irradiated tube. Decrease in striation spacing in irradiated material has been attributed to the increasing yield strength of the matrix. The results generated give an understanding of the fracture behaviour of irradiated Indian pressure tubes and serve a valuable role in LBB based safety analysis of the coolant channels.

Contents

Nomenclature

α	Alpha
β	Beta
Δa	Crack growth
dJ/da	Crack growth rsistance
E	Young modulus
f_a	Fraction of basal pole in axial direction
f_r	Fraction of basal pole in radial direction
f_t	Fraction of basal pole in transverse direction
H_{eq}	Hydrogen equivalent
J_i	Initiation fracture toughness
J_{max}	Mazimum load fracture toughness
K_I	Stress intensity factor in Mode I loading
K_{max}	Maximum load stress intensity factor
kN	kilo Newton
MeV	Mega electron Volt
MPa	Mega Pascal

P_f	Precrack load limit
P	Load
V_A	Axial DHC velocity
V_R	Radial DHC velocity
wppm	Parts per million by weight
W	Width of specimen
ASME	American Society of Mechanical Engineers
ASTM	American Society for Testing and Materials
BCC	Body Centred Cubic
BWR	Boiling Water Reactor
CANDU	Canadian Deuterium Uranium
CCL	Critical Crack Length
CCT	Curved Compact Tension
COD	Crack Opening Displacement
CRSS	Critical Resolved Shear Stress
CT	Calandria Tube
CW	Cold Worked
CWSR	Cold Worked and Stress Relieved
DCPD	Direct Current Potential Drop
DCT	Disk Compact Tension
DHC	Delayed Hydride Cracking

DM	Double Melted
DSC	Differential Scanning Calorimetry
EFPY	Effective Full Power Year
EMCCR	En-Masse Coolant Channel Replacement
EOL	End of Life
GDOES	Glow Discharge Optcal Emission Spectroscopy
HCP	Hexagonal Close Packed
HOY	Hot Operating Years
HT	Heat Treated
IPHWR	Indian Pressurised Heavy Water Reactor
KAPS	Kakrapar Atomic Power Station
LBB	Leak Before Break
LLD	Load Line Displacement
NFC	Nuclear Fuel Complex
ORT	Operator Response Time
PHWR	Pressurised Heavy Water Reactor
PT	pressure tube
QM	Quadruple Melted
R/J	Roll Joint
RAPS	Rajasthan Atomic Power Station
SD	Standard Deviation

SEM	Scanning Electron Microscope
SIF	Stress Intensity Factor
SZW	Stretch Zone Width
TE	Total Elongation
TEM	Transmission Electron Microscope
TSS	Terminal Solid Solubility
UE	Uniform Elongation
UTM	Universal Testing Machine
UTS	Ultimate Tensile Strength
YS	Yield Strength

List of Figures

List of Tables

Chapter 1

Introduction

1.1 Background

India at present has 22 operating nuclear power reactors with an installed capacity of 5780 MWe. These include two Boiling Water Reactors (BWRs), 18 Pressurised Heavy Water Reactors (PHWRs) and two VVERs (Pressurised Water Reactor type). Thus PHWRs are the mainstay of the Indian nuclear power program. Pressure tubes, made of zirconium alloy (Zr-2.5Nb), are the primary pressure boundary material for the PHWRs. These zirconium alloy tubes are the main structural component of the reactor core and have a design life of the order of 25-30 years. The pressure tube properties important for the performance of the reactor are: (i) fracture toughness (ii) delayed-hydride-cracking (DHC) (iii) deformation (iv) corrosion and hydrogen ingress [1]. These properties are dependent on the chemical composition and microstructure of the pressure tubes and thus are a function of the manufacturing process and operating conditions.

The pressure tubes are the primary pressure boundary of the reactor, which house nuclear fuel bundles and guides the coolant over it for nuclear heat removal. Its integrity and reliability is essential for the reactor operation. Due to their location in the core region of the reactor the pressure tubes are exposed to aggressive environment of high temperature, high stress, corrosive media and neutron radiation. Neutron irradi-

ation induced changes and hydrogen/deuterium pick-up from corrosion reaction with hot water coolant are the two most important sources of damage in pressure tube alloys. The damage is manifested in one or more form of (a) dimensional changes, in form of axial elongation and diametral creep of the tube (b) changes in its mechanical properties, mainly reduction in fracture toughness and increase in delayed hydrided crack growth velocity, which is accompanied by changes in microstructure/chemical composition. One or some of these changes may limit the useful operating life of the pressure tubes. Information on in-service behaviour and extent of ageing induced degradation in these properties of the zirconium alloy components, are therefore essential for the un-interrupted and safe running of nuclear power plants.

Thus, behaviour and properties of Zr-2.5Nb pressure tube has been an area of continued study and research over last several decades. Canadian PHWR program has been the leading one among them. The as-fabricated properties of the pressure tubes, show inherent variability in the as-fabricated properties due to minor variation in the alloy chemistry and fabrication process variables [2, 3]. This variability has been found to persist even after irradiation [4, 5]. It is important to study various operating damage mechanisms given earlier and monitor changes occurring during its operating life for any PHWR program.

1.2 Objectives of this research

Though extensive work has been carried out on the pressure tube materials and some of it is available in the open literature, mostly from Canada, very limited amount of work on mechanical property of irradiated Indian PHWR pressure tube is available so far. It is important to note that the manufacturing route used for Indian pressure tubes differ from Canadian route and there are differences in the microstructure and texture of pressure tubes. In this research work an attempt has been made to study the variation in important mechanical properties of Indian Zr-2.5Nb pressure tube with respect to different parameters such as temperature, hydrogen concentration and

irradiation to different fluences. The fracture toughness and delayed hydride cracking (DHC) behaviour of Indian irradiated Zr-2.5Nb pressure tubes and rolled joint stub have been studied and compared with the data available in open literature. These two parameters are important for Leak before Break (LBB) behaviour of the tubes. Thus the main idea has been to study the mechanical properties of Zr-2.5Nb pressure tubes, that are currently in use in Indian PHWRs.

This research work has made following contributions to the existing knowledge base on the Indian Zr-2.5Nb pressure tube material;

1. Extensive work has been carried out to characterize the tube to tube variability in the mechanical properties of Indian pressure tubes, fabricated using double melted and quadruple melted fabrication routes, along axial and transverse orientation, at front and back end of the pressure tubes. This study on variability in the mechanical properties shall give insights into expected behaviour of irradiated pressure tubes of different types and location in terms of front and back end of the tube.

2. Dynamic impact test behaviour for both as-received and hydrided Zr-2.5Nb pressure tubes over a range of temperature, along axial and circumferential direction has been studied in this work. Nature of fracture morphology and energy absorbed during dynamic fracture along two major directions of the tube has been studied.

3. Fracture toughness and DHC velocity behaviour of Zr-2.5Nb Indian pressure tubes, after irradiation, is studied in the present work using the Disk Compact Tension (DCT) specimens. The test specimen preparation and fracture toughness evaluation for indigenous irradiated pressure tubes has been established during this work. In this research work an attempt has been made to study the variation of fracture properties of irradiated Indian Zr-2.5Nb pressure tubes and its rolled joint portion, with respect to different parameters such as temperature, hydrogen concentration and irradiation to different fluences. The results of

current work has been compared with the data available in open literature. The fracture toughness and DHC velocity are two important parameters for safety assessment, including leak before break analysis, of the pressure tubes over its operating life. The main idea has been to understand End of Life (EOL) properties for irradiated pressure tubes, that are currently in use in Indian PHWRs.

1.3 Structure of the thesis

This work comprises four components. First is to characterize the inherent tube to tube variability in the properties by studying the tensile and fracture toughness properties of the as-fabricated pressure tube offcuts. The study would give an idea of the amount of scatter that can be expected in the properties due to variations within the specified limits in the fabrication parameters and chemical composition. It is important as it has been found that this variability in properties persist even after irradiation. Second part is to study the effect of hydrogen concentration and dynamic loading on the fracture behaviour of the tubes. These two parts have been carried out on the unirradiated materials to have larger data base, which would otherwise be very difficult to obtain using irradiated alloys. Third and fourth part of this work studied the two important mechanical properties of the tubes that is; fracture toughness and the delayed hydride crack growth behaviour using actual irradiated pressure tubes taken out of reactor service after different operating years.

The outline of the thesis is as follows: Chapter 2 gives a brief literature review of the topics directly related to the present studies on pressure tube. Chapter 3 presents an overview of various experimental methods followed in the present study of unirradiated and irradiated pressure tubes. Chapter 4, 5 and 6 present the research work carried out on Indian Zr-2.5Nb pressure tubes. Chapter 4 presents a statistical study carried out on the tensile and fracture properties of Indian Zr-2.5Nb pressure tubes. Chapter 5 covers the study on anisotropy in the impact behaviour of the as-fabricated as well as the hydrided pressure tube material. Chapter 6 covers the research studies carried out

on fracture toughness of Indian irradiated Zr-2.5Nb pressure tubes, rolled joint stub and the delayed hydride crack growth study carried out on Indian irradiated PHWR pressure tube. Chapter 7 gives the summary of salient observation and conclusions. Chapter 7 also gives scope of further research work that seems pertinent to gain further insights into this area. Finally a list has been presented of the publications made from the present research.

The thesis work has resulted in publication of four international journal papers, two on unirradiated pressure tubes and two on irradiated pressure tubes. The research also includes the additional works carried out on unirradiated and irradiated pressure tube and roll joint stub that is yet to be published.

Chapter 2

Literature review

2.1 PHWR reactor and pressure tubes

A simplified schematic diagram of a PHWR and its coolant channel assembly are shown in Figure 2.1 and Figure 2.2 respectively [6, 7]. PHWRs design is characterized by its use of natural uranium dioxide as fuel, heavy water as moderator, and high pressure heavy water as coolant. The reactor consists of a low-pressure horizontal reactor vessel, called as calandria, containing heavy water moderator at near ambient pressure and temperature. The calandria is pierced by a large number of pressure tubes, which contain the fuel bundles, and through that pressurized heavy water coolant circulates as shown in Figure 2.1 [6]. The calandria houses all reactivity and reactor shutoff devices in the low-pressure low temperature environment. The pressure tubes are separated from the cool heavy water moderator by calandria tubes. A gas of low thermal conductivity (dry CO_2) flows through the annulus to thermally insulate the hot pressure tube from the cold calandria tube. Each end of a pressure tube is roll expanded into the hub of a thicker Martensitic stainless steel end fitting to form a pressure tight, high strength roll joint (R/J) [8]. End fittings are supported on the calandria vessel end shields. There are 306 coolant channel assemblies in a 220 MWe Indian Pressurised Heavy Water Reactors (IPHWRs) and 392 assemblies in a 540/700 MWe IPHWRs [9]. Each coolant channel assembly of a PHWR comprises mainly of a

pressure tube (PT) concentrically located inside a calandria tube (CT) and four tight fit garter springs spacers between these two tubes, as shown in Fig. 2.2 [7]. All these components are made up of zirconium base alloys because of their unique combination of good corrosion resistance in water, good mechanical properties, and low capture cross section for thermal neutrons [10–14]. The calandria tube is surrounded by heavy water moderator. The pressure tube houses the fuel bundles and heavy water coolant flows through it to extract the heat of fission reaction. A schematic diagram of the flux, temperature profile along the length of the pressure tube and roll joint region is shown in Figure 2.3 [15] and is representative of the the temperature, flux profile in Indian PHWR reactors.

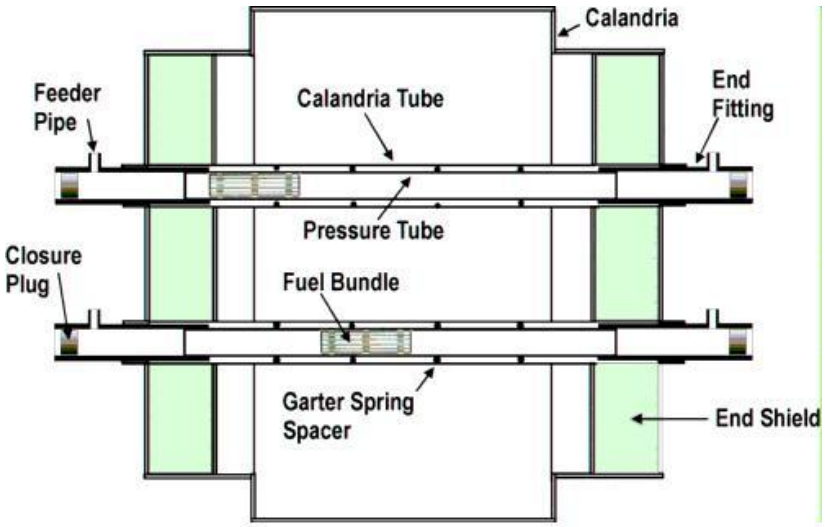

Figure 2.1: A simplified schematic diagram of PHWR system [6].

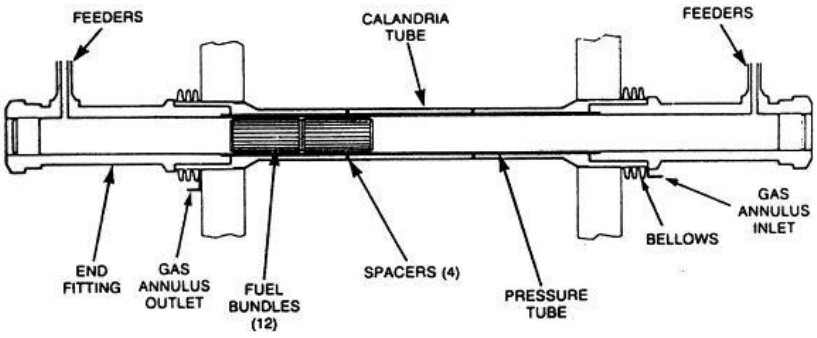

Figure 2.2: A simplified schematic diagram of PHWR coolant channel assembly [7].

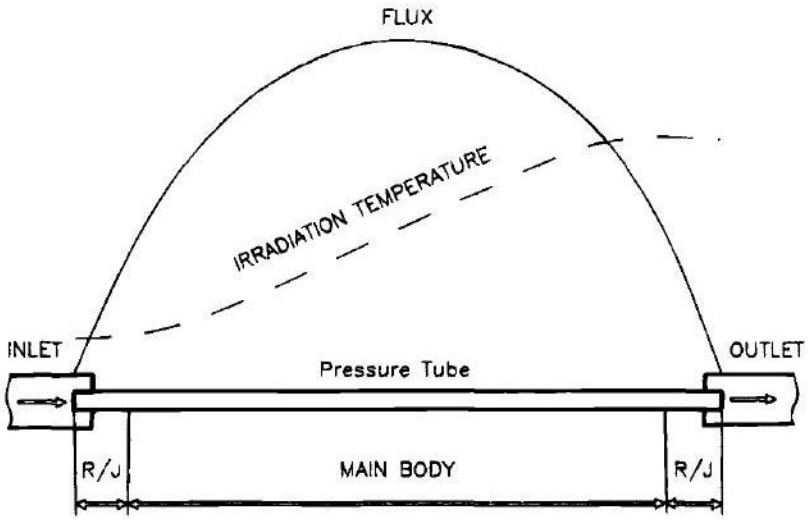

Figure 2.3: A schematic diagram of the flux and temperature profile for the pressure tube main body and roll joint region [15].

Zr-2.5Nb alloy is presently being used as the pressure tube material due to its high strength, and creep and fracture resistance [14]. The pressure tubes serve as miniature pressure vessels operating at about 300 $^{\circ}C$, with a coolant pressure of about 10 MPa. The design of the pressure tube is based on section III of the ASME pressure vessel code, which specifies the criteria for maximum design stress on the basis of ultimate tensile strength, yield strength, creep and stress-rupture strengths at the operating temperature. For pressure tube alloys (both Zircaloy-2 and Zr-2.5Nb alloy) one third of the ultimate tensile strength has been found to be the limiting design stress [16].

The fuel bundle assembly sets the minimum size for inside diameter, and the materials UTS at the operating temperature sets the minimum wall thickness required [17]. The pressure tube characteristics important for the performance of the reactor are: (i) fracture toughness, (ii) delayed hydride cracking (DHC) (iii) deformation (iv) corrosion and hydrogen ingress (v) manufacturing variability and (vi) microstructure evolution during service [18]. Dimensional change due to irradiation creep and growth leads to increase in pressure tube length as well as diameter of tube and sagging of pressure tubes. The diametral expansion limits are established by considerations of the coolant flow through the fuel bundles and elongation can only be accommodated to the design limit of the bearing travel [19]. The limits in sag are determined by interference with other in-core devices or by contact of the pressure tube with the calandria tube in between spacers. Thus the satisfactory performance and the life of the pressure tube depends heavily upon its dimensional stability in the reactor, which is a strong function of several metallurgical parameters [20]. These parameters include the shape, the size and the size distribution of the grains, the distribution of various phases, dislocation density and the crystallographic texture. Embrittlement is caused by the neutron irradiation damage to the crystal lattice that increases the strength and decreases the ductility and fracture toughness [19]. The corrosion resistance of the pressure tube, mainly hydriding and oxidation rate, also depends strongly on the microstructure and texture of the tube [21]. Hydrogen in solution has very little effect on mechanical properties but when precipitated as hydrides it can reduce fracture toughness and increase the ductile-brittle transition temperature. The amount of this reduction depends on the hydride density and their orientation relative to the stress direction. Hydrogen concentration more than solubility limit may also lead to delayed hydride cracking and it is one of the main crack growth mechanism in the pressure tubes. The pressure tubes are the primary pressure boundary material for the hot pressurised coolant and they should have good fracture toughness. The excellent performance of the pressure tube is due to the inherent safety of the design and the principle of Leak-before-Break [19]. If a defect forms and propagates until it is through wall, the small leakage of heavy

water coolant will be detected and the reactor would be shut down before the defect can grow to the critical size. Since the pressure tubes operate in a high neutron flux at high pressure and temperature their properties change during service and confidence is needed that the properties particularly those that influence leak before break behaviour, remain within acceptable limits.

The pressure tubes of 220 MWe IPHWR are about 5.2 meter long, and have internal diameter of 82.5 mm and nominal wall thickness of 3.5 mm and they operate in the temperature range of about 250 - 300 $^{\circ}C$ under an average coolant pressure of about 10 MPa and maximum fast neutron flux up to 3.2×10^{17} $n/m^2/sec$ [22].

2.2 Pressure tube fabrication

In efforts to improve the properties of pressure tubes, several major changes in their fabrication flow sheet have been explored and implemented [17, 18]. Zircaloy-2 was replaced with Zr-2.5Nb because of its greater strength and smaller pick-up of hydrogen/deuterium from corrosion reaction with hot heavy water coolant. The fabrication route of Zr-2.5Nb itself has had several versions. Pressure tubes made by routes based on quenching and heat-treatment (annealed or age hardened) were installed in reactors located at Ignalina in Lithuania, Kanupp in Pakistan, and Fugen in Japan, whereas routes based on cold working and stress relieving are used for pressure tubes in CANDUs of Canadian and Indian design [12, 18, 23–25]. With cold-worked tubes, the focus of current improvements in fabrication process, is to have better creep and fracture properties and to reduce microstructural variability to increase the predictability of in-service behaviour. The fabrication route of the pressure tubes is a critical factor, which can significantly influence the metallurgical parameters and hence the mechanical behaviour of the tube over its long operating life.

The heat treated (HT) Zr-2.5Nb pressure tubes were fabricated from the sequence of: extrusion, solution treatment in the $(\alpha + \beta)$ phase, water quenching, cold working about 15%, ageing 24 h at 500 $^{\circ}C$. All of the pressure tubes in the KANUPP, Fugen

and Gentilly-1 reactors were installed in this metallurgical condition. This fabrication procedure produced a mixture of primary α-grains in a matrix of martensite and gave a more random texture than the cold worked (CW) tubes, which has a concentration of basal normals in the transverse direction [26]. The conventional fabrication process for CANDU cold worked Zr-2.5Nb tubes was: extruded at $840\,^{\circ}C$, cold-drawn 25%, and autoclaved for 24 h at $400\,^{\circ}C$. It was felt that the tubes in the cold worked condition could be fabricated with greater confidence in the uniformity of their mechanical properties and that they could be produced at lower cost than heat treated tubes [27].

Cold-worked and stress relieved Zr-2.5Nb tubes are the standard pressure tubes for Indian and CANDU Pressurized Heavy Water Reactors (PHWR). Pressure tubes of Indian Pressurized Heavy Water Reactor (IPHWR) of 220 MWe are made of Zr–2.5Nb alloy manufactured either from Double Melted (DM), in older reactors, or from Quadruple Melted (QM) ingots for newer reactors [28]. Pressure tubes of the Indian PHWRs were manufactured at Nuclear Fuel Complex (NFC), Hyderabad [29], following a fabrication route similar to, but not same as the modified route II developed for the manufacture of PTs of CANDU reactors [11]. This modified route consisted of two cold working steps (instead of one cold working step for the conventional route followed for CANDU PTs) with an intermediate annealing step [12]. The intermediate annealing step was required to attain recovery, so as to facilitate second stage of cold working. However, there are three major differences between modified route II developed for CANDU pressure tubes and that used at NFC. These are the mode of hot working (extrusion at NFC and forging for CANDU), amount of cold work imparted during first cold working stage of tube fabrication (50–55% at NFC, as compared to 20% for CANDU tubes) and mode of imparting cold work (cold pilgering at NFC, as compared to cold drawing practiced for CANDU tubes) [12]. The fabrication route for CANDU and Indian pressure tube is shown in Figure 2.4. The fabrication of pressure tubes for upcoming Indian PHWRs of 700 MWe capacity and other future tubes shall be produced using new forging route [30] and differences in microstructure and properties between the pressure tubes fabricated through this new route with that of

existing route is available in open literature [20, 30].

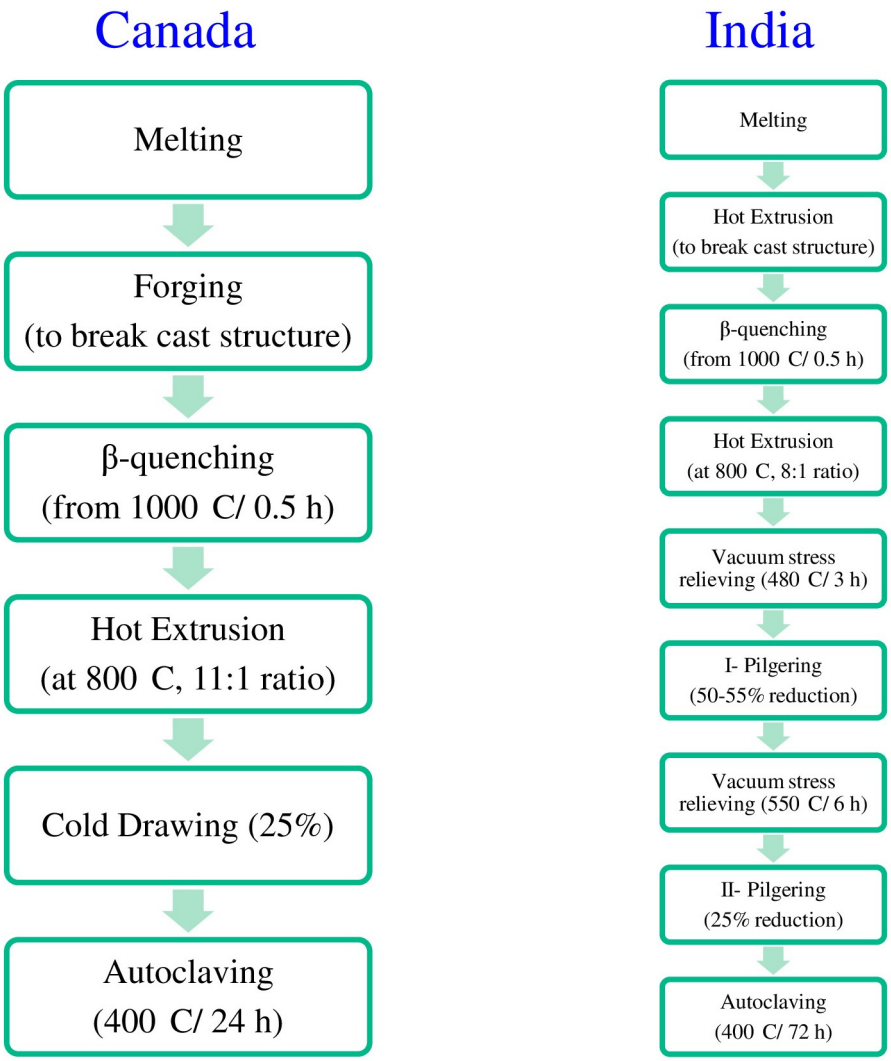

Figure 2.4: Pressure tube fabrication route followed at Canada and India.

2.3 Microstructure and texture

Microstructure plays an important role in the performance of Zr-2.5Nb pressure tube in the reactor. Zr-2.5Nb contains 2.4–2.8 wt% of niobium, and major alloying elements in the form of 900–1300 *wppm* oxygen and <650 *wppm* iron [31]. Oxygen stabilizes the hcp α-phase, whereas niobium stabilizes the body-centred cubic (bcc) beta (β)-phase [32]. The equilibrium phase diagram of Zr-Nb system is shown in

Figure 2.5 [31, 33]. Niobium has a very low solubility in the α-phase so that the equilibrium microstructure of Zr-2.5Nb at room temperature is α-grains that contain about 0.2%Nb and a β-phase that contains 95%Nb [17]. The β-phase is normally present in metastable β-Zr phase having around 20% Nb.

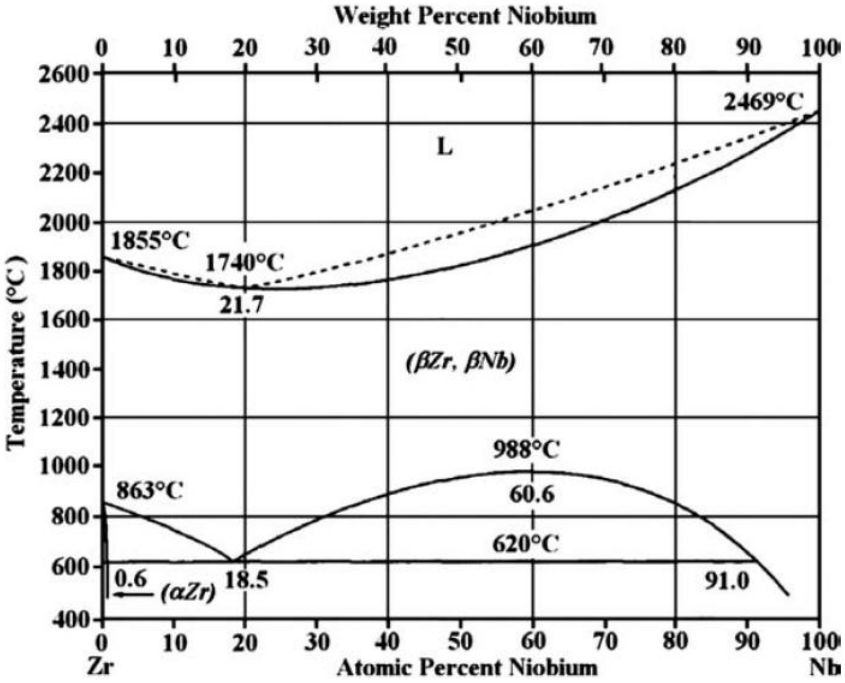

Figure 2.5: The Zirconium–Niobium equilibrium phase diagram [33].

The typical grain structure of as-installed Zr-2.5Nb pressure tube in CANDU reactors is shown in Figure 2.6(a) [31, 34, 35]. The microstructure of CANDU reactor pressure tubes consists of elongated, platelet like grains of hexagonal-close-packed (hcp) α-Zr, partially surrounded by a thin network of filaments of body-centered-cubic β-Zr. These β-Zr filaments are metastable and initially contain about 20% Nb. The stress-relief treatment results in partial decomposition of the β-Zr filaments with the formation of hcp ω-phase particles that are low in Nb, surrounded by an Nb-enriched β-Zr matrix [36, 37]. The α-grain is about 0.3–0.5 μm thick in the radial direction and has an aspect ratio of around 1:5:50 in the radial, circumferential (transverse), and longitudinal (axial) directions of the tube, respectively [38]. CANDU pressure tubes

had dominant transverse basal pole texture, with fraction of basal pole of hcp α-Zr (f_t) along this direction being around 0.58-0.6. The fraction of radial and axial basal poles being around 0.35 and 0.05 respectively.

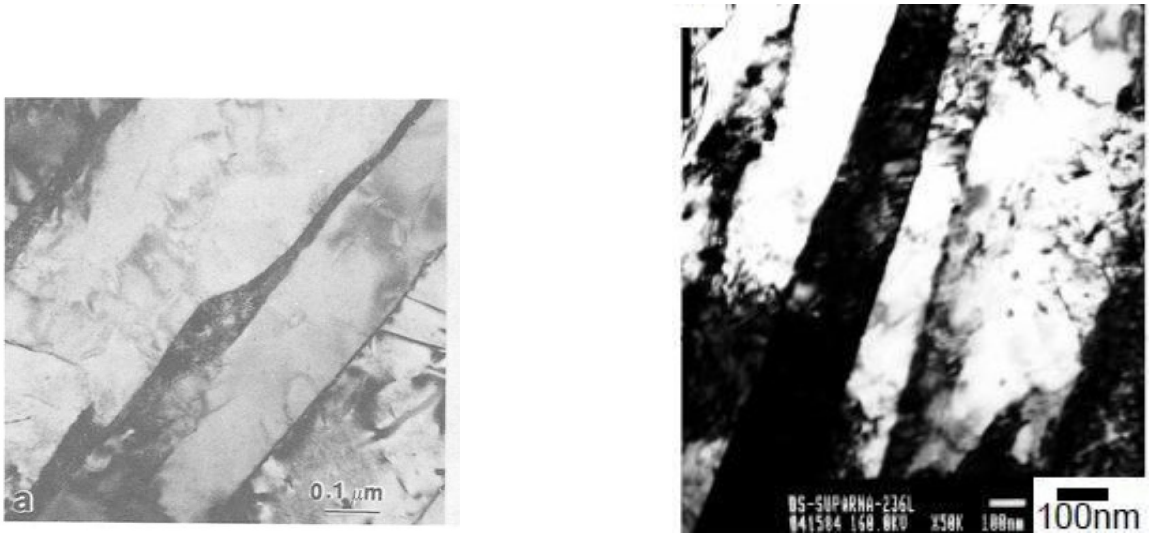

(a) (b)

Figure 2.6: Typical grain structure of Zr-2.5Nb pressure tube in (a) CANDU reactors [35] and (b) Indian PHWRs [39].

Microstructural observation of unirradiated Indian pressure tube off-cuts showed the lamellar morphology of the α-Zr along with the β-phase present as stingers between two α-laths as well as fine and coarse β globules shown in Figure 2.6(b) [39]. TEM-EDS analysis showed that the niobium concentration was less than 1% in the α-Zr phase. Niobium concentration was 10-12% in the continuous film of β-Zr and 20-40% percent in case of globulised β-phase [39]. The size of α -Zr lamellae was found to be in the range from 0.17 to 0.2 μm, 1.8 to 2.4 μm and 1.7 to 2.8 μm in the radial, circumferential and axial direction respectively (aspect ratio of 1:7:8).

The pressure tubes have dominant transverse basal pole texture, i.e. the α-grains are oriented such that the large fraction (0.55-0.6) of basal poles of hcp α-phase are oriented close to transverse direction. The basal pole fractions in radial and axial directions are around 0.35 and 0.05 respectively.

The microstructural parameters of the hot extruded structures obtained in Canadian and Indian pressure tube material are available in open literature [12]. The

volume fraction of β-phase in the Canadian pressure tube and Indian pressure tube extruded structure is 11-13% and 20-28% respectively and the Nb-concentration in β-phase in them is respectively 18-20% and 8-12% [12].

2.4 Degradation mechanism in pressure tubes

Pressure tubes, due to their location in the core region of the reactor, are exposed to aggressive environment of high temperature, high stress, corrosive media and neutron radiation. Neutron irradiation induced changes and hydrogen/deuterium pick-up are the two most important sources of damage in zirconium alloys. The main factors that are known to govern the integrity of the Zr-2.5Nb tubes are firstly, their dimensional change by irradiation growth and creep, secondly, embrittlement by neutron irradiation and delayed hydride cracking at the surface flaws or near the rolled joint regions with high residual tensile stress [40]. Information on in-service behaviour and extent of ageing induced degradation in these properties of the zirconium alloy components, are therefore essential for the un-interrupted and safe running of nuclear power plants.

To serve up to designed life of around 25 years, pressure tubes must be able to provide sufficient resistance against the in-reactor degradation mechanisms [8].

2.4.1 Microstructural changes due to irradiation :

Irradiation of pressure tubes at moderate temperatures changes the microstructure of the pressure tube in several ways e.g. [5]: dislocation loops are generated from the point defects and β-Nb precipitates in the supersaturated α-phase and the stringer of β-Zr phase decomposes in shorter lengths [41] and formation of Nb rich β-Nb and Nb depleted ω-phase regions. The density of dislocation loops and the resultant hardening approaches an asymptotic value. Both interstitial-type and vacancy-type loops form during irradiation. The relative proportion of each depends on the irradiation temperature. Griffiths et al. [42] have shown that the c-component dislocation loops in Zr-2.5Nb samples formed during irradiation are vacancy-type in nature [38]. Irradiation

enhances the precipitation of β-Nb in the α-phase [43], enhances the decomposition of the β-phase, and disperses iron from the β phase.

Post irradiation examination of a Zr-2.5Nb pressure tube from Wolsong1 nuclear power plant [40] after 9.3 effective full power years (EFPY) showed that neutron irradiation changed the dislocation density and the Nb concentration in the β-Zr grains. The a-type dislocation density in the irradiated tube was as much as 2 times that of the unirradiated tubeand was the largest at the pressure tube coolant inlet end subjected to the lowest operating temperature in reactor [40, 42]. This difference in dislocation density indicated that the irradiation temperature and not the flux or fluence, which is maximum at the central location of the pressure tube, played a major role in change in dislocation density. The outlet location of the Wolsong1 Zr-2.5Nb with the highest operating temperature had the higher decomposition of the β-Zr, leading to the formation of the β-Nb, while the inlet location had a lesser amount. Irradiation leads to increase in the dislocation density and also to the decomposition of the β-Zr phase. Decomposition and reconstitution of β-Nb phase has been reported along CANDU pressure tubes due to combination of irradiation temperature and flux.

The TEM study of irradiated Indian Zr-2.5Nb pressure tube has shown that it had an average α-grain width, grain length and aspect ratio in the range of 0.17-0.27 micron, 1.7-2.3 micron and 7.1-8.5 respectively [44]. The grain morphology of α-Zr phase in the Zr-2.5Nb alloy pressure tube did not change appreciably after irradiation. The grain size in terms of length and aspect ratio and the size distribution were nearly similar to that seen in the unirradiated sample [39]. Extensive modification in β morphology was seen at the high flux and high temperature regions of the pressure tubes [44]. The β phase was observed to have globulised completely in many regions. β precipitates were present at the interface of α-Zr laths as well as within the lath. The Nb concentration of the β phase appeared to have increased and the volume fraction had reduced.

2.4.2 Deformation behaviour

The satisfactory performance and the life of the pressure tubes depend mainly on its dimensional stability in the reactor [45]. The diametral expansion and axial elongation rates of pressure tubes in CANDU reactors due to irradiation deformation are important properties that limit the useful life of the reactor and the maximum power for reactor operation. The dimensional changes in the axial and diametral directions are due to the net effect of thermal creep, irradiation creep, and irradiation growth [46]. Both irradiation creep and growth are strong functions of several metallurgical parameters, which include the shape, the size, and the size distribution of the grains, the distribution of various phases, the interfacial structure, and the crystallographic texture and oxygen concentration [1]. The major factors controlling the creep rates in pressure tubes include grain size, texture, and oxygen concentration. Deformation rates are also a direct function of operating conditions such as stress, temperature, and neutron flux. It is also indirectly dependent on the operating conditions because of the modifying effects of the irradiation on the microstructure [47, 48]. Therefore, the in-reactor deformation behavior of pressure tubes is controlled both by the as-fabricated microstructure and the microstructure that evolves during irradiation.

For a given set of operating conditions there is considerable variability in deformation behavior of as-fabricated pressure tubes that can be related to variations in the material chemistry and microstructure [3]. Texture and grain thickness can affect both the anisotropy and magnitude of deformation strain. In general, pressure tubes that have a higher radial basal pole texture parameter and have grains that are thinner in the radial direction tend to exhibit higher diametral strain and lower elongation rates [3]. These microstructural variables also affect the deformation behavior along the length of a given tube because of a gradual change in grain structure and crystallographic texture occurs from one end of the tube to the other. Tube-to-tube variability is likely to result from differences in microstructure, texture and cold work caused by differences in the manufacturing process such as alloy chemistry, quenching practices, extrusion variables, and stress-relieving treatments. Variability from one end of the

pressure tube to the other end is also likely by microstructural and texture changes that occur due to the difference between the starting and final extrusion temperature [18]. Comparing the front and backends of the tube reveals the most prominent correlation; front-ends show larger grain thickness and lower radial texture than back-ends [42]. The front end and back end of pressure tube refers to the end emerging first and last, respectively, from the extrusion press [49].

CW Zr-2.5Nb tubes in CANDU power reactors display higher maximum creep strains when the back-end of pressure tubes installed at the outlet end of the coolant channel [50]. For these tubes, this behavior is attributed to end-to-end variations in the creep and growth properties of the tube. The higher transverse and lower axial strain in the HT Zr-2.5Nb pressure tube than the CW tube are consistent with the known effects of crystallographic texture on anisotropy of the in-reactor deformation of zirconium alloy tubes [26, 27, 51].

2.4.3 Mechanical properties of pressure tubes

The mechanical properties of Zr-2.5Nb are largely dependent on the microstructure and crystallographic texture of the α -phase that constitutes over 90% of the material volume [52]. The texture of pressure tube, developed during its fabrication, leads to its mechanical properties being different in different directions i.e axial and transverse directions.

Tensile and impact behaviour

Differences in the ingot chemistry from which pressure tubes are fabricated and also variations in the fabrication parameters within the limits of specification lead to tube to tube variation in the microstructure and texture. The extrusion process has a significant effect on the pressure tube properties, in particular, the mechanical strength and microstructural features important for deformation, such as basal pole texture and grain shape and size [1]. Even the differences in the extrusion temperature along the length of the tube lead to variations in grain size, texture and dislocation density along

the length of the pressure tube. These, in turn, may lead to differences in mechanical properties from tube to tube as well as from one end of the tube to the other end of the tube. In general, strength increases from the front-end to back-end of the tube [53]. Mechanical property of Zr-2.5Nb is also different in different direction. Other than anisotropic crystal structure, the texture developed during fabrication leads to differences in tensile property along the axial and transverse directions of the pressure tubes.

Directional dependence of the impact energy is required for safety assessment of the pressure tubes under accidental condition. Very little information is available in literature on the impact behavior of Indian pressure tube material [54–56].

Neutron irradiation dramatically alters the microstructure of Zr-2.5Nb [31]. Both the yield strength and the ultimate tensile strength increase with fluence due to the formation of a high density of dislocation loops during irradiation that harden the material, and to lesser extent cause the dissolution of precipitates [4, 5, 38, 41, 57–59]. The irradiation hardening is accompanied by a reduction in ductility, mostly due to strain localization when irradiation damage gets cleared out in bands during plastic deformation. The increase in strength and decrease in ductility arises from the interaction of moving dislocations with irradiation induced localised obstacles like interstitials, dislocations, dislocation loops distributed in the glide plane [60]. The change in transverse ultimate tensile strength with irradiation is shown Figure 2.7 [17]. Irradiation temperature, metallurgical condition (heat treatment, cold work) and the alloy composition each affect the change in properties with irradiation [32].

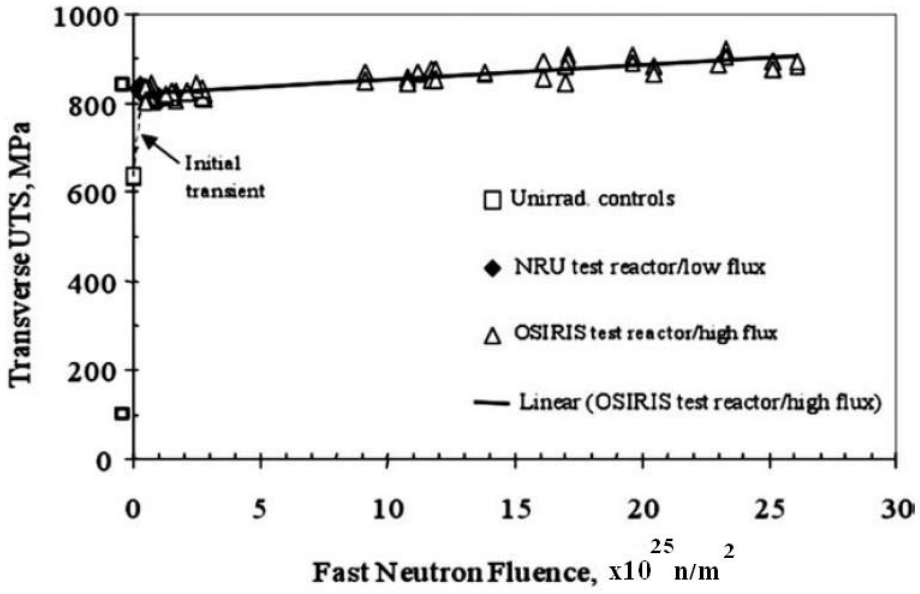

Figure 2.7: Effect of irradiation on ultimate tensile strength showing initial sharp transient and saturation effect [17].

For irradiated, cold-worked Zr-2.5Nb, the ultimate tensile strength (UTS) generally occurs at very low plastic strains, indicative of the low work-hardening behavior of this material and it results in little distinction between the 0.2% offset yield stress and the UTS in the transverse direction [4, 5, 61].

During tensile deformation of irradiated zirconium alloys, the dislocation loops that cause the hardening either are annihilated by mobile dislocations or cause deformation twins [62]. Both processes lead to strain localization. Void formation takes place in the intense shear bands. Pre-irradiation tensile strength did not seem to correlate to the fracture toughness of the irradiated material as the alloys having different initial strength would get saturated to near similar irradiation hardening afterwards and hence would not affect toughness [4]. The fracture properties and DHC velocity are closely linked with the radiation-induced microstructural evolution [37, 38, 63].

Fracture behaviour

Fracture toughness is a property that describes the ability of a material containing a crack to resist fracture and it gives an idea of amount of stress required to propagate

a pre-existing flaw of a given size or the maximum length of crack a component can withstand for a given stress before failure. This fracture toughness is very important property as the occurrences of flaws is not completely avoidable in processing, fabrication or servicing of a material or a component. Flaws may appear as cracks, voids, inclusions and design discontinuities. Fracture toughness depends on strength, ductility, microstructural features like grain size, void nucleation sites and dislocation density.

Neutron irradiation increases the strength and consequently reduces the ductility and fracture toughness of cold worked Zr-2.5Nb pressure tube material [4, 5, 38, 41, 57, 58]. For pressure tube, the fracture toughness is characterized by the parameters such as initiation toughness (J_i), dJ/da, which is a measurement of the crack growth resistance at small crack extension from curved compact specimens of irradiated surveillance pressure tubes [58]. Irradiation initially rapidly reduces the fracture toughness and critical crack length (CCL), but further reduction with fluence is small as shown in Figure 2.8 [17, 38]. The results from the tests irradiation in reactors with different fast neutron fluxes indicate that the fast flux intensity does not have a major effect on the irradiated toughness and microstructure evolution, rather its the total fast neutron fluence that matters [5].

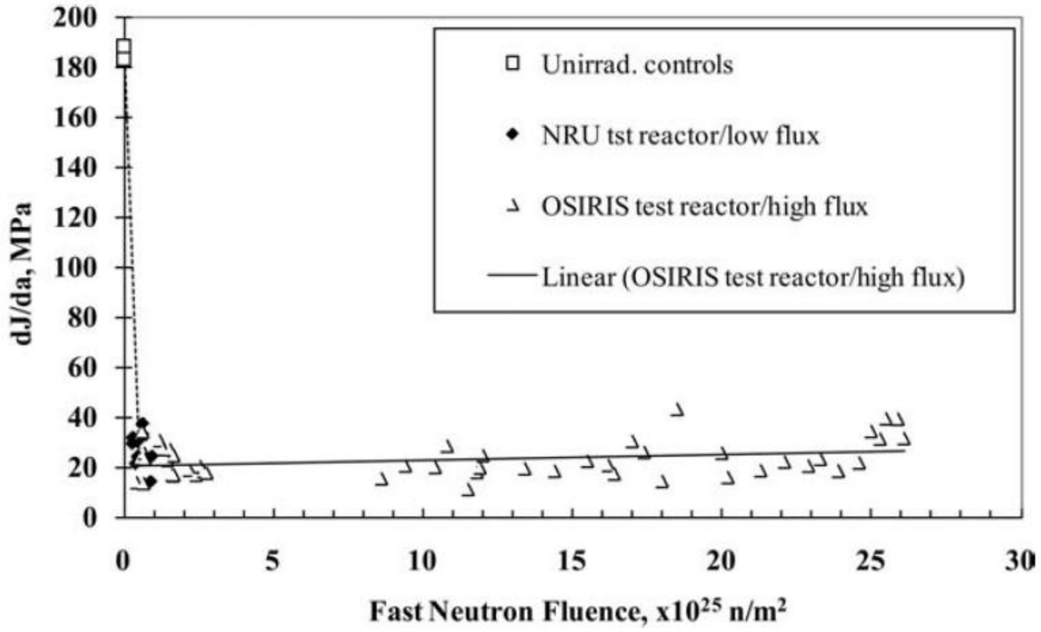

Figure 2.8: Effect of irradiation on fracture toughness showing sharp initial transient and marginal effect of flux [17,38,].

The fracture toughness of cold-worked Zr-2.5Nb shows large lot to lot variability, which persists even after irradiation as shown in Figure 2.9 [4, 5]. When sufficient data on the effect of fluence on fracture behaviour had been gathered, it became apparent that the reduction in the fracture toughness of some tubes was considerably less than that in other nominally similar tubes. The possible causes of this variability were variations in grain size and shape, variations in distribution of the β-phase, crystallographic texture, and variations in concentration and distribution of trace elements [2]. A low fracture toughness was found to be associated with fissure like features on the fracture surface, with small inter-fissure spacing and large size of the fissures in low toughness tubes. The trace element impurities chlorine, phosphorus in combination with carbon, formed planes of weakness shown by fissures on the fracture surface due to the presence of microsegregated species (Zr-CI-C complex) and particles (phosphides and, to a lesser extent, carbides) [2, 5, 41, 64]. They are especially damaging to the toughness of

cold-worked Zr-2.5Nb pressure tube material since they effectively divide the specimen into a series of thinner specimens or ligaments, each of which may then fail at a lower fracture strain [5, 61, 64]. The fracture surface of material containing little chlorine had no fissures, and the fracture toughness was found to be quite high. This result strongly suggested that if the chlorine concentration was minimized, toughness would be increased, as shown in Figure 2.10 [64]. It also provided another reason to control the carbon concentration [2].

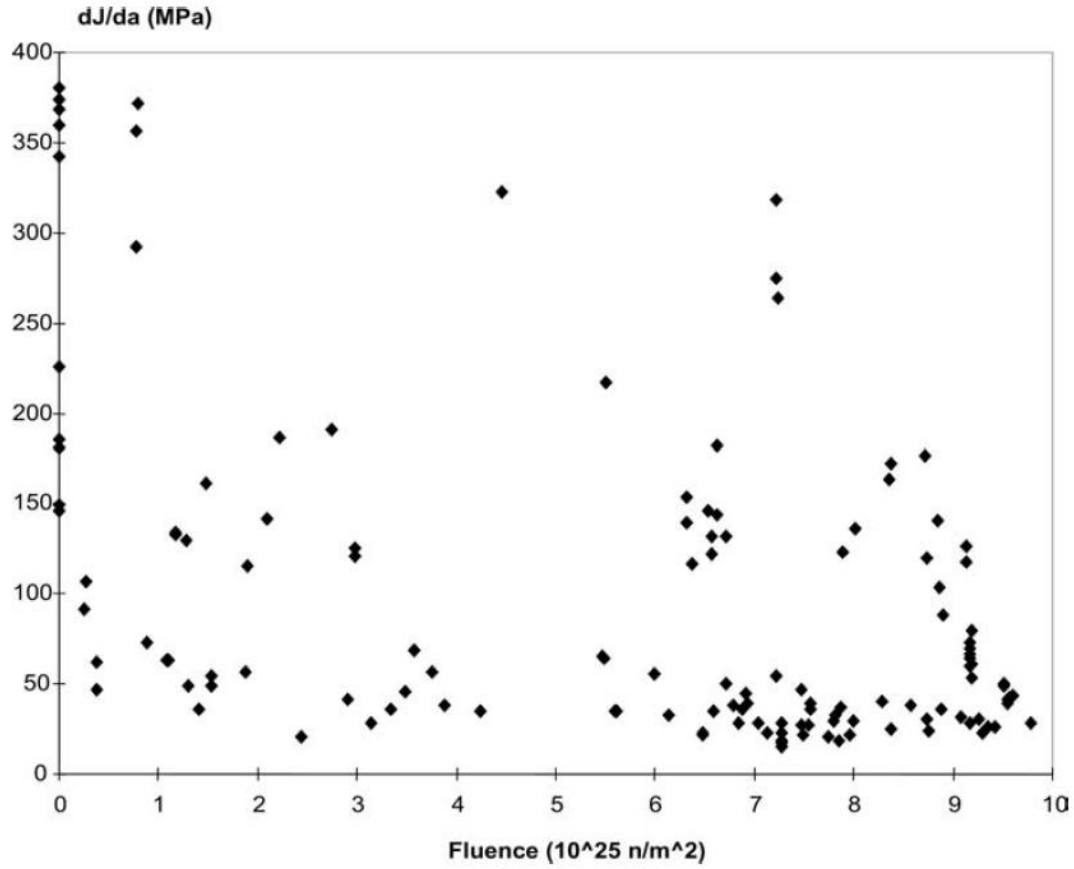

Figure 2.9: The fracture toughness of cold worked Zr-2.5Nb pressure tubes at 240-300$^{\circ}C$ after service in a CANDU reactor showing large variability in toughness [4,5,17].

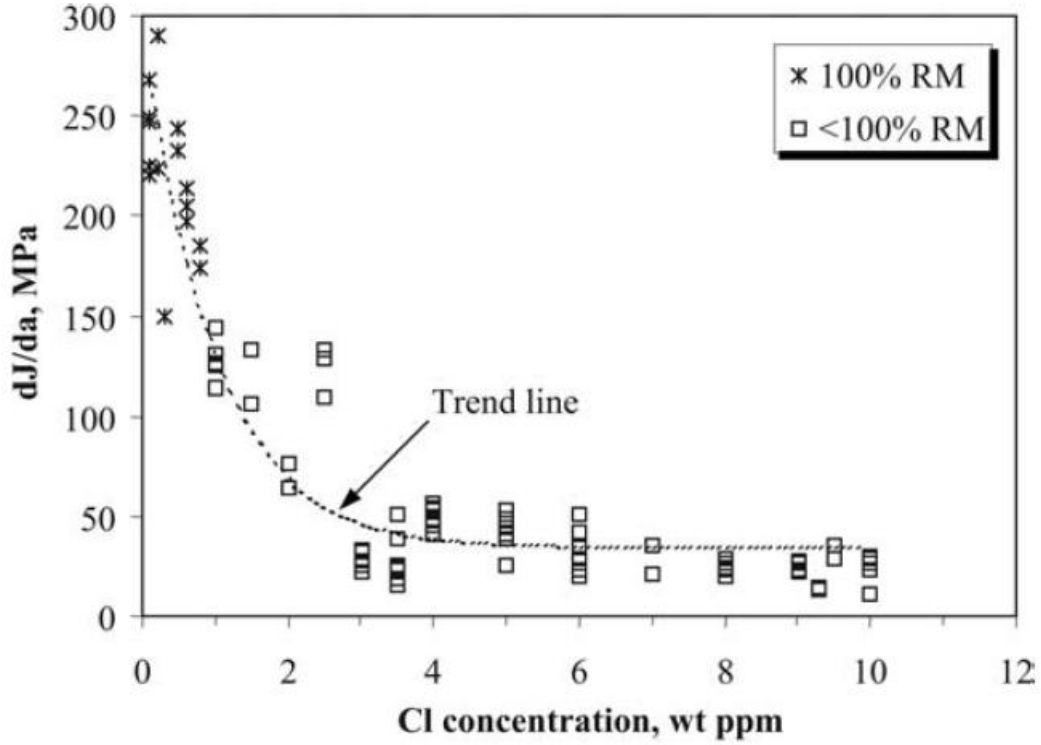

Figure 2.10: Effect of chlorine on fracture toughness of Zr-2.5Nb pressure tube showing large increase in toughness with low concentration of chlorine [64].

It has been found that minimizing trace quantities of some impurity elements (Cl, C, H, P) in the alloy is very effective in increasing fracture toughness of Zr-2.5Nb [2, 49, 64, 65]. Chlorine is a residual element coming from the fabrication process, and it turned out that the tubes that had the low chlorine concentration had been made from ingots that had been made from 100 % recycled material. This resulted in the adaption of a practice of material being vacuum melted four times rather than the normal twice, which resulted in the removal of volatile chlorine from ingot. Carbon and phosphorus concentrations are controlled by judicious choice of starting materials. Initial hydrogen concentration is minimized by careful attention to surface preparation and ingot processing at each stage of fabrication. Thus fabrication route of Zr–2.5Nb has changed from double melted ingot to quadruple melted ingot. The efficacy of these changes is demonstrated in the distribution of the values of crack growth resistance in tubes made by double and quadruple melting of ingots made from

Kroll sponge and double melted ingots made from electrolytic powder, Figure 2.11 [66]. This improved fracture resistance was gained without sacrificing strength [66]. These changes in pressure tube fabrication have led to a more consistent product with smaller variation in microstructure and subsequent improved properties than could be attained previously [1]. For example, although ultimate tensile strength has increased slightly in more recent production tubes, the variability in properties has decreased as seen in Figure 2.12 [1].

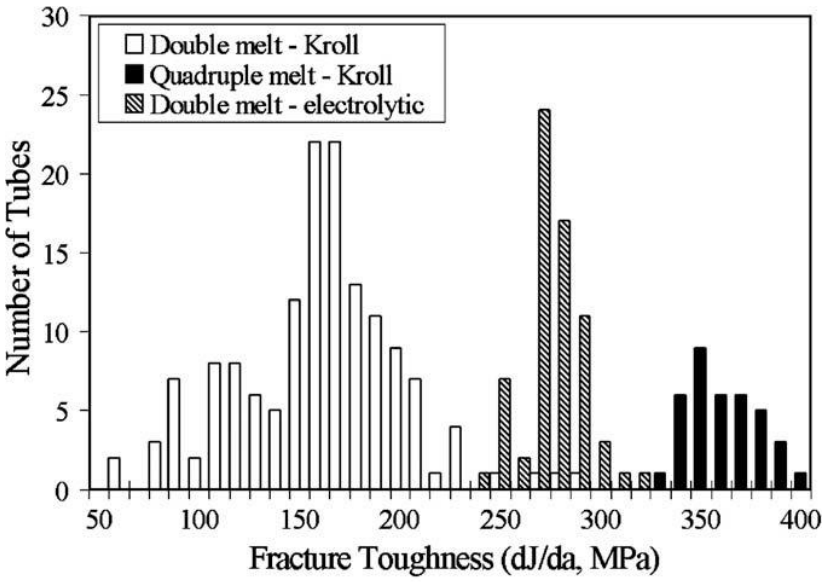

Figure 2.11: Variation of crack growth resistance at 250$^{\circ}C$ for three versions of Zr–2.5Nb pressure tubes showing significantly higher toughness for quadruple melted tubes [66].

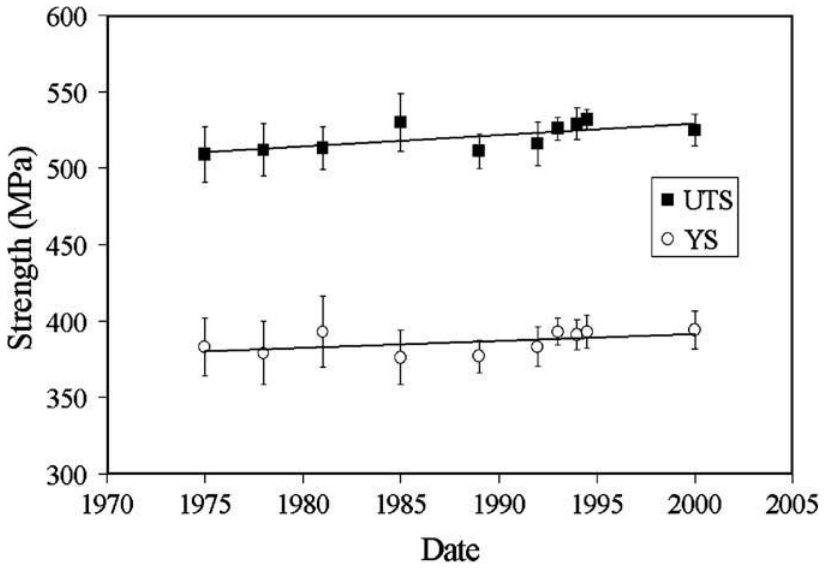

Figure 2.12: Reduction in variability of yield strength (YS) and ultimate tensile strength (UTS) of pressure tubes with year of tube production [1].

Specimen size effect

A procedure was developed for fracture toughness testing of zirconium alloy pressure tubes using 17-mm curved compact tension specimens [67], and it was shown that because of the small size of the specimens, the curvature of the specimen did not introduce significant errors [68]. The curvature of the tube was retained because flattening the material to produce flat specimens would be difficult due to irradiation embrittlement and the possibility that any dislocation movement induced by the flattening process would destroy the defect structure produced by irradiation [27].

To study the relationship between small specimen results and large-scale toughness tests, systematic studies were carried out on unirradiated and irradiated materials [61, 62, 69, 70]. For irradiated material, the evaluation of fracture toughness was also done using curved compact tension specimen [27, 69, 71]. Geometry constraint was seen to affect the test results on samples of different sizes [69]. A 500 mm long tubes burst specimen was used for large-scale fracture toughness determination and a curved compact tension CT specimen with a 17 mm width was used for the small sized specimen [70]. The J versus $\triangle a$ curve for small specimen and full-scale burst type

specimen from pressure tubes were compared and the results from the small curved CT specimen were found to be conservative. This difference in the measured toughness values from CT specimen and burst test specimen arise due to differences in the triaxiality and the crack tip stress-state ahead of the growing crack in these geometries [72]. In the case of small specimen, the fracture surface in the central region shows more fissure like features due to higher crack tip constraint. In the burst type specimen, the high constraint central region is smaller, and the corresponding plastic zone size is larger, which yields higher toughness.

Effect of hydrogen

During reactor operation the pressure tubes undergo corrosion by reacting with hot coolant heavy water and hydrogen or deuterium is generated as a product of this reaction. Deuterium is also generated due to radiolytic decomposition of coolant heavy water. A part of the hydrogen/deuterium evolved during service is picked up by the pressure tubes [73]. Approximately 2%–10% of the deuterium generated by the corrosion process is absorbed along the body of the tube. Additional deuterium may also enter the pressure tube through the rolled joint between tube and end fitting, which leads to higher hydrogen concentration in the rolled joint region. Figure 2.13 shows a typical deuterium concentration profile along the length of a pressure tube [18]. Along the main body of the pressure tube the deuterium concentration increases and peaks near the outlet end that is at higher temperature.

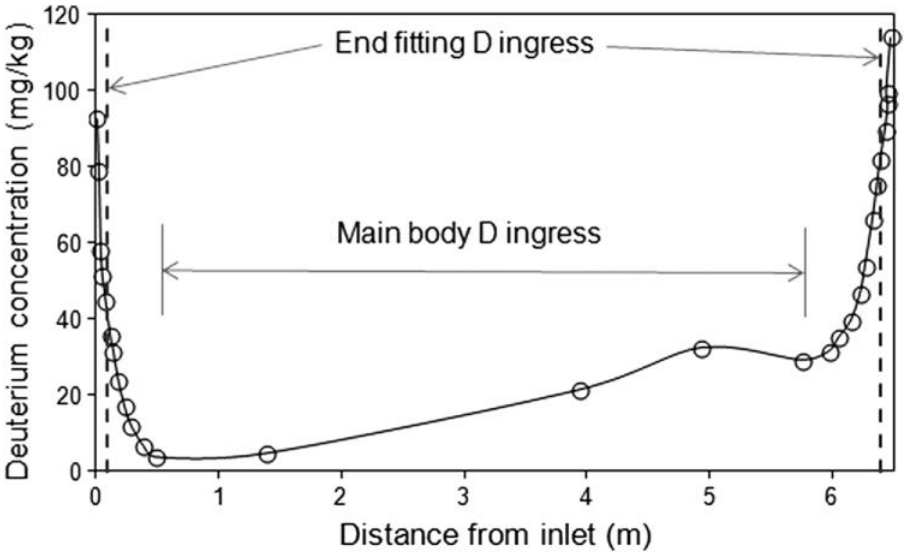

Figure 2.13: Deuterium/Hydrogen concentration profile along the pressure tube length, showing high hydrogen concentration in rolled joint regions and gradual increase from inlet to hotter outlet end [18].

Hydrogen or deuterium, if present in excess of terminal solid solubility (TSS) forms zirconium hydride phase [54]. Depending on the hydrogen concentration, cooling rate and temperature of hydride precipitation, either of three γ , δ or ε hydride phases can form in dilute zirconium alloys [73, 74]. However under reactor operating conditions only δ hydrides have been found to form [73]. Depending on the temperature and hydride orientation, the zirconium-hydrides can be brittle and can lead to either overall loss of fracture toughness i.e hydride embrittlement or time dependent fracture known as delayed hydride cracking.

Hydride embrittlement

Studies have shown that a large decrease in tensile ductility can take place in Zr-alloys as a result of hydride precipitation [57, 75–78]. The extent of hydride embrittlement depends, not only on the quantity of hydride present, but also on its morphology, distribution and in particular the orientation of hydride platelets with respect to the applied stress [78, 79]. Hydride platelets oriented normal to the stress axis have been found to cause large reductions in strength and ductility, while hydride platelets ori-

ented parallel to the stress axis have little effect. For a tubular component internally pressurized in service, it is desirable to have the hydride platelets oriented with their major axis in the circumferential direction [79]. Closely spaced hydride platelets lead to brittle fracture, but ductile fracture prevails in materials containing widely spaced hydrides [78, 80].

Effect of hydrogen concentration and temperature on Zr-2.5Nb pressure tube have shown that hydrogen concentration of around 100 to 140 $wppm$ significantly reduced the initiation fracture toughness J_i to around 80% of the initial values [81]. But at higher temperature effect was not so prominent. Work on Indian Zr-2.5Nb pressure tube has also shown that in unirradiated pressure tube material the fracture toughness parameters J_i and maximum load fracture toughness J_{max} decreases mildly with hydrogen concentration above a threshold value of around 25 $wppm$, and crack growth resistance $\frac{dJ}{da}$ remains practically unaffected by the hydrogen above this concentration [82]. In a similar work on unirradiated Zircaloy-2 pressure tube it was found that circumferential hydrides were less damaging as compared to radial hydrides [83].

The effects of hydride morphology on the axial fracture toughness of cold-worked Zr-2.5Nb pressure tube material have been determined with different morphologies and hydrogen concentrations [84]. The morphologies were characterized by a parameter referred to as the hydride continuity coefficient (HCC), which provides a measure of the extent to which hydrides are oriented in the axial- radial plane of the pressure tube. Hydrides in this orientation are known to be detrimental to the fracture properties of the tube. The effects of increasing HCC and hydrogen concentration on the fracture toughness are clearly evident. Specimens having low HCC values have relatively high toughness at room temperature and achieve an upper shelf toughness, indicative of a plastic tearing failure mode, above $100\,^{\circ}C$. For the specimens containing reoriented hydrides, HCC > 0.5, toughness is significantly lowered at all temperatures below about $240\,^{\circ}C$. Above $240\,^{\circ}C$ specimens can be expected to exhibit upper shelf toughness. Fracture behavior at $240\,^{\circ}C$ may be either brittle or ductile [84].

Delayed Hydride Cracking

Delayed hydride cracking (DHC) is a well known stable crack growth mechanism in zirconium alloys. Hydrogen accumulates at a stress raiser in component. If sufficient hydrogen is present, hydrides form and, if the stress is above a threshold value, the hydrides fracture and the crack advances and then gets arrested in the ductile zirconium alloy matrix. This hydride formation and fracture process then repeats until the crack grows to larger size and becomes unstable. The two main characteristic parameters of DHC are the crack velocity, V, and the threshold loading below which cracks do not grow; this threshold stress intensity factor is called K_{IH}. The dependence of DHC velocity on stress intensity factor, K_I, is schematically shown in the Figure 2.14 [85]. It shows [86] three stages: Stage 1) no cracking up to a threshold, called K_{IH}, after which the cracking rate increases rapidly with K_I, Stage 2) Stable crack growth, having little rate change with further increase in K_I and Stage 3) onset of unstable cracking when fracture toughness K_{Ic} is reached.

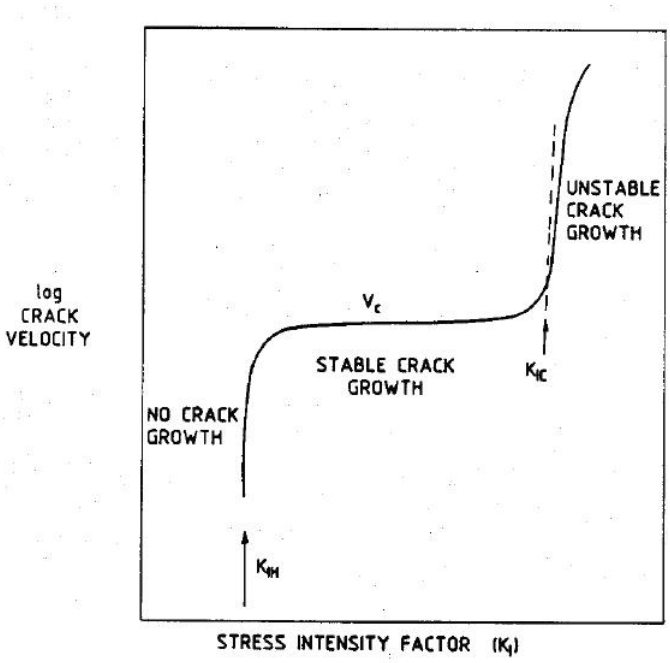

Figure 2.14: Schematic diagram of dependence of DHC velocity on applied stress intensity factor [85].

A number of instances of DHC in the nuclear industry have occurred in pressure tubes of CANDU PHWRs. The pressure tubes in Units 3 and 4 of the Pickering Nuclear Generating Station were made from Zr-2.5Nb, and several of them cracked and leaked in 1974 and 1975 [87, 88]. All the cracks in these tubes initiated at the inside surface of the pressure tubes where they were attached to the end fittings of the reactor by rolled joints. At this position there were high residual tensile hoop stresses that resulted from an incorrect procedure of making the rolled joint [89]. The crack surfaces were characterized by coloured, concentric bands, centered about the crack origin, corresponding to portions of the fracture surfaces covered with different thicknesses of oxide [89, 90].

In the unirradiated PT the DHC velocity in the axial direction was found to be 1.7 to 1.9 times higher than that in the radial direction. It has been also reported that the temperature dependency of DHCV in the axial direction (V_a) is smaller than that in the radial direction (V_R). At low temperature, $V_A > V_R$, but at 300 $^{\circ}C$ both velocities have about the same value [15].

Neutron irradiation at operating temperatures increases DHCV and reduces K_{IH} [91, 92]. The neutron irradiation reduced K_{IH} by about 20% and increased the velocity of cracking by a factor of about five [15]. The rate of cracking is used in estimating the action time for detecting propagating cracks before they grow and become unstable. Hence, it is important for reactor operators to know how these properties change during service in reactors where the components are exposed to neutron irradiation at elevated temperatures. The increase in crack velocity was greatest with the lowest irradiation temperature. The crack velocities are higher at the inlet end than at the outlet end of the coolant flow. The average crack velocity at the inlet end has been reported to be about twice that at the outlet end. These changes in the crack velocity by neutron irradiation are explained in terms of the combined effects of irradiation hardening associated with increase in <a>-type dislocation density, and β-phase decomposition [4, 15, 21, 38, 41, 93]. While the former process increases crack velocity, the latter process decreases it. The combined contribution is controlled by

the irradiation temperature.

Figure 2.15 [1] shows the effects of irradiation and fluence on the radial DHC crack growth rate at 240 $^{\circ}C$. The data show that irradiation increases the DHC crack growth rate by a factor of about 10 and the effect saturates after a fluence between 5 and 10×10^{25} n/m^2. Higher yield strengths lead to higher crack-tip stresses that increase the driving force for hydrogen/deuterium diffusion and also affect the critical condition for hydride fracture [18]. The axial crack growth rate relationship with temperature on irradiated pressure-tube material is shown in Figure 2.16 [1]. It is an Arrhenius relationship because the main temperature dependence of DHC growth rates resides in the temperature dependence of hydrogen diffusion and its solubility limit [18].

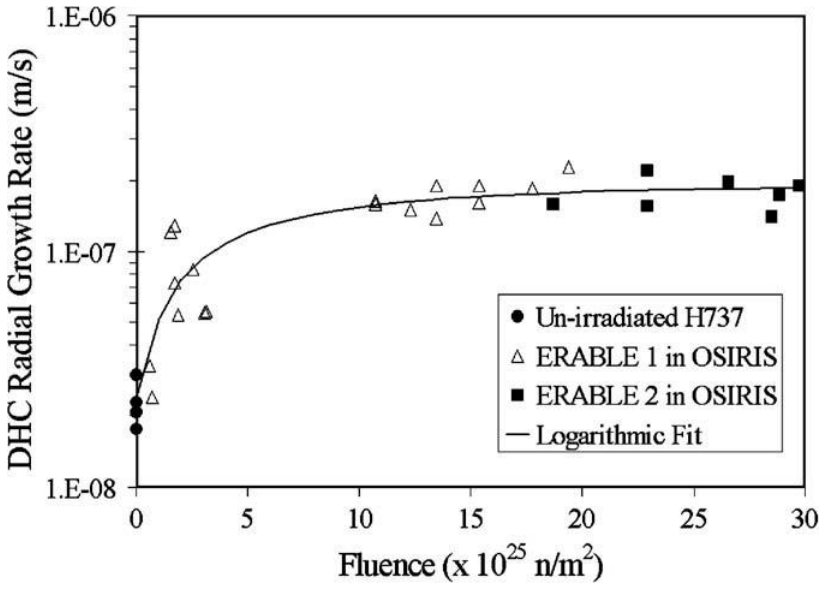

Figure 2.15: Effect of fluence on DHC radial growth rates at 240 $^{\circ}C$ showing sharp initial increase due to irradiation hardening and saturation after that [1].

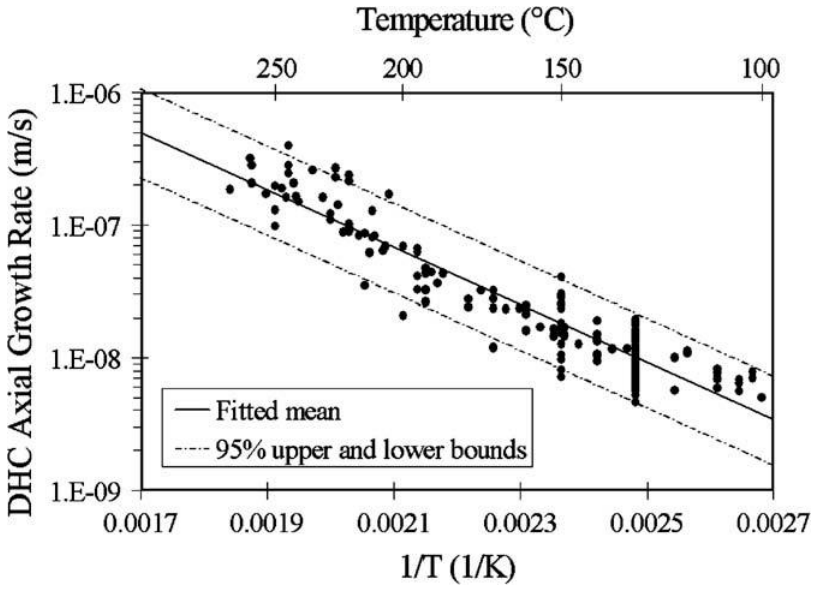

Figure 2.16: The upper bound, mean and lower bound axial DHC crack growth rates for irradiated Zr–2.5Nb pressure tubes showing Arrhenius dependence on temperature [1].

2.5 Leak Before Break approach

As part of a defence-in-depth approach to fitness for service, the pressure tubes are operated in a regime that satisfies the leak-before-break (LBB) criterion [91]. Satisfying LBB criteria requires that any undetected flaw in a pressure tube, if it grows in a subcritical manner, across and along the tube, must produce sufficient leakage of primary coolant for detection and sufficient time is available for safe shutdown of the reactor before leaking crack grows to the critical crack length (CCL) [41]. The structural integrity of the pressure tubes is periodically assessed by means of mechanical testing of surveillance tubes removed from service [94]. Such testing provides information on any degradation in the mechanical properties due to the effects of irradiation damage and deuterium pick-up, as well as demonstrates safety margins for continued tube operation.

One of the criteria for limiting the lifetime of a pressure tube would be an inability to defend "leak-before-break". The most likely crack propagation mechanism for Zr-2.5Nb pressure tubes is delayed hydride cracking, which determines the rate of crack

growth and CCL is governed by the fracture toughness [41]. CCL is the minimum length of an axial, through-wall crack that would be unstable under reactor operating conditions [66]. Critical crack length may be determined from the burst tests on 500-mm tube sections with axial, through-wall defects [4]. Estimates of CCL may also be obtained from the small curved compact toughness specimens machined directly from the irradiated tube material [67, 68]; such specimens generally produce conservative results [4, 61].

The best way to estimate CCL is by iteration of the plane stress fracture toughness calculated from closed end burst tests on sections of irradiated, full-size pressure tubes containing axial cracks [66]. Although this test method represents reactor conditions, it is impractical for new materials. The CCL estimation from burst tests for new materials would need irradiation of half meter or more tube sections and its testing. For development and evaluation of new materials it is much more practical to irradiate small specimens and use the correlation observed earlier between dJ/da values obtained on small specimens and CCL values obtained in burst tests of irradiated tubes removed from reactors.

Another measure chosen to compare fracture toughness is the slope of the crack growth resistance curve, dJ/da, measured on curved compact specimens [66, 67]. An acceptable value of dJ/da has to be derived to provide a guideline for new processes. Using small specimens machined from archive tubing, dJ/da of unirradiated material was compared with the CCL derived from burst tests on the same tubes that had been removed from power reactors after several years of service and is shown in Figure 2.17 [66]. The tests were done at $250\,^{\circ}C$ to represent the inlet temperature of a CANDU fuel channel. The initial benefit of the higher CCL of irradiated material with increase in dJ/da of unirradiated material is not maintained beyond about 200 MPa. In the guidelines for new materials or process improvements, target dJ/da was set at 250 MPa to provide both an acceptable CCL during service and a margin for unknown factors [66].

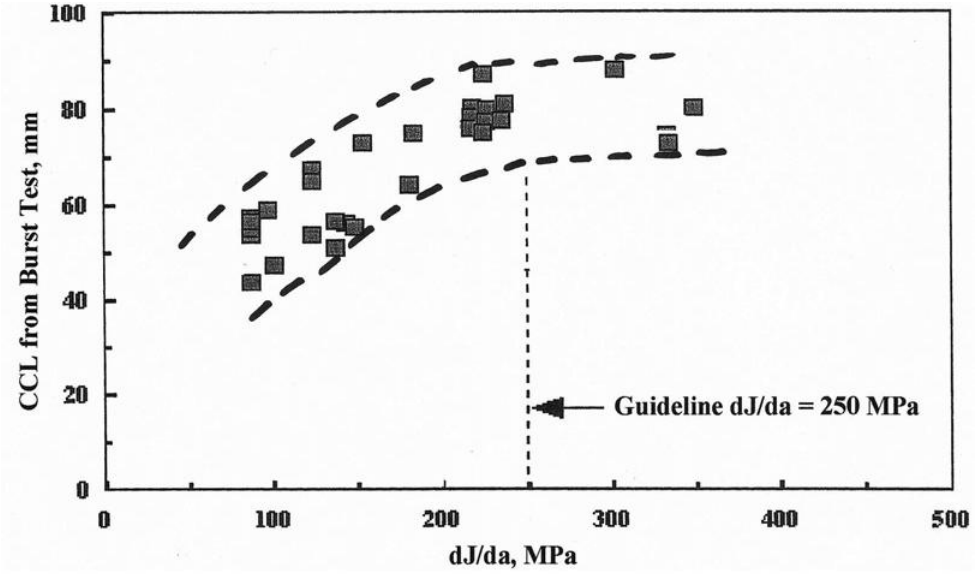

Figure 2.17: Relationship between the critical crack length (CCL) of irradiated Zr-2.5Nb pressure tubes obtained from burst tests and crack growth resistance of unirradiated archive material at 250 °C. CCL calculated for internal pressure of 10 *MPa*, tube internal diameter of 51.7 mm, and wall thickness of 4 mm [66].

Operator response time (ORT)

DHC cracks may initiate at flaws, which are locations with higher tensile stresses. The crack grows in both the through-thickness (radial) and longitudinal (axial) directions until it penetrates the wall of the tube and starts leaking [86]. Figure 2.18 shows the schematic geometry of a growing crack [91]. At through-wall penetration, a leak of coolant into the annulus gas system begins and the crack continues to grow towards both end in the longitudinal direction. To satisfy the LBB criteria the important question that the reactor operators need to answer is "How much time is available to detect the leak and to take action before the crack becomes unstable?" [95]. The time available can be estimated using the simple model shown in Figure 2.18, which represents the fracture face [95]. The tube wall thickness is W, the crack length at leakage is L and the CCL is C, assuming C>L. In cold-worked Zr-2.5Nb pressure tubes, cracks tend to grow about twice as fast in axial direction as compared to radial or thickness direction. Thus if a crack is initiated almost at a point on the inside surface,

then L=4W at the point of through wall crack generation. If the crack continues to grow in both directions axially, the amount of crack growth available in each direction is 0.5(C-4W), and with a crack velocity V the time, t, available to detect the leak from first penetration to the attainment of the CCL is [95]

$$t = \frac{C - L}{2V} \tag{2.1}$$

This time is known as operator response time (ORT). Thus to estimate the response time when the crack has penetrated through the thickness of the pressure tube, we need to know critical crack length, C which we can get from the fracture toughness test, and V, delayed hydride crack growth velocity which we can get from the DHC test.

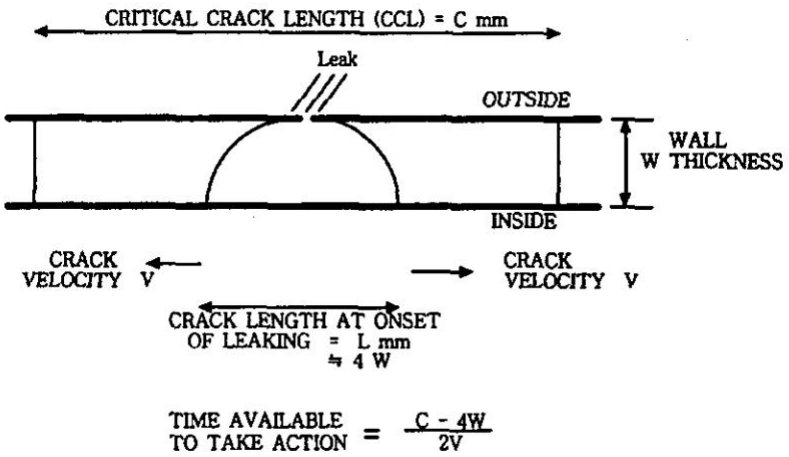

Figure 2.18: Schematic diagram of crack dimensions at onset of leaking [91,95].

2.6 Relevance of current work

Extensive literature, mostly from Canada, is available on the works that have been carried out on the CANDU pressure tube materials. Also studies on unirradiated Indian PHWR pressure tube material Zr-2.5Nb with respect to microstructure, tensile, fracture toughness and DHC velocity have been reported [9, 12, 16, 23, 28, 29, 53, 96,

97]. Mechanical properties and deformation of Indian irradiated Zircaloy-2 pressure tube material, used in early reactors, is available to some extent [39, 98–101]. However, very limited studies on Indian irradiated Zr-2.5Nb PHWR pressure tube material has been carried out [39, 44, 102–105]. It is important to note that the manufacturing route used for Indian pressure tubes differ from that of Canadian route and there are differences in the microstructure of the as-fabricated and irradiated pressure tubes of these two types.

Extensive work has been carried out in present study to characterize the tube to tube variability in the mechanical properties of Indian pressure tubes, fabricated using double melted and quadruple melted fabrication routes, along axial and transverse orientation, at front and back end of the pressure tubes. Dynamic impact test behaviour for both as-received and hydrided Zr-2.5Nb pressure tubes over a range of temperature, along axial and circumferential direction has been studied. Fracture toughness and DHC velocity behaviour of Zr-2.5Nb Indian pressure tubes, after irradiation, have been studied using the Disk Compact Tension (DCT) specimens. The results generated have been used to demonstrate Leak Before Break safety criteria for coolant channels.

Chapter 3

Materials and experimental procedures

In the present thesis experiments have been carried out on the Zr-2.5Nb pressure tube materials that are being used in Indian PHWRs. Materials of pressure tubes in Indian PHWRs have been changed progressively matching with the development sequence. Figure 3.1 shows the types of pressure tube materials used in different Indian PHWRs.

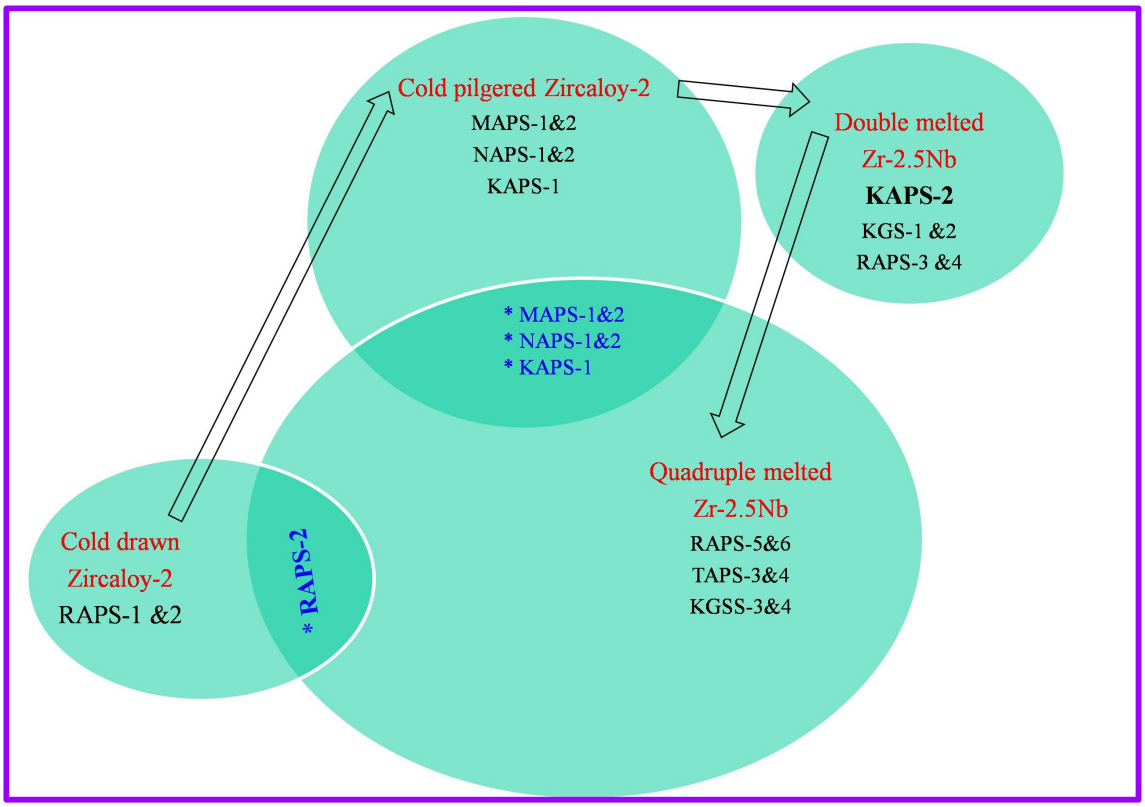

Figure 3.1: Progressive changes in Indian PHWR pressure tube materials.

The materials used and the experiments carried out in this work on these materials are shown as block diagram in Figure 3.2 and Figure 3.3 respectively. Kakrapar Atomic Power Station-2 (KAPS-2) is the lead reactor having double melted Zr-2.5Nb pressure tubes and Rajasthan Atomic Power Station-2 (RAPS-2) is the lead reactor having quadruple melted pressure tubes. Extensive work on unirradiated material has been carried out on the offcuts of pressure tubes of these two reactors. The irradiated materials used in the present experiment were two pressure tubes S-7 and Q-10 removed from KAPS-2 reactor. KAPS-2 is a 220 MWe PHWR type reactor. Typical cross-section of the core of Indian 220 MWe PHWR with channel location is shown in Figure 3.4. It also shows the locations of S-7 and Q-10 channel in PHWR.

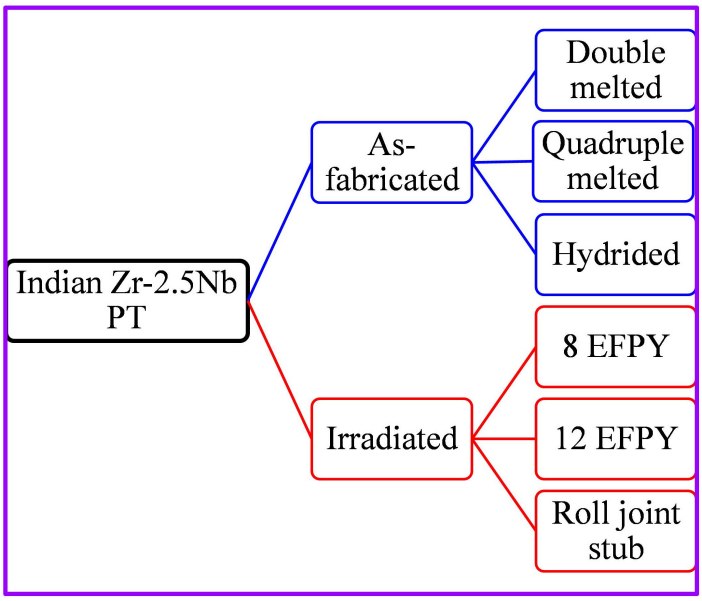

Figure 3.2: Materials used in the present experiments.

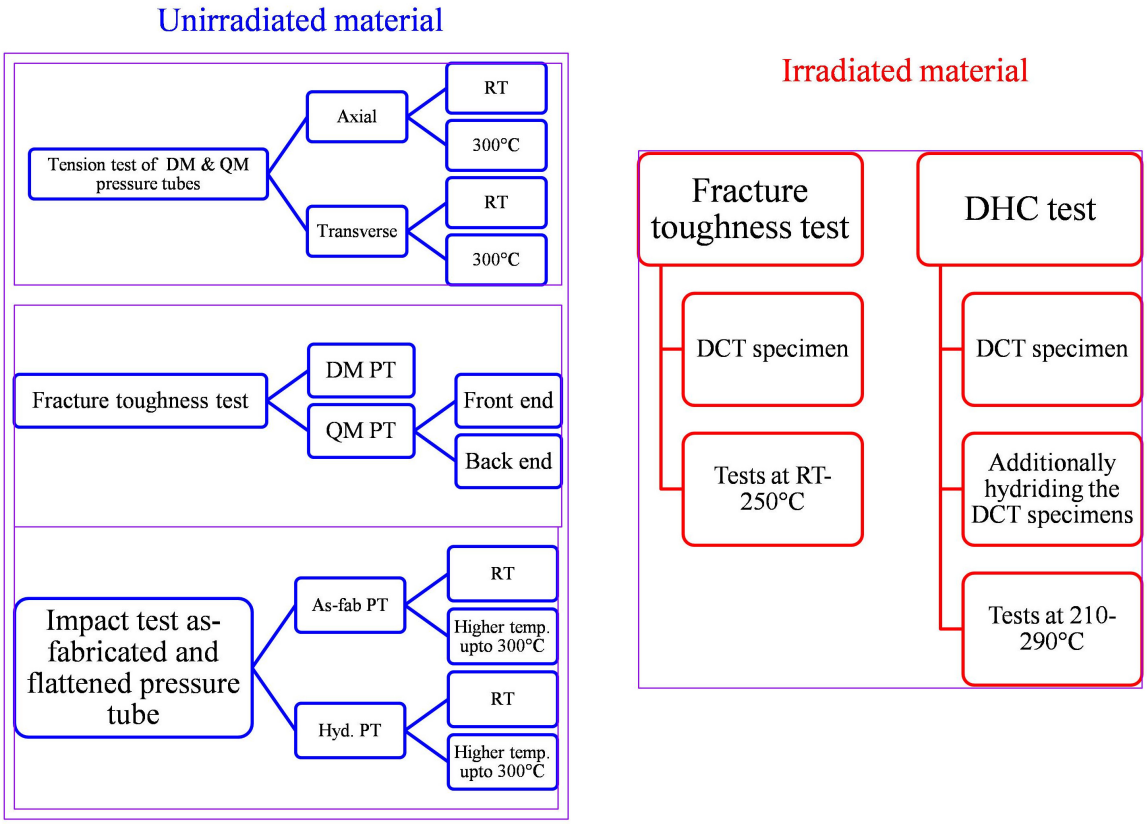

Figure 3.3: Experiments carried out in the present study.

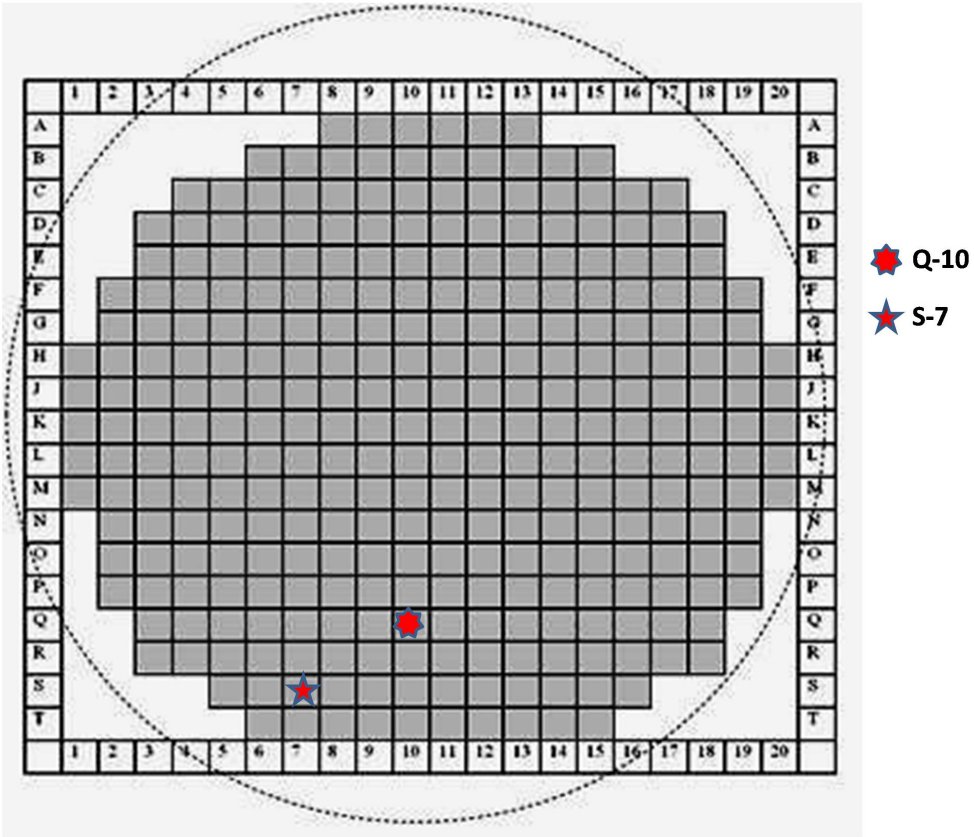

Figure 3.4: Typical cross-section of the core of Indian 220 MWe PHWR with channel location.

3.1 Materials

The materials under study were essentially Zr-2.5Nb pressure tubes made at NFC using the cold pilgering route described earlier in section 2.2. The Indian PHWR pressure tubes are of ≈82.5 mm average internal diameter and ≈3.5 mm thickness. The pressure tubes in the present study, were tested in (i) as-fabricated condition (ii) after hydriding the tubes and (iii) also after irradiation of the tubes in the pressurised heavy water reactor. The material, microstructure, texture, hydrogen concentration and irradiation have been given in detail in the context where they appear in the thesis. The specified chemical composition and mechanical properties of IPHWR pressure tube are given in Table 3.1 [96] and Table 3.2 [106].

Table 3.1: Major specified chemical composition of Zr-2.5Nb pressure tubes [96]

Elements alloyed to zirconium	Specified values	
(by Weight)	Double-melted	Quadruple-melted
Niobium, %	2.4-2.8	2.4-2.8
Oxygen, *wppm*	900-1300	900-1300
Iron, *wppm*	1500 max	650 max
Hydrogen, *wppm*	25 max	5 max
Carbon, wppm	270 max	125 max
Chlorine, *wppm*	...	0.5 max
Phosphorous, *wppm*	...	10 max

Table 3.2: Specified axial tensile properties for the Indian pressure tubes [106]

Properties	Zr-2.5Nb	
	$25\,^{\circ}C$	$300\,^{\circ}C$
Ultimate tensile strength (MPa)	-	$\geq$462
0.2% Yield strength (MPa)	$\leq$586	$\geq$324
Percentage elongation	-	$\geq$14.0

3.2 Hydriding

Zr-2.5Nb material has limited solid solubility for hydrogen that varies with temperature. Hydrogen, more than the solubility limits forms hydride phase, which depending upon its concentration, distribution and orientation may affect the properties of the pressure tube. Pressure tubes, both as-fabricated and irradiated were hydrided to study the effect of hydrogen concentration on the mechanical properties of Indian Zr-2.5Nb pressure tubes.

3.2.1 Gaseous hydriding

Gaseous hydriding method [107] was used to hydride the as-fabricated pressure tube in the present investigation. As-fabricated pressure tube of around 150 mm spool (spool is a tubular portion of certain length cut from the full length pressure tube) length was used for hydrogen charging. The spool piece was first polished up to 1200 grit emery paper to obtain oxide free surface. The piece was cleaned thoroughly with acetone. The polished and cleaned tube spool was gaseously charged in a modified Sievert's apparatus with target hydrogen concentration around 75 *wppm* [108]. After hydrogen charging the spool piece was homogenised at $400\,^{\circ}C$ for 24 hours to get uniform distribution of hydrides through out the PT spool piece.

The hydrogen charging system consisting of two glass chambers to hold the specimen and a hydrogen source, a vacuum pumping system, a capacitance based manometer and resistance heated furnaces to heat the specimen and the hydrogen source (pure zirconium hydride). The system is first evacuated to a dynamic vacuum of the order of 10^{-5} torr using a diffusion pump. After this the hydrogen source is heated using the resistance heating furnace. Once the source temperature $550\,^{\circ}C$ is attained, the system is isolated and heating of source is continued. The amount of hydrogen evolved is proportional to the pressure indicated by the capacitance based manometer. Depending upon the weight of the sample, hydrogen is released up to a predetermined pressure, source heating is discontinued and the source tube is isolated. Subsequently the specimen chamber is heated to a temperature in the range of 350 to $400\,^{\circ}C$. Amount of hydrogen picked up by the specimen, is indicated by the pressure change indicated by the manometer. The amount of hydrogen picked up is computed from the difference between the initial and the final pressure readings recorded at room temperature.

3.2.2 Cathodic hydrogen charging

The hydriding of the irradiated Zr-2.5Nb pressure tube for delayed hydride crack growth study was carried out by cathodic hydrogen charging method [109]. Test spec-

imens were cleaned mechanically by grinding paper using hand grinder to remove the oxide layer before subjecting to hydrogen charging. Cleaning was done in a fixed enclosure to avoid spread of loose contamination. The oxide free surfaces were ultrasonically cleaned to remove loose particles and taken for hydrogen charging after contamination monitoring. The specimens were spot welded with Zircaloy-4 wires for the ease of holding during hydrogen charging. The hydriding set up used in the study is shown in Figure 3.5. Electrolytic hydrogen charging was carried out using 0.2M H_2SO_4 solution in de-mineralised water after preheating the solution to 70 $^{\circ}C$ using sample as cathode and Lead (Pb) as anode. The bath was homogenized by magnetic stirring. Current density was maintained at 0.2 Amp/cm^2 using DC power. Charging was carried out in a ventilated system for 5 hours for a target hydrogen concentration of about 100 $wppm$. The temperature was attained with a heater attached with the system. Lead sulphate layer deposited over the specimen was cleaned immediately after charging hydrogen by wiping with tissue paper. The hydride deposited over the surface was homogenized by heating in furnace in air environment at a temperature of 335°C for 48 hours.

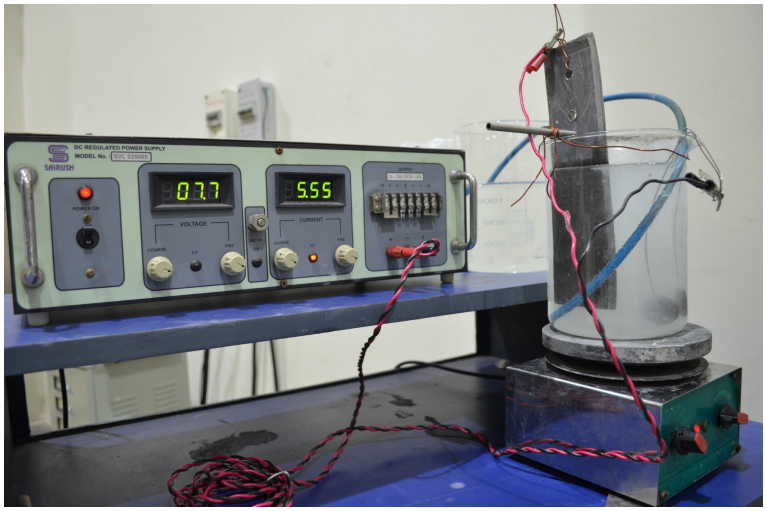

Figure 3.5: Set up used for hydriding the DCT specimens for DHC test, which was located in a shielded facility.

3.3 Hydrogen and hydrogen equivalent (H_{eq}) measurement by Differential Scanning Calorimeter (DSC)

The hydrogen equivalent concentration of the as-fabricated hydrided PT, as-received irradiated pressure tube and also the hydrided irradiated pressure tube were measured by DSC technique. DSC is a very sensitive instrument that is used to measure the changes of the difference in the heat flow to the sample with respect to a standard sample when both of them are subjected to a controlled temperature program [110]. The difference in the heat flux between the sample and the reference is sensed by thermopiles and is plotted against temperature. The solubility of hydrogen in zirconium matrix has strong temperature dependence and follows an Arrhenius relationship. The Arrhenius type of relationship that governs the equilibrium Terminal Solid Solubility (TSS), C_T , at any temperature T, can be expressed as follows [110, 111]:

$$C_T = 1.2 \times 10^5 \exp(-\frac{Q}{RT}) \tag{3.1}$$

where, Q = 35786 J/mol, R = 8.314 J/mol/K and T is temperature in K.

In other words, the terminal solid solubility temperature for hydride in the material can be used as a measure of C_T , the hydrogen concentration. The plot of (1/T) against $\ln C_T$ is a straight line.

The process of hydride dissolution (which is an endothermic reaction) can be monitored by DSC and from the DSC scan the TSS temperature can be estimated. Substituting the TSS temperature T, in the above equation, the hydrogen concentration C_T can be estimated.

In case of irradiated Zr-2.5Nb pressure tube since the hydrogen species picked up is made up of Deuterium ($_2H^2$)and Hydrogen ($_1H^1$), the composition estimated by DSC technique represents Hydrogen equivalent (H_{eq}), which is the composition of hydrogen species expressed in terms of equivalent composition of Hydrogen.

$$ppmw\ of\ H_{eq} = \frac{1}{2}(ppmw\ of\ 2H^2) + ppmw\ of\ {}_1H^1 \tag{3.2}$$

Small pieces, cut from the mechanical tested specimens, were used as samples for determination of H_{eq}. The samples were cleaned with acetone, CCl_4 and dried. Subsequently, they were cut into very small pieces to accommodate into the Al pan of diameter 4 mm and height 3 mm. The aluminium pan was crimped with the sample and was used for the DSC scans. The DSC unit was calibrated for temperature and heat flow using standard In and Zn samples. The test samples, along with the reference, were subjected to a linear heating program, under a constant flow of Argon. The reference material chosen was Al_2O_3, which acts as an inert material over the range of temperature of our interest and gives stable, horizontal thermal base line. The derivative DSC (DDSC) plot was used to identify the point of inflexion on the DSC scan corresponding to the TSS temperature value as shown in Figure 3.6. The hydrogen concentration was estimated using the TSS values obtained from the DSC scan

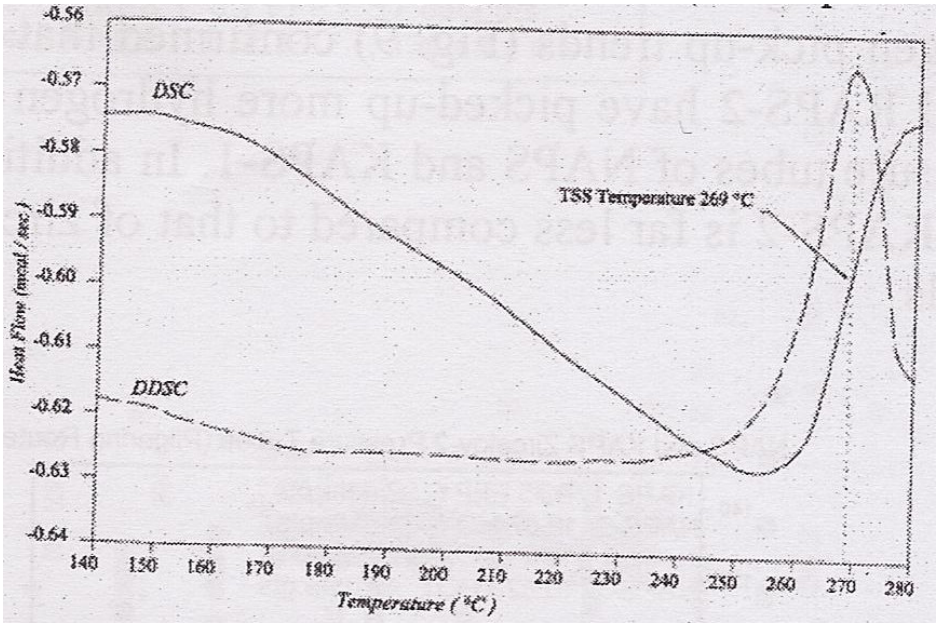

Figure 3.6: Typical DSC plot and the DDSC plot for determining the TSS temperature.

3.4 Irradiation details

Two irradiated pressure tubes studied were received from Indian PHWR Kakrapar Atomic Power Station-2 (KAPS-2) and they were removed from reactor as surveillance pressure tubes after different Hot Operating Years (HOY) and Effective Full Power Years (EFPY). The channel locations were S-7 and Q-10 in the reactor. The pressure tubes, S-07 and Q-10, were in service for ≈8.3 HOY (≈7.9 EFPY) and ≈15.28 HOY (≈12.66 EFPY) respectively. The average inlet and outlet temperature of the pressure tube in the reactor was around 250 $^{\circ}C$ and 300 $^{\circ}C$. The neutron flux varied along the length of the tube and peaked near the midpoint of the tube. The maximum fast neutron fluence experienced by the pressure tubes were $\approx 4 \times 10^{25}\ n/m^2$ and $\approx 6 \times 10^{25}\ n/m^2$ respectively. The neutron fluence and the temperature profile along the length of the S-7 pressure tube is shown in the Figure 3.7 [112].

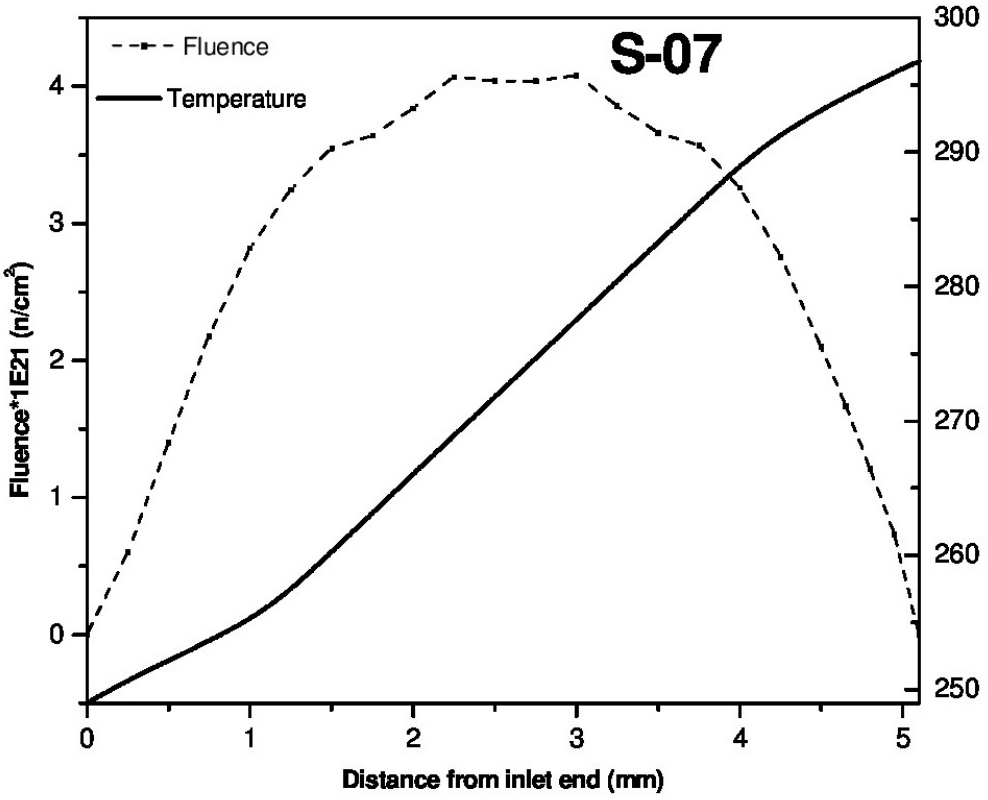

Figure 3.7: Neutron fluence and temperature profile along the length of the irradiated pressure tube S7 [112].

3.5 Tension and fracture toughness test on pressure tube offcuts

3.5.1 Tension test on offcuts

Miniature flat tensile specimen geometry was selected for mechanical property evaluation of the off-cuts from different pressure tubes from double melted and quadruple melted ingots. Schematic diagram of the type of tensile specimens (transverse and longitudinal) prepared from pressure tube off-cuts is shown in Figure 3.8. Flat longitudinal and transverse tensile specimens were prepared from the offcuts. Longitudinal (or axial) and transverse (or circumferential) specimens are prepared from the longitudinal (i.e. axial) and transverse (i.e. circumferential) direction of the pressure tube with the tensile axis being parallel either to the longitudinal or to the transverse directions of the pressure tube, respectively. Tensile specimens had 1.8 mm width, 1.5 mm thickness and 7.6 mm gauge length. Specimens of both orientations were prepared without any flattening treatment. Wire cut EDM was used for tensile specimen preparation. Tension tests were carried out at room temperature and 300 $^{\circ}C$ in a 100 KN capacity screw driven universal testing machine (UTM). The crosshead speed during the testing was 0.25 mm/min. The tests were carried out without any extensometer. Tests were conducted in air atmosphere. The shoulder type grip used for tension testing of miniature flat specimens is shown in Figure 3.9.

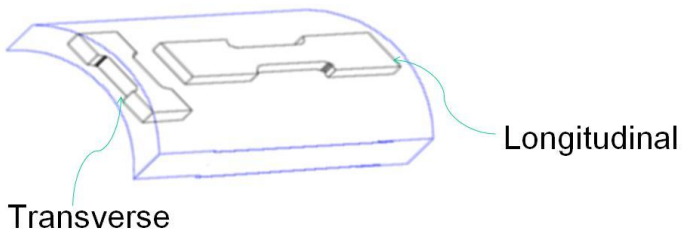

Figure 3.8: Type of tensile specimens (transverse and longitudinal) prepared from pressure tube off-cuts.

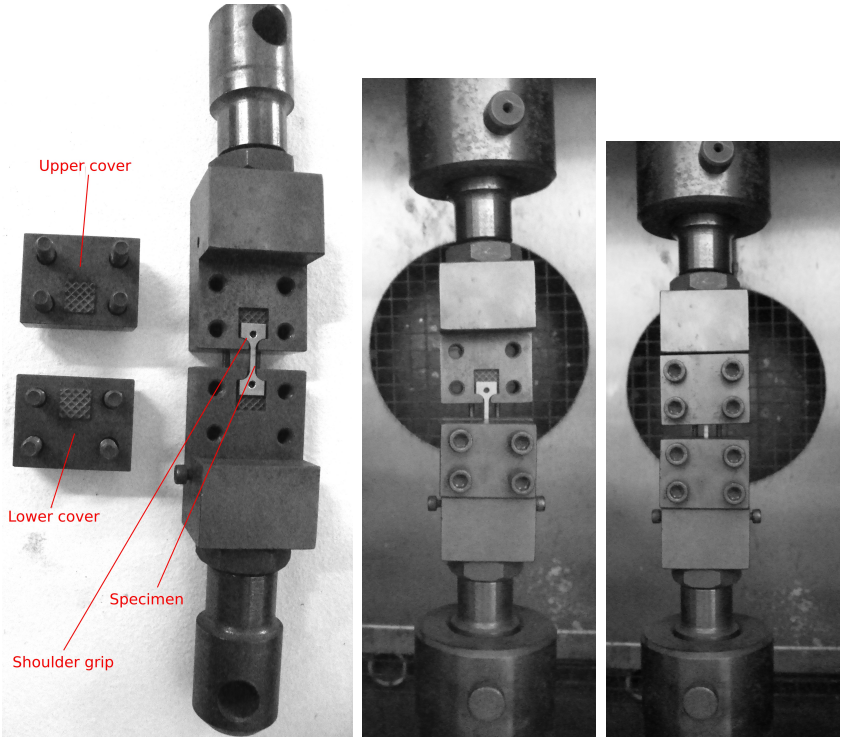

(a) (b) (c)

Figure 3.9: (a) Shoulder type grip with specimen, also shown upper and lower cover to be used during testing (b) Bottom cover attached to the grip and (c) Both top and bottom cover attached to the grip to hold the specimen tight during testing .

3.5.2 Fracture toughness test on offcuts

Fracture toughness tests were carried out using a 15 kN capacity servo hydraulic UTM. Single specimen J-test method was used for this purpose. Fracture toughness tests were carried out using curved compact tension (CCT) specimens, as shown in Figure 3.10, prepared from the offcuts of some of the double melted (of KAPS-2 reactor) and quadruple melted (of RAPS-2 reactor) pressure tubes. The width (W) of the specimen was 17 mm and notch length was 6.8 mm. The CCT specimens were fabricated, using wire cut EDM, with a notch orientation to get fracture on the radial-axial plane and crack growth in the axial or longitudinal direction of the tube. The experimental procedure involves fatigue precracking, loading of specimen, heat tinting, post-test fatigue fracture, initial and final crack length measurement, experimental output data analysis and J-calculation. Finally J versus Δa plot was

obtained for different test temperatures. Single specimen J-test method, using direct current potential drop (DCPD) system for crack length measurement, was followed for the present study. Specimens were precracked using tapered pins to get uniform crack front across the specimen thickness and decreasing load steps were followed during precracking.

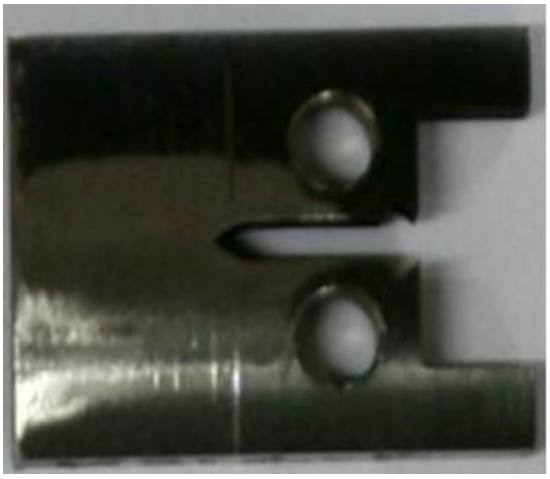

Figure 3.10: Curved compact tension (CCT) specimen, having 17 mm width, prepared from the pressure tube off-cuts.

Fatigue precracking of the CCT test specimens were carried out using a table top servo-hydraulic universal testing machine at room temperature such that, a/W, was $\sim$0.5 (where a is the crack length and W is the width of the specimen). The starting notch length of the specimen was such that initial a/W was 0.4. Thus the total crack growth during fatigue precrack was around 2 mm for each specimen. The mean load and load amplitude was reduced in four stages such that maximum load was 0.9 kN in the first stage and 0.6 kN in the fourth stage of fatigue precracking. The loads used, as per ASTM E 1820-11, were such that maximum loads were less than the limit load (P_f) defined by Equation 3.3 and the ratio of maximum stress intensity factor (SIF) K_I to Young modulus (E) is less than 0.0002 $m^{1/2}$.

$$P_f = \frac{0.4Pb_0^2\sigma_Y}{(2W+a)} \tag{3.3}$$

$$K_I = \frac{P}{BW^{1/2}} f\,(a/W) \tag{3.4}$$

where,

$$f\left(a/W\right) = \frac{[2+\frac{a}{W}][0.886+4.64\frac{a}{W}-13.32\left(\frac{a}{W}\right)^2+14.72\left(\frac{a}{W}\right)^3-5.6\left(\frac{a}{W}\right)^4]}{\left(1-\frac{a}{W}\right)^{\frac{3}{2}}}$$

P is the maximum load used,

B is the thickness of the specimen,

b_o is the initial remaining ligament in the specimen

σ_Y is yield strength of the test material

Table 3.3: Mean load and amplitude used during fatigue pre-cracking of 17 mm CCT specimens.

Precracking stage	Mean load (kN)	Load amplitude (kN)	Target K_{max} ($MPa\sqrt{m}$)
1^{st}	0.495	0.405	15.2
2^{nd}	0.440	0.360	14.7
3^{rd}	0.385	0.315	14.0
4^{th}	0.330	0.270	13.0

After precracking the specimens were pulled at a crosshead speed of 0.25 mm/min. Four Zircaloy-4 wires were welded to the specimens for testing with DCPD system. A constant current of 3 amp was used and the DCPD voltage drop was continuously monitored in the data acquisition system. All the tests were carried out at room temperature. After the fracture toughness tests, the specimens were heat tinted at 350 ^{o}C for an hour and then fractured using fatigue loading. The fractured specimen surfaces were seen under stereo microscope for initial and final crack length measurement using nine point average method. From the total voltage drop and crack growth observed during the J-test, the calibration constant was derived for each of the specimen tested. Thus the intermediate crack lengths for each test were calculated from the DCPD voltage output readings.

For each of the tested specimens, the digital outputs from the machine and DCPD

unit, i.e. load–displacement and DCPD voltage output, were analysed to get the crack lengths and corresponding area under the load–displacement plot. Crack growth initiation was detected from the intersection point of the two tangents drawn at the two slope regions in the voltage drop versus displacement output. Since the total crack extension was very limited (around 2 mm), a linear relationship was assumed between measured voltage drop and measured crack length. These data were then analyzed as per ASTM E 1820-11 to get the J versus Δa plot for each of the specimen tested.

The total J values were split into elastic (J_{el}) and plastic (J_{pl}) part as per Equation 3.5 where J_{el} and J_{pl} are as given in Equations 3.6, and 3.7 respectively.

$$J = J_{el} + J_{pl} \tag{3.5}$$

$$J_{el} = \frac{K^2(1-\upsilon^2)}{E} \tag{3.6}$$

$$J_{pl(i)} = [J_{pl(i-1)} + \frac{\eta_{(i-1)}}{b_{(i-1)}} \frac{\left(A_{pl(i)} - A_{pl(i-1)}\right)}{B}][1 - \gamma_{(i-1)} \frac{\left(a_{(i)} - a_{(i-1)}\right)}{b_{(i-1)}}] \tag{3.7}$$

where,

$$\eta_{(i-1)} = 2 + \frac{0.522 b_{(i-1)}}{W} \tag{3.8}$$

$$\gamma_{(i-1)} = 1 + \frac{0.76 b_{(i-1)}}{W} \tag{3.9}$$

$[A_{pl(i)} - A_{pl(i-1)}]$ is the increment of plastic area under the load vs. plastic load line displacement record between lines of constant displacement at points $(i-1)$ and i as described in equation below and shown in Figure 3.11 (where 'i' is any point corresponding to which load and displacement data are used for calculations involved in fracture toughness test analysis):

$$A_{pl(i)} - A_{pl(i-1)} = \frac{\left(P_{(i-1)} + P_{(i)}\right)\left(v_{(i)} - v_{(i-1)}\right)}{2} \tag{3.10}$$

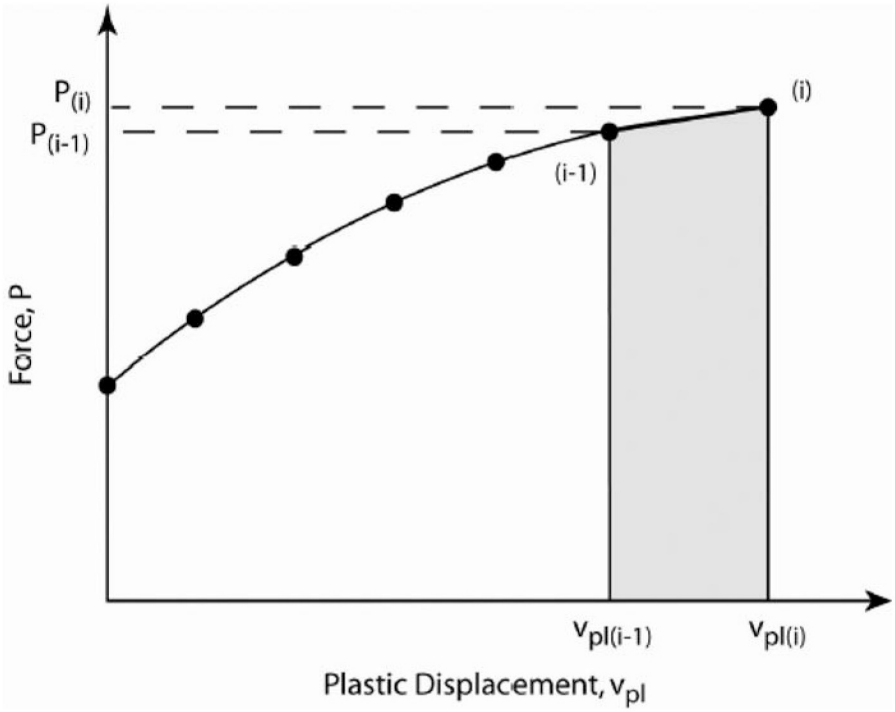

Figure 3.11: Schematic plot showing points $'i'$, $'i-1'$ and corresponding load, plastic displacements and plastic area obtained during fracture toughness test analysis [115].

The values of Young's modulus $E = 95900 - 57.4(T - 273)\ MPa$ [82, 113, 114], and $\nu = 0.436 - 4.8 \times 10^{-4}\,(T - 300)$ [82, 113, 114] were used in the above equation, where T is the test temperature in $^{\circ}C$. The blunting line computed using $J_{blunt} = 2\sigma_{flow}\,(\triangle a)$, where $\sigma_{flow} = (\sigma_{YS} + \sigma_{UTS})/2$, was superimposed over J vs. $\triangle a$ plot. The blunting line is a construction line that is drawn in accordance with $J_{blunt} = 2\sigma_{flow}\,(\triangle a)$ and this accounts for deflection that occurs due to plastic deformation near the crack tip prior to the onset of stable crack growth i.e blunting line characterises the apparent crack advance that occurs due to a geometric blunting before sharp tearing crack begins. Two exclusion lines parallel to the blunting line were drawn at an offset of 0.15 and 1.5 mm crack length extension. The J-Δa data that fall between the the construction lines parallel to blunting line but at 0.15 mm offset and 1.5 mm offset are the qualified data. Another offset line parallel to the blunting line was drawn at an offset of 0.2 mm and the intersection point of the 0.2 mm offset line with the power law curve passing through the qualified data was taken as the J_Q value as shown in Figure 3.12 [115]. The qualified data were fitted to a power law $\left(J = C_1\,(\triangle a)^{C_2}\right)$ and straight line as shown

in Figure 3.13 [115]. The slope of the best fit straight line, over crack extension of 0.5 to 1.5 mm, yielded the mean dJ/da value. The J_{max} value is obtained corresponding to the maximum load taken by the specimen during the fracture toughness testing.

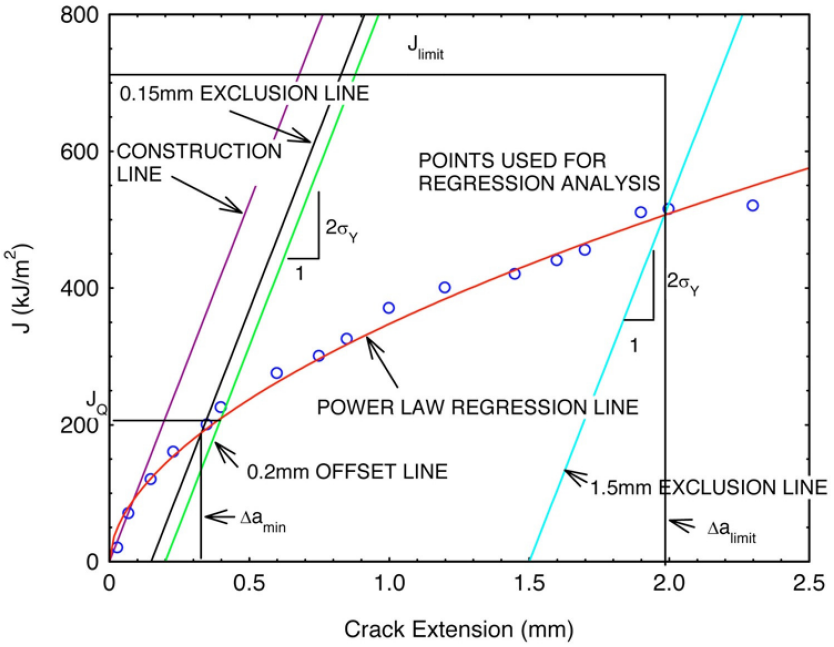

Figure 3.12: Construction line for data qualification of $J-R$ curve evaluation for fracture toughness tests [115].

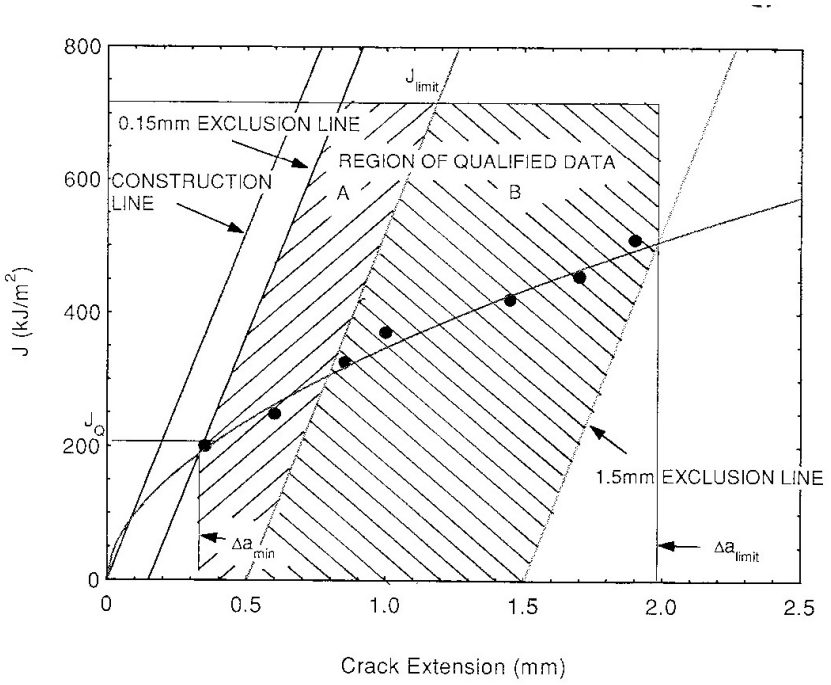

Figure 3.13: Region of qualified data in the J vs crack extension plot for $J-R$ tests [115].

3.6 Texture measurement and dislocation density determination of pressure tube offcuts

3.6.1 Texture measurement

Kearns texture parameter representing the distribution of basal poles of the α-phase of the Zr-2.5Nb pressure tube material in the three principal directions namely, transverse (f_t), radial (f_r) and axial (f_a) can be estimated from the intensity data of X-Ray Diffractometer scan using the methodology given by J. J. Kearns [116]. The idealized orientation of basal pole in these directions are shown schematically in Fig 3.14. The Kearns parameters for the basal poles represent the effective volume fraction of the basal poles in transverse, radial and axial directions. The effective volume fraction of orientation parameter (f) of a particular plane in a particular tube direction is given by the following equation: [116]

$$f = \frac{{}_0\int^{\frac{\Pi}{2}} I_\phi sin\phi cos^2\phi}{{}_0\int^{\frac{\Pi}{2}} I_\phi sin\phi d\phi} \tag{3.11}$$

where I_ϕ is the average x-ray intensity (in units of times random) at angle of tilt ϕ of the plane from a reference direction.

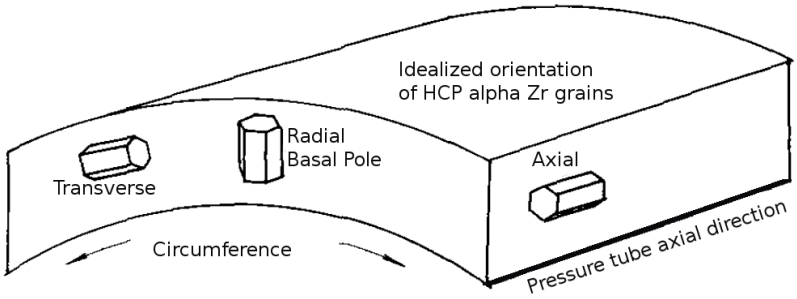

Figure 3.14: Idealized orientation of basal poles of α-Zr grains along the three principal directions of the pressure tubes.

Texture samples were prepared from the three directions, of the pressure tube offcuts, e.g. transverse, radial and axial in such a way that the sample surface was normal to the selected direction as shown in Figure 3.15(a). X-Ray diffractograms from

these sample surfaces were used to determine the Kearns texture parameter for basal pole in these three tube directions [117]. In case of texture parameter determination for transverse and axial directions, the texture samples were prepared by keeping a number of small specimens close by to provide a surface area of around 15 mm x 10 mm for exposure to X-Ray beam, as the wall thickness of the tube was small (3.5 mm). Each specimen piece in the sample is obtained by removing inner and outer layers by EDM as shown in Figure 3.15(b). Sample surface for determination of radial Kearns parameter is normal to the tube radial direction and is curved. It is made flat by removing outer and inner surface perpendicular to the radial direction and obtaining a rectangular sample as shown in Figure 3.15(b).

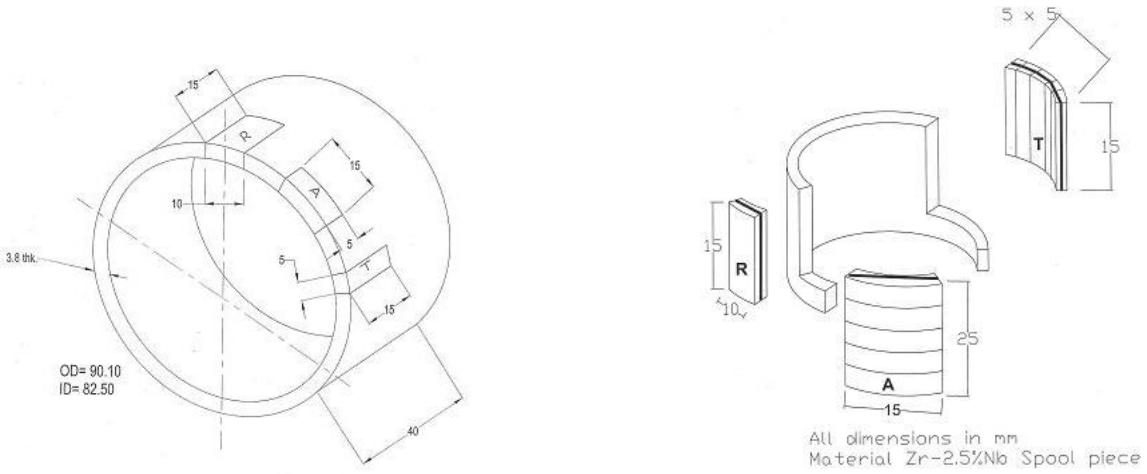

(a) (b)

Figure 3.15: Schematic diagram showing (a) sample cutting plan from offcut for radial, axial and transverse texture determination and (b) method for obtaining rectangular flat samples by removal of outer and inner surface layers using EDM as shown by thick line.

All samples were chemically polished in 45% HNO_3, 5% HF and 50% H_2O to dissolve around 0.05 mm thickness of the sample. Samples were stacked together closely and mounted in Araldite glue. Light mechanical grinding, polishing and finally chemical polishing was carried out to ensure that the sample in the composite sample is in the same level.

The XRD scans were recorded on the samples in the 2θ angle range of $30° - 140°$, on a Diffractometer using CuK_α radiation in scan steps of 0.05^0 2θ / step and X-ray

counts for 1 second. An XRD scan of zirconium powder sample was also recorded in identical condition to represent a random sample. Diffraction patterns were background corrected using software based on Sonnerveld Visser background correction method and integrated intensity for 18 reflections were obtained. Ratios of the integrated intensities (I/I_0) of reflections of the sample with the same reflection of the powder sample were obtained.

Preferred orientation parameters in the three principal directions of the pressure tubes were calculated by evaluating Equation 3.11 following a summation procedure of 18 reflections integrated intensities using the tilt angles of these reflections in standard projection of diffracting planes of alpha zirconium, $c/a = 1.59$.

3.6.2 Dislocation density determination

X-Ray diffractograms from radial (R-sample) sample surface were used to determine the dislocation density for the pressure tubes [117]. The correction for instrumental broadening (B_{inst}) is most important step in the estimation of material properties from line profile analysis. Integral breadth (B_{inst}) due to instrumental broadening is defined as ratio of the area under the peak (A) and the maximum intensity (I_0) when the sample is free from the microstructural broadening effects. The instrumental broadening (b) is a function of Bragg's diffraction angle, θ and is given as $(B_{inst})^2 = U\tan\theta + Vtan\theta + W$. Small diffraction angles (2θ less than 30°) were excluded from the calculation. Once the instrumental broadening is determined it has to be fitted in the above equation to get degree of fit. Various samples were used for calculation of instrumental broadening as suggested in literature, for example, annealed powder zirconium, crystal bar zirconium, CW and fully annealed Zircaloy sheet. In this case, best fit was obtained using a fully annealed Zircaloy material. Using high intensity peaks a curve with Y-axis as $(integral\,breadth)^2$ and X-axis as $tan\theta$ was obtained (Figure 3.16). The fit was done using second order polynomial for $tan\theta$ (X-axis) and yielded the following equation for instrumental broadening:

$$(B_{inst}\,in\,radian)^2 = 8.23402 \times 10^{-6}\,tan^2\theta + 1.43322 \times 10^{-5}\,tan\theta + 1.4657 \times 10^{-6}$$

The above equation was used for calculating instrumental broadening (B_{inst}) at any given θ. The observed integral breadth in the sample (for measurement of D,ρ and ε) is corrected for instrumental broadening to give corrected integral breadth.

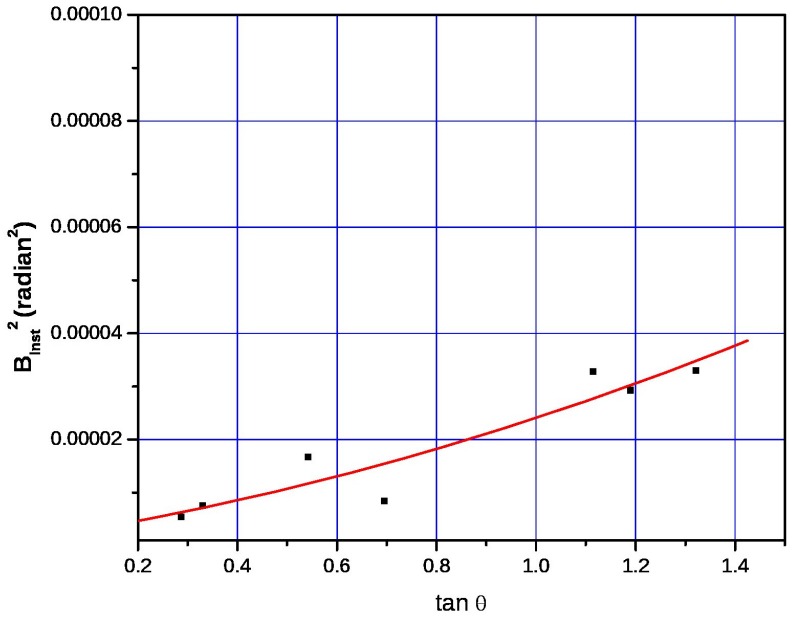

Figure 3.16: Fitting of curve for high intensity peaks of fully annealed Zircaloy sample [117].

At least 4-5 peaks of high intensity between $2\theta = 30$ to 100° were taken and plots of $(\beta cos\theta/\lambda)^2$ vs $(sin\theta/\lambda)^2$. A typical graph obtained is shown in the Figure 3.17.

From the plots, coherent domain size (D) in $\mathring{A}$ and micro-strain (ε) were calculated using the following equations:

$intercept = 1/D^2$,

$slope = 16\,\varepsilon^2$

After calculation of D and ε,

Dislocation density corresponding to domain $\rho_D = 3 \times \eta/(D^2)$ where $\eta = 1$;

Dislocation density corresponding to strain $\rho_\varepsilon = 2.K.\varepsilon^2/b^2$, where b =Burgers vector of the majority of existing dislocations. The Burgers vector is taken as, $b = \frac{1}{3}[11\bar{2}0]$, $K = 10$;

Total dislocation density is $\rho = (\rho_D \times \rho_\varepsilon)^{0.5}$.

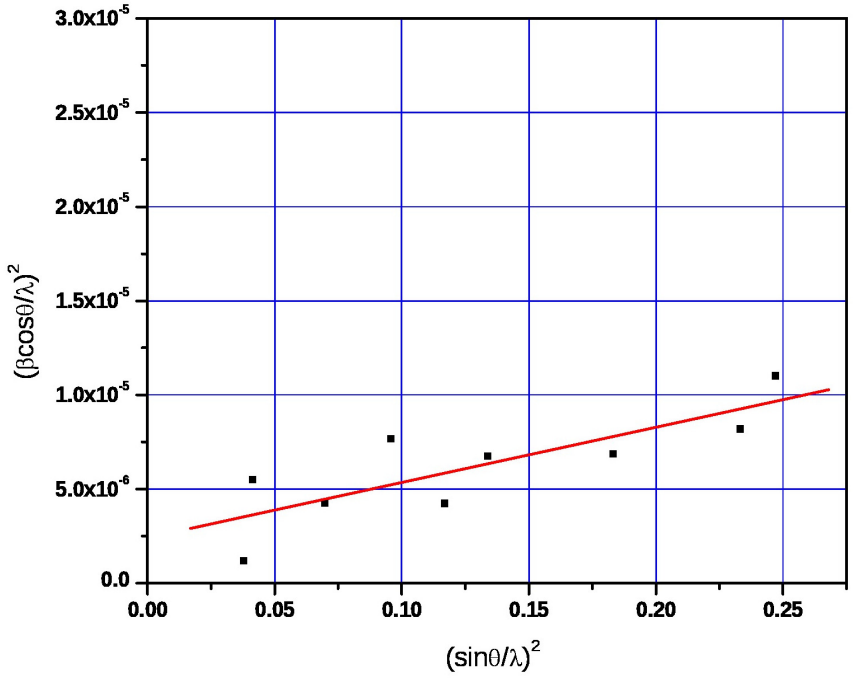

Figure 3.17: $(\beta cos\theta/\lambda)^2$ **vs** $(sin\theta/\lambda)^2$ **plot for a typical radial sample of the off-cut [117].**

3.7 Impact test of as-received and hydrided pressure tube

The impact tests were carried out on as-received and hydrided Zr-2.5Nb pressure tube material. Impact samples of dimension $55 \times 10 \times t$ mm were machined from the pressure tube spools where t is the thickness of the pressure tube, which is 3.5 mm in IPHWRs. The orientations of the notch was such that it facilitated crack growth either along axial or along circumferential directions of the pressure tube. These samples will be referred as axial and transverse samples respectively throughout this manuscript. Dimensions of the Charpy specimens used in the present study and their orientations with respect to the pressure tube are schematically shown in Figure 3.18 (a) and (b). The specimens had a machined V-notch of dimension shown in Fig. 3.18(a) [118]. Drop tower impact testing machine, CEAST make with instrumented ISO Charpy tup, with an environment chamber for thermal conditioning of the specimens, was used for testing. The machine had automated weight lifting and drop arrangements

with high rate data acquisition system and personal computer. A specially designed anvil, for axially notched specimens of as-fabricated type (i.e curvature being same as that of as-fabricated pressure tube), was fitted in place of standard Charpy anvil, and located in the environment chamber. The specially designed anvil for holding the as-fabricated axial notched impact specimen and the exploded view of the specimen are schematically shown in Figure 3.18 (c). It was ensured that the specimen sits freely in the slot of the anvil at all temperatures of testing. Velocity of pendulum was 3.5 m/s (corresponding to a drop height of 0.625 m).

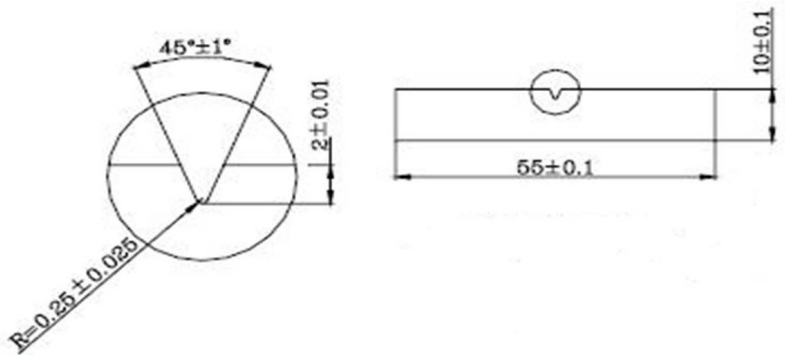

(a)

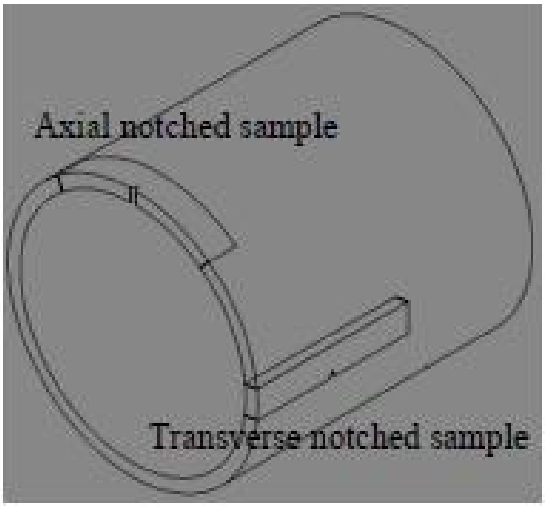

(b)

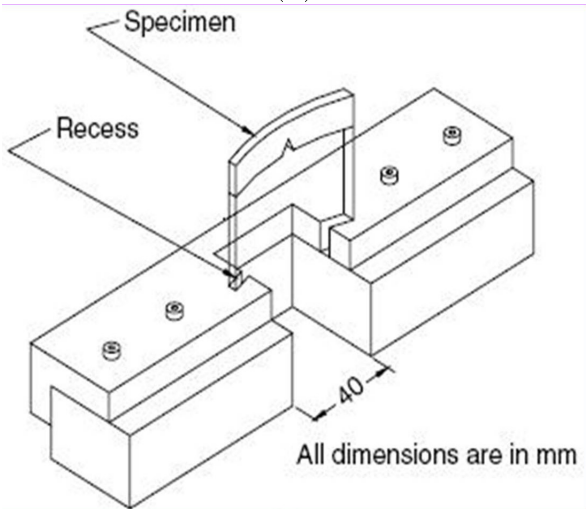

(c)

Figure 3.18: Schematic diagram of (a) dimension of Charpy sample (b) sample orientation in the pressure tube and (c) fixture for holding the axial notched sample during test in drop tower impact testing machine.

3.8 Fracture toughness and DHC test of irradiated pressure tube

Fracture toughness measurements were carried out on two irradiated Zr-2.5Nb pressure tubes (S-7 and Q-10) and delayed hydride crack growth study was carried out on the irradiated pressure tube S-7.

The specified chemical composition of the double melted Zr-2.5Nb pressure tube is given in Table 3.1 [96, 106]. Chemical analysis of S-7 and Q-10 pressure tube offcuts were done using glow discharge optical emission spectroscopy and is given in Table 3.4.

Table 3.4: Chemical composition of as-fabricated S-7 and Q-10 pressure tubes.

Pressure tube	Niobium (wt%)	Oxygen (*wppm*)	Chlorine (*wppm*)	Phosphorus (*wppm*)	Hydrogen (*wppm*)	Carbon (*wppm*)
S-7	2.71	1019	1.37	12.83	11.9	244
Q-10	2.79	882	1.21	7.97	7.45	25.1

Texture of the as-fabricated pressure tube used for DHC study and S-7 pressure tube before irradiation are given in Table 3.5. Fractions of basal pole in the transverse, radial and axial direction are represented as f_t , f_r and f_a respectively.

Table 3.5: Texture of the as-fabricated pressure tubes used for DHC test.

Pressure tube	f_t	f_r	f_a
As-fabricated PT	0.57	0.35	0.08
S-7 (before irradiation)	0.51	0.37	0.12

The resistance offered by the pressure tube to the initiation and propagation of cracks will depend primarily on the fracture toughness. This is generally evaluated by developing $J-R$ curves from pressure tests (slit burst test) carried out on the tubes with through wall cracks [119–121]. The slit burst test simulates the actual component

geometry and condition. However, slit burst tests require handling of larger amount of irradiated material, around 500 mm of pressure tube spool and may lead to larger manrem exposure. Curved Compact Tension (CCT) test specimens have also been used for the evaluation and mapping of fracture toughness of such tubes [4, 68]. Apart from the CCT geometry, Disk Compact Tension (DCT) specimens can also be used for the evaluation of fracture toughness. The advantage of using the disk geometry is that it can be punched out or trepanned from the irradiated pressure tube and specimens can be prepared in absence of other machining methods such as electric discharge spark machining. In a relatively brittle irradiated pressure tube, punching a rectangular coupon for CCT specimen at room temperature, may lead to some cracking of the tube and the specimens due to the sharp edges. Such sharp edges are avoided in the disk configuration that was chosen to be punched out or trepanned out from the irradiated pressure tube. In this research work, DCT specimens were used for the fracture toughness study of irradiated material. Hence, an attempt was made to study the effect of specimen size and test method on the fracture toughness of unirradiated Zr-2.5Nb pressure tube using more widely used CCT specimen with DCT specimens.

Fracture toughness, as per ASTM E 1820-11[115], was measured using single specimen test method. Analysis of the experimental data gives J versus crack extension ($\triangle a$) plot and different fracture toughness parameters like initiation fracture toughness (J_i), maximum load fracture toughness (J_{max}) and crack growth resistance (dJ/da) were evaluated from this. The J-values are measured as a function of area under the load vs. corrected load line displacement, specimen dimension and a geometry factor defined in standard for various specimen geometries. As per the standard there are three methods that can be used for measuring the crack extension such as unloading compliance, direct current potential drop (DCPD) and load normalization techniques. Unloading compliance needs special grooves on the specimen for attaching the crack opening displacement (COD) gauge to the specimen. This type of grooved specimen was not possible to fabricate at our laboratory for the irradiated pressure tubes. DCPD system, which needs welding of wires to the specimen for voltage drop measurement,

was used for crack length measurement in irradiated pressure tube S-7. Welding of wires to the specimens of irradiated pressure tube Q-10 was giving sparking problem most likely due to wear near electrode area. This sparking was leading to problem of spread of radioactive contamination. So, load normalisation technique was used in case of analysis of irradiated pressure tube Q-10 data.

3.8.1 Specimen preparation

The irradiated pressure tubes received were around of 5 meter length. Circular disk coupons of 30 mm diameter were punched out or trepanned at distances of around 1 meter from both the inlet end and outlet end of the irradiated pressure tubes. The coupons were transferred to a custom made drilling and notching set-up, inside the lead cells, to drill out two pin holes and a central slit with a sharp V-notch tip to get Disk Compact Tension (DCT) specimens. The specimen dimension, except for the thickness and small curvature, were as per ASTM E 1820-11 [115]. The width (W) of the specimen was 22.22 mm and notch length was 8.7 mm. The thickness of the specimen was same as the thickness of the pressure tube. The design dimension of the specimen is shown in Figure 3.19. The DCT specimens were fabricated with a notch orientation to get fracture on the radial-axial plane and crack growth in the axial direction of the tube. For DHC test on irradiated S-7 pressure tube, the DCT specimens prepared from the irradiated pressure tube had to be hydrided additionally because the as-received irradiated pressure tubes had $H_{eq} \sim 20$ $wppm$. The DHC test specimens were hydrided by cathodic hydrogen charging method and homogenised for uniform hydride distribution before DHC test.

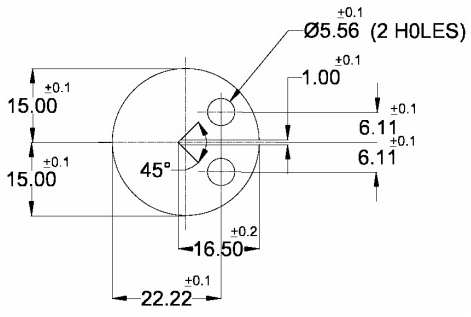

Figure 3.19: Dimension of the disk compact tension (DCT) test specimen.

3.8.2 Zircaloy wire welding

For testing with the DCPD system, four Zr-4 wires, each of 1.0 mm diameter and around half meter length, were spot welded in a custom made automated machine, at the slit mouth and at the top and bottom side of each of the DCT specimen to function as potential drop and current input leads. The wires were covered with asbestos sleeves to electrically insulate them during the test. These wires were then connected to DCPD system for online crack length monitoring during precracking, fracture toughness and DHC test of irradiated pressure tube S-7.

3.8.3 Fatigue precracking

Both fracture toughness and DHC testing both require the specimens to be precracked before actual loading of the specimens for the corresponding tests. A sharp crack tip was obtained by fatigue precracking the DCT specimens using a servo-hydraulic universal testing machine located inside a lead-cell. Fatigue precracking was carried out at room temperature, up to a crack length (a) such that a/W ratio was in the range of 0.48 to 0.60. The starting notch length of the specimen was such that the normalized crack length, a/W, was 0.4. Thus the length of fatigue precrack was around 2 to 4 mm from notch tip. The mean load and load amplitude during fatigue precracking was reduced in four stages such that maximum load was 1.8 kN in the first stage and 0.8 kN in the fourth stage and is given in Table 3.6. This procedure was such that the precracking load used was around 42%-50% of the maximum load

allowed, as per ASTM E1820. The DCPD output voltage reading was used to get an estimate of crack growth during each stage of precracking when DCPD system was used during the fracture toughness test. Change in voltage of around 70 mV corresponded to a change in crack length of around 1.0 mm for the input current of 3.0 A and the preamplifier gain set at 1000. In tests without the DCPD system, the maximum encoder position reading for actuator was used to monitor crack growth during each stage of precracking. Change in maximum encoder position of around $30\mu m$ corresponded to a change in crack length of around 1.0 mm. The load values were reduced at each stage of precracking after around 1 mm of crack growth.

Table 3.6: Mean load and amplitude used during fatigue pre-cracking of DCT specimens.

Precracking stage	Mean load (kN)	Load amplitude (kN)	Target K_{max} ($MPa\sqrt{m}$)
1^{st}	1.01	0.73	28
2^{nd}	0.80	0.64	26
3^{rd}	0.70	0.50	25
4^{th}	0.44	0.36	20

3.8.4 Loading for fracture toughness test

After precracking the DCT specimens were loaded in the servo-hydraulic Universal Testing Machine (UTM). The experimental set-up consisted of the UTM located inside a lead-cell. The fracture toughness testing procedure recommended in ASTM E-1820-11 [115] was followed in the present experiment. The crack lengths were determined using DCPD technique for the irradiated S-7 pressure tube while load normalisation method was used for irradiated pressure tube Q-10 and its roll joint, which facilitated the use of single specimen technique for fracture toughness parameter determination. The machine, with movable lower crosshead, had computerized test control and data acquisition systems. The DCPD unit was of the pulsed DC current type. Tests were stopped and specimens were unloaded when the crack was estimated to have grown

around 2 to 3 mm, or when the load had dropped by about 25% from the maximum load applied on the specimen. Throughout the test, the values of load, crosshead displacement, and potential drop were continuously recorded. Fracture toughness tests were carried out at different temperatures ranging from 25 $^{\circ}C$ to 300 $^{\circ}C$. A resistance heated furnace was attached to the testing machine for carrying out the test at high temperatures with a temperature control within $\pm 4\,^{\circ}C$.

3.8.5 Loading for DHC test

For the DHC test, the specimens were precracked and then put into a dead-weight/loading test set-up. The specimens were first heated up to 350 $^{\circ}C$ (at 5 $^{\circ}C$/min) and soaked at that temperature for 1 hour and then cooled to the test temperatures (210, 250, 265 and 290 $^{\circ}C$ at 1 $^{\circ}C$/min). The specimens were then kept under constant load (such that stress intensity factor was around 15 $MPa\sqrt{}$m and 20 $MPa\sqrt{}$m respectively at the beginning and end of DHC test) and temperature was held constant for the test duration. Direct current potential drop (DCPD) system was used to get indication of crack initiation and monitor the extent of crack growth.

3.8.6 Crack length measurement

The DHC tested specimens and the fracture toughness tested specimens, after heat tinting (the process of heating the specimen at some temperature for certain time, which gives different colours to fracture surface depending on its surface appearance is known as heat tinting) at 350 $^{\circ}C$ for an hour, were fractured using fatigue loading. The fractured specimen surfaces were photographed and these photographs were used for initial and final crack length measurement using nine point average method.

From the total voltage drop and crack growth observed during the J-test, the calibration constant was derived for each of the specimen tested for fracture toughness tests with DCPD system. The intermediate crack lengths were then calculated from the DCPD voltage output readings using linear interpolation. The linear relationship between crack length and voltage drop was checked using two 30 mm diameter Disk

CT specimens of Zr-2.5Nb. In these two specimens voltage drop was measured at different crack lengths and then crack length versus voltage drop were plotted. This showed linear correlation between DCPD voltage drop and crack length ($R^2 > 0.987$) as shown in Figure 3.20.

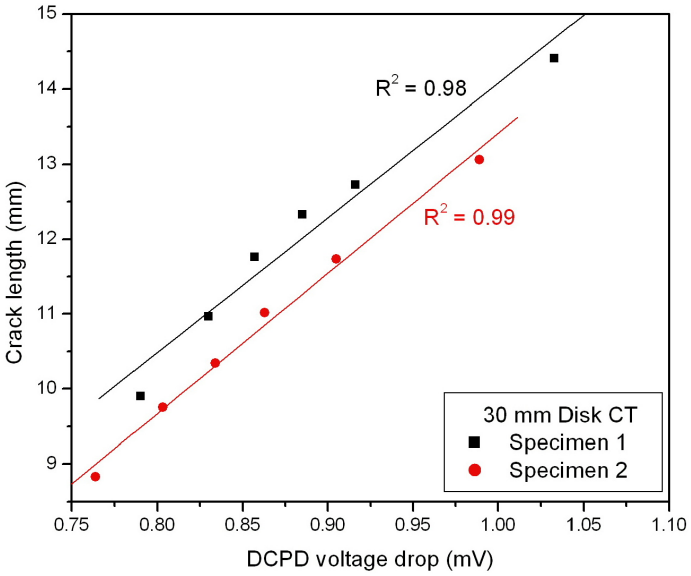

Figure 3.20: Crack length versus voltage drop obtained for two DCT specimens.

For tests that did not use DCPD, the intermittent crack lengths were measured by load normalisation technique [83, 115].According to load normalisation principle, the load (P) may be written as a function of crack length(a) and plastic deformation or displacement (v_{pl}), by two separate multiplicative functions as shown in Equation 3.12

$$P = G\left(\frac{a}{W}\right) H\left(\frac{v_{pl}}{W}\right) \tag{3.12}$$

where W is the specimen width. The plastic load line displacement can be expressed as

$$v_{pl} = v - v_{el} = v - PC\left(\frac{a}{W}\right) \tag{3.13}$$

where $C\left(\frac{a}{W}\right)$ is the elastic compliance, and is a function of actual crack length.

A normalized load (P_N) can then be defined as a function of only plastic displacement:

$$P_N = \frac{P}{G\left(\frac{a}{W}\right)} = H\left(\frac{v_{pl}}{W}\right) \tag{3.14}$$

The geometry calibration function $G\left(\frac{a}{W}\right)$is dependent on the specimen geometry and can be determined from the J calibration [122, 123]

$$G\left(\frac{a}{W}\right) = BW\left(\frac{b}{W}\right)^{\eta_{pl}} \tag{3.15}$$

where uncracked ligament length $b = W - a$ and η_{pl} is the geometry correction factor, which depends only weakly on material properties. It has been shown that η_{pl} is independent of crack growth and has the value of 2.130 for compact tension specimens[122, 123] and the same value has been used for calculation using DCT specimen as no other value for this type of specimen is available as of now. Several kinds of material deformation functions $H\left(\frac{v_{pl}}{W}\right)$ have been proposed, but Landes et al. have demonstrated that LMN function gives good fit over the large range of plastic displacement values [124]. The LMN function is given by

$$P_N = \frac{\left[L + M\left(\frac{v_{pl}}{W}\right)\right]}{N + \left(\frac{v_{pl}}{W}\right)}\left(\frac{v_{pl}}{W}\right) \tag{3.16}$$

The technique involves first finding the P_N verses $\frac{v_{pl}}{W}$, based on initial crack length from the load-load line displacement data. Thereafter for few initial points, points B, P_N values, are recalculated after allowing crack growth due to blunting. At the final point, point A, the final crack length is known, as it can be physically measured after the J test, so there actual P_N is known. As for LMN function to be defined at least, three points are required. The third set of intermediate points, point C, is chosen at an intermediate value of $\frac{v_{pl}}{W}$, e.g. $\frac{1}{3}\,of\,\left(\frac{v_{pl}}{W}\right)$. The P_N at these intermediate points are not known to any close approximation as is the case with points taken for blunting. Therefore, a range of P_N is taken at these intermediate C points. The parameters L, M, and N are calculated for final point, set of blunting points, and one of these intermediate points. This is repeated for all the intermediate calibration points. The fitted LMN curve is compared for their deviation from these calibration points. The

value of L, M, and N, giving the best fit, defines the function $H\left(\frac{v_{pl}}{W}\right)$. Once $H\left(\frac{v_{pl}}{W}\right)$ is known, $G\left(\frac{a}{W}\right)$ can be calculated for each point of load-load line displacement data curve, which will give the value of crack extension at each point.

3.8.7 Estimation of fracture toughness

All the measured and calculated data were used for J-integral calculation at different crack extensions. Finally J versus $\triangle a$ plots were obtained for different test temperatures.

3.8.8 Evaluation of DHC velocity

Incubation time (T_i) for the crack to start growing by DHC was evaluated from the start of change or increase of slope in DCPD voltage drop once the specimen was loaded at the test temperature. The time (T_{DHC}) taken for crack to grow by DHC is then obtained by subtracting the incubation period (T_i) from the total time (T_{Load}) the specimen was loaded. DHC velocity ($DHCV$) was measured from the extent of crack growth ($\triangle a_{DHC}$) by DHC to the time taken for crack to grow by DHC.

$$T_{DHC} = T_{Load} - T_i \tag{3.17}$$

$$DHCV = \frac{\triangle a_{DHC}}{T_{DHC}} \tag{3.18}$$

3.9 Metallography, SEM and Hydrogen equivalent estimation

Small pieces were cut, from some of the as-fabricated and hydrided specimens as well as from irradiated, irradiated and hydrided tested specimens, for metallography and determination of H_{eq} using the Differential Scanning Calorimetric technique as has been explained in Section 3.3.

Specimens from the undeformed end of the tested samples were sectioned along axial–radial (longitudinal direction of the tube) and radial–circumferential (transverse direction of the tube) planes of the pressure tube. Standard metallographic techniques were used to prepare the samples. The samples were mounted in the stainless steel rings using cold setting resin. Metallographic samples were prepared by sequential grinding and polishing of samples and for irradiated samples this action has been carried out inside the hot cells. The morphology and distribution of hydride platelets were revealed after swabbing sample surfaces for few seconds with an etchant of 10%HF, 45%HNO_3 and 45% lactic acid.

The fracture surfaces of the tested samples were examined using Scanning Electron Microscope (SEM) to study the fracture morphology.

Chapter 4

Variability in mechanical properties of Zr-2.5Nb pressure tubes

4.1 Objective

Indian Zr-2.5Nb pressure tube fabrication route has changed from double melted (DM) ingot to quadruple melted (QM) ingot route. Few reactors in India are still operating with double melted ingot route pressure tubes and Kakrapar Atomic Power Station-2 (KAPS-2) is the lead reactor with this type of pressure tube. Rajasthan Atomic Power Station-2 (RAPS-2) is the lead reactor that is running with quadruple melted Zr-2.5Nb pressure tubes. The objective of the present work was to study the variability in mechanical properties, like tensile and fracture toughness, in Indian Zr-2.5Nb PHWR pressure tubes of both double melted and quadruple melted types using the offcuts from KAPS-2 and RAPS-2 pressure tubes that are in service. The study would give an idea of expected variability in properties after irradiation also, as limited data are available in irradiated condition. The experimental results can also be used for probabilistic safety assessment of the coolant channels. As the mechanical properties for anisotropic material like Zr-2.5Nb varies with orientation, tensile properties have been studied along both axial and transverse direction of the pressure tubes. Again the mechanical properties may vary along the length of the 5.2 meter long pressure

tube so tensile and fracture toughness variability have been studied for front end and back end of the pressure tubes, which cover the extreme ends of the tubes. As the amount of material available in the offcut, which is ring of around 35 mm width, is limited so detailed study could be carried out only on tensile properties of the pressure tubes. Fracture toughness properties and texture variability have been studied for a limited number of pressure tubes.

4.2 Experimental

4.2.1 Material

Before installing the pressure tubes into the reactor, rings of material (off-cuts) are removed from the front and back end of each pressure tube, this distinction referring to the end emerging first and last, respectively, from the extrusion press [49]. The front-end and back-end off-cuts used in the present study were from the double and quadruple melted Zr-2.5Nb pressure tubes. Test specimens were prepared from 32 offcuts (from both front end and back end of each of 16 pressure tubes) from pressure tubes of quadruple melted origin and 15 offcuts from pressure tubes of double-melted origin. The location of front-end off-cut and back-end off-cut in a pressure tube is shown in Figure 4.1. The specified chemical composition and tensile properties for the Indian PHWR pressure tubes are given in Table 3.1 . KAPS-2 is the first Indian PHWR that started using Zr-2.5Nb pressure tubes instead of Zircaloy-2 pressure tubes. RAPS-2 is the first reactor in which all the Zircaloy-2 pressure tubes were replaced with quadruple-melted Zr-2.5Nb pressure tubes during en-masse coolant channel replacement (EMCCR).

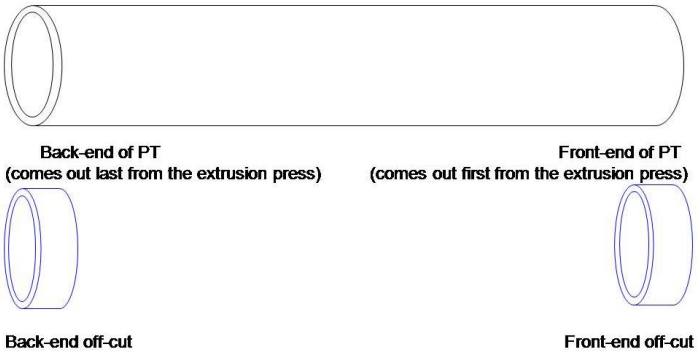

Figure 4.1: Front-end off-cut and back-end off-cut in a pressure tube.

4.2.2 Tension test

As the maximum length of the off-cuts available was 35 mm, miniature flat tensile specimen geometry was selected for tensile property evaluation of the off-cuts from different pressure tubes. Flat longitudinal and transverse tensile specimens, as shown in Figure 3.8, were prepared from pressure tubes. The details of specimen orientation, dimensions and test temperature are explained in Section 3.5. The shoulder girder type tensile test jig was used to put the specimen on the grip easily.

The load and crosshead displacement data obtained from the tests were, recorded in personal computer, and analysed to get engineering stress strain plots and tensile properties of the pressure tube offcuts.

4.2.3 Fracture toughness test

Fracture toughness tests on the pressure tube offcuts (of both double melted and quadruple melted type) were carried out using the 17 mm width curved compact tension specimens. All dimensions of the specimen, except curvature and thickness, were as per the standard ASTM E 1820 [115]. The curvature and thickness of the specimen were same as that of as-fabricated pressure tubes. Due to limited amount of material, fracture toughness tests were carried out on limited number of offcuts and only at room temperatures. Toughness was evaluated using single specimen test method where direct current potential drop (DCPD) system was used to monitor the

extent of crack growth in the test specimens. The experimental details are given in Section 3.5.

4.2.4 Texture measurement and dislocation density determination

Texture samples were prepared from some of the pressure tube offcuts on which tension tests were carried out. The details of specimen preparation and method of texture measurement and dislocation density determination are given in Section 3.6.

4.3 Results and Discussion

The off-cuts used in the present study were from double-melted and quadruple melted Zr-2.5Nb pressure tubes. The fabrication process resulted in two phase microstructure of strongly textured α-grain and a grain boundary network of β-phase. The α-grains have a hexagonal close packed (hcp) crystal structure. Evolution of texture mainly takes place during the second hot extrusion process and subsequent pilgering elongates the α-grains and thus affect the grain aspect ratio. Tube to tube variation in the chemical composition and hot working process parameters, within the limits of specification, may cause the variation in their micro-structure, texture and mechanical properties. During second hot extrusion, the microstructure and texture of the leading end to the trailing end vary due to the variation in the hot working temperature [12]. The crystallographic texture, grain size and grain aspect ratio, dislocation density developed during fabrication of pressure tube govern mechanical properties. To achieve improved in-reactor performance in terms of dimensional changes, it is desirable to produce pressure tubes with uniform microstructure, texture and mechanical properties. This uniformity is ensured by adopting good manufacturing practices that produces pressure tubes with variation in the microstructural parameters and mechanical properties within a narrow band.

4.3.1 Axial and transverse tensile properties

A typical stress-strain plot obtained in room temperature testing of axial and transverse specimen for the Zr-2.5Nb alloy pressure tube material manufactured by double/quadruple melting is shown in Figure 4.2. Typical tested specimens of longitudinal and transverse orientation is shown in Figure 4.3. The effect of orientation on the fracture features can be clearly seen from this figure. For the axial samples the shear failure is nearly normal to the axial direction, with little reduction in specimen width along the transverse direction. The transverse tensile specimens showed shear failure that is inclined to the transverse loading direction, with specimen width reduction along the axial direction. Table 4.1 shows the average room temperature axial and transverse tensile properties evaluated from double melted and quadruple melted pressure tube offcuts. In general the transverse specimens showed higher yield strength (YS) and ultimate tensile strength (UTS) as compared to the longitudinal specimens . The tensile strength of the transverse specimens is relatively closer to the yield strength compared to that in the axial specimens. That means transverse specimens showed less strain hardening as compared to the longitudinal specimens. The uniform and total elongation also depends on specimen orientation. The axial specimens showed higher uniform and total elongation compared to the transverse specimens.

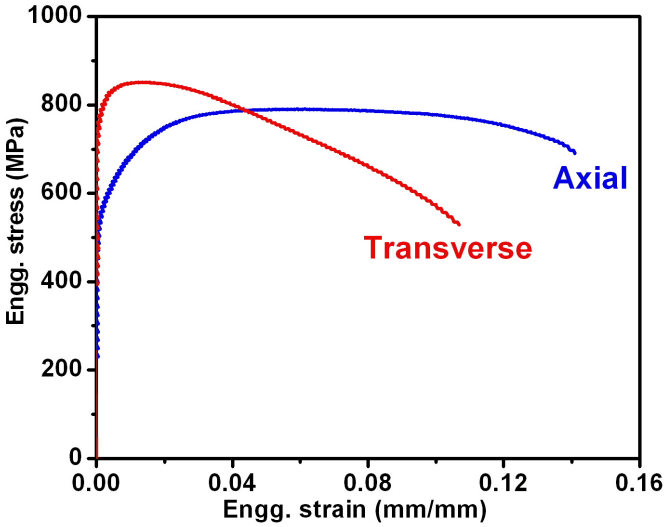

Figure 4.2: Typical room temperature stress-strain plot obtained in testing of Zr-2.5Nb pressure tube material using axial specimen and transverse specimen.

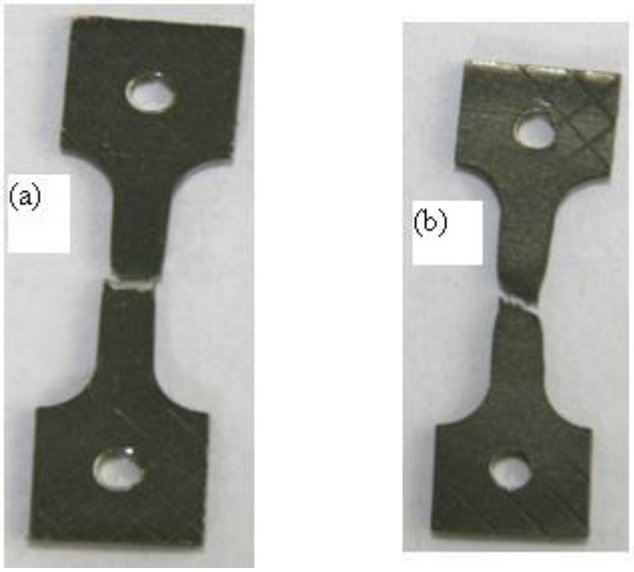

Figure 4.3: Typical tensile tested specimens (a) axial specimen (b) transverse specimen.

Table 4.1: Room temperature tensile properties of Zr-2.5Nb pressure tube in axial and transverse orientation (averaged for double melted and quadruple melted pressure tubes).

Tensile properties	Axial	Transverse
YS (MPa)	601	787
UTS (MPa)	798	835
UE (%)	6.1	2.3
TE (%)	15.0	12.4

Deformation of metal requires a minimum of 5 independent deformation systems for an arbitrary plastic strain. The face-centered cubic system has 12 slip systems, and the body-centered cubic system has 48 slip systems and satisfy this criteria easily. Hexagonal close-packed system of α-Zr, has lower symmetry and typically only 3 slip systems are easily activated. The deformation in this case is achieved through either dislocation slip on less preferred planes, or by twinning. Deformation by these alternative modes, particularly twinning, results in the evolution of preferred crystallographic orientation, or texture.

Plastic deformation occurs in Zr-2.5 Nb occurs by dislocation glide upon either prismatic or pyramidal slip system [125]. The primary slip system in α-Zr is on the prism planes $\{10\bar{1}0\}$ and in $\langle 11\bar{2}0\rangle$ directions, commonly referred as prismatic slip. Slip has also been observed along the basal $\{0001\}$ planes in the $\langle 1\bar{2}10\rangle$ direction, and is known as basal slip.

A majority of the basal poles in the pressure tubes are oriented in the circumferential or transverse direction and to some extent, in the radial direction with fraction of basal pole in transverse and radial direction in the range of 0.3-0.4 and 0.5-0.6 respectively. With majority of $\{0001\}$ poles aligned in the transverse direction, it requires the plastic flow to occur primarily by the more difficult $\{10\bar{1}1\}\langle\bar{1}\bar{1}23\rangle$ pyramidal slip [125] or by twinning [126] when straining along transverse direction. Thus pyramidal slip and twinning is responsible for higher YS in the transverse specimen because the

critical resolved shear stress(CRSS) for pyramidal slip and twinning are higher than that for prismatic slip. Once yielding occurs by twinning, further deformation occurs primarily in the twinned regions that are now better aligned for slip. The deformation will then take place locally there, leading to localized deformation in the necked region [126] as shown in Figure 4.3(b) showing failed transverse specimen.

The axial specimens when loaded deform by slipping as the prismatic slip systems are better oriented in this orientation of specimen and the CRSS for this slip is lower than that for twinning. This lower CRSS leads to lower YS in the axial specimen of the Zr-2.5Nb pressure tube. Slip fosters uniform deformation along the gauge section and leads to greater extent of strain hardening. It can also be observed from the Figure 4.2 that the difference between YS and UTS for the longitudinal specimens is higher than that for the transverse specimens, which is an indication that axial specimens strain harden more than that of transverse specimens. The average value ratio of UTS to YS is 1.33 and 1.06 respectively for axial and transverse specimens. As compared to the localized deformation in transverse specimen, the axial specimens show more uniform deformation along the gauge length as shown in Figure 4.3.

4.3.2 Double-melted and quadruple-melted pressure tube tensile properties

Table 4.2 shows the mean value and standard deviation of the tensile properties of double-melted and quadruple melted pressure tube off-cuts at room temperature. Normal distribution of tensile properties at room temperature for double-melted and quadruple melted Zr-2.5Nb pressure tube off-cuts are shown in Figure 4.4 and Figure 4.5. Though the data set was limited, the Kolmogorov–Smirnov test [127], which is a non-parametric test to compare a sample with a reference probability distribution indicated significant p values, which showed it was reasonable to assume normal distribution to graphically represent the scatter and variations in offcut tension test results. It is clear from these tables and figures that double-melted pressure tubes show wider scatter as compared to the quadruple-melted pressure tubes. Double-melted pressure

tubes have relatively higher strength and lower elongation as compared to quadruple-melted pressure tubes in the longitudinal direction as seen in Figure 4.4. Figure 4.5 shows that the transverse property is quite comparable for these two types of pressure tubes.

Table 4.2: Room temperature tensile properties of double-melted and quadruple-melted pressure tube off-cuts (Numbers in brackets indicate the number of specimens tested at room temperature).

Properties	Double melted				Quadruple melted			
	Longitudinal (30)		Transverse (25)		Longitudinal (32)		Transverse (32)	
	Mean	Std. Dev.	Mean	Std. Dev.	Mean	Std. Dev.	Mean	Std. Dev.
YS (MPa)	618	29	793	77	583	23	780	29
UTS (MPa)	803	43	833	68	792	26	836	28
UE (%)	5.7	0.62	2.5	0.62	6.4	0.35	2.14	0.24
TE (%)	14.0	2.29	12.5	1.65	16.0	1.59	12.3	1.87

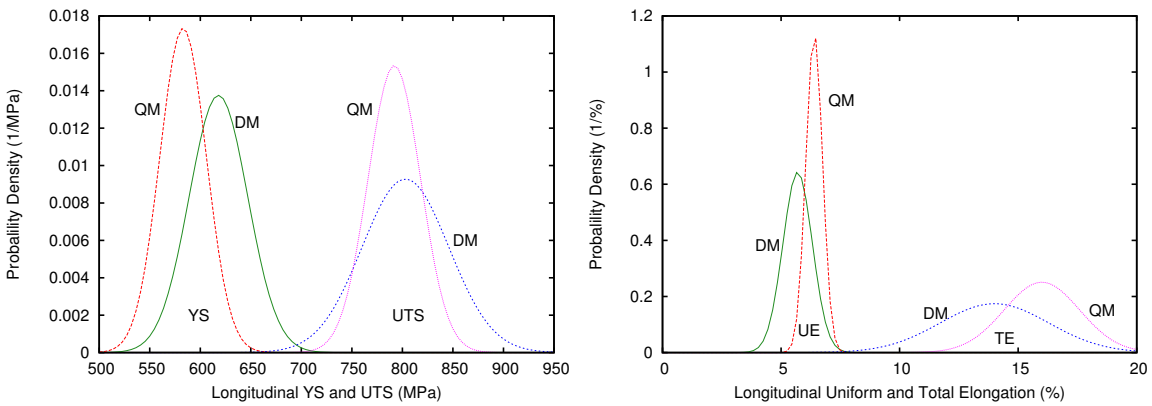

(a) (b)

Figure 4.4: Distribution of (a) strength and (b) elongation properties at room temperature in longitudinal direction for double-meted and quadruple-melted pressure tube off-cuts.

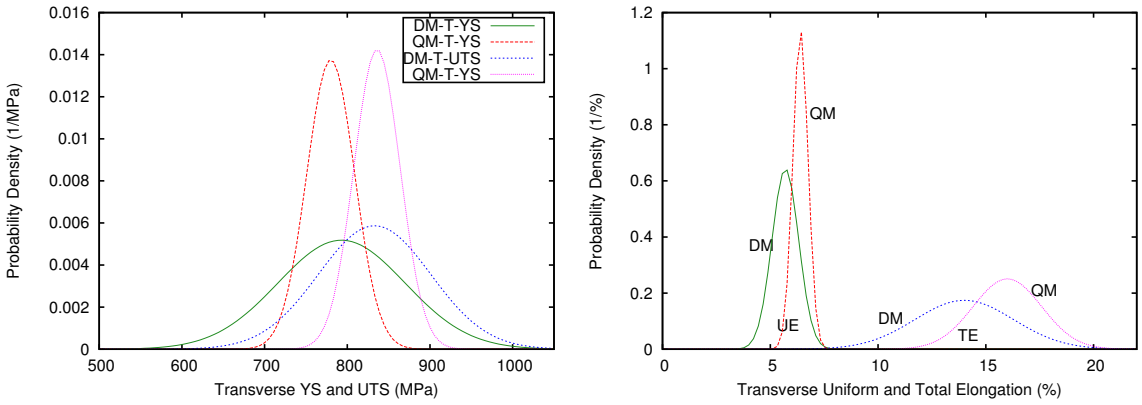

(a) (b)

Figure 4.5: Distribution of (a) strength and (b) elongation properties at room temperature in transverse direction for DM and QM pressure tube off-cuts.

The resolved fraction of basal plane normal in the axial, transverse and radial directions (f_a, f_t *and* f_r) and the dislocation density of pressure tubes as measured by X-ray line broadening for the DM and QM pressure tubes are shown in Figure 4.6 and their normal distribution is shown in Figure 4.7. The pressure tube has the majority of basal poles in the transverse direction [11, 128] as shown in the Figure 4.6. The higher strength in double-melted pressure tube may be partly due to higher dislocation density as the texture in double-melted and quadruple-melted are in close proximity as seen in Figure 4.7. There are many other sources of strengthening like chemical composition and grain size. Grain sizes of the offcuts have not been measured but since the fabrication route is same it is expected to be more or less similar. Quadruple melted tubes, have lower specified values on elements like C, P and Cl. Also the maximum specified iron concentration in DM and QM tubes were 1500 wppm and 650 wppm respectively. Differences in these chemical composition seem to be primary reason for higher strength of DM PTs.

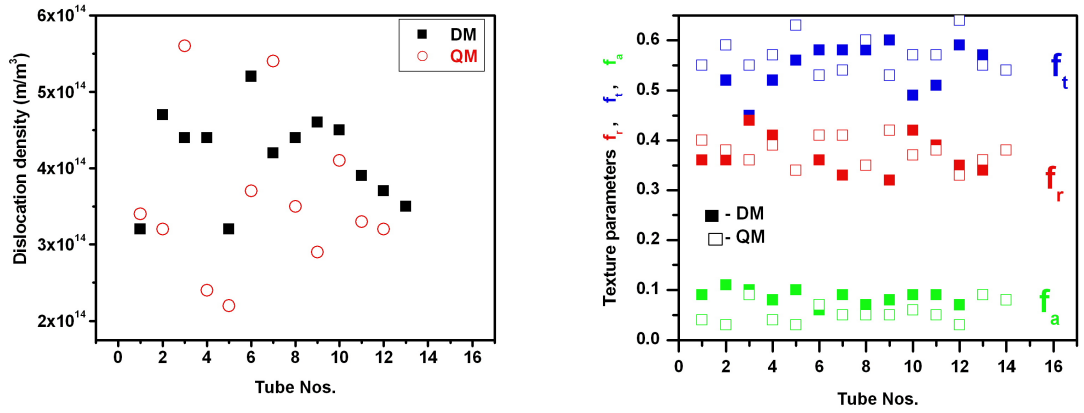

(a) (b)

Figure 4.6: Data plot of (a) dislocation density and (b) texture in DM and QM pressure tube off-cuts.

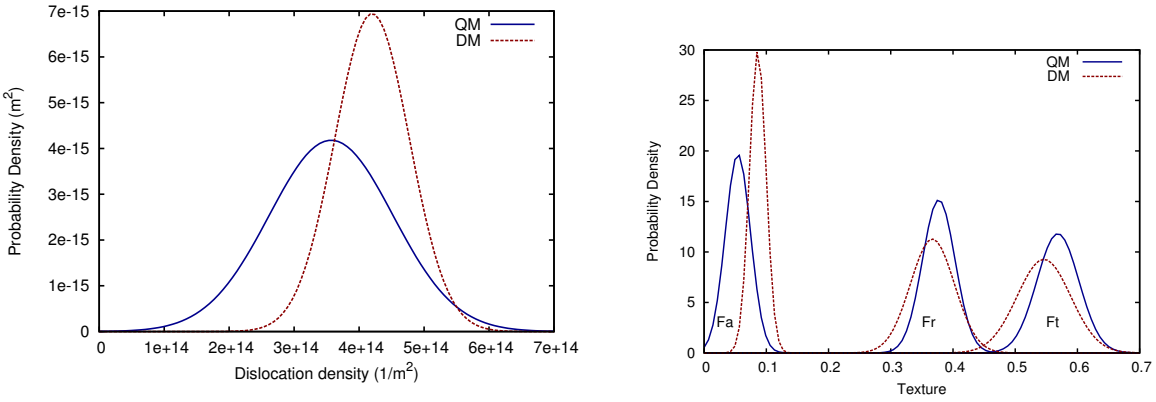

(a) (b)

Figure 4.7: Distribution of (a) dislocation density and (b) texture in DM and QM pressure tube off-cuts.

4.3.3 Tensile properties at frontend and backend of the quadruple melted pressure tubes

For the quadruple melted pressure tubes the tensile properties were evaluated for both frontend and backend of each of the sixteen pressure tube offcuts at room temperature and at 300 $^{\circ}C$. The comparison of tensile properties of the frontend and backend of pressure tubes in the axial and transverse has been shown respectively in Figure 4.8 and Figure 4.9. It is seen in the figures that in most of the pressure tubes backend has shown slightly higher strength and lower elongation as compared to that of frontend

offcuts except for few pressure tubes the both end properties are nearly equivalent or frontend is slightly stronger. The mean and standard deviation of the tensile properties in longitudinal and transverse direction of frontend and backend pressure tube off-cuts is shown in Table 4.3 and 4.4 respectively for room temperature and for 300 $^{\circ}C$. The statistical analysis result in these tables indicate that backend is relatively stronger and less ductile as compared to the frontend offcut.

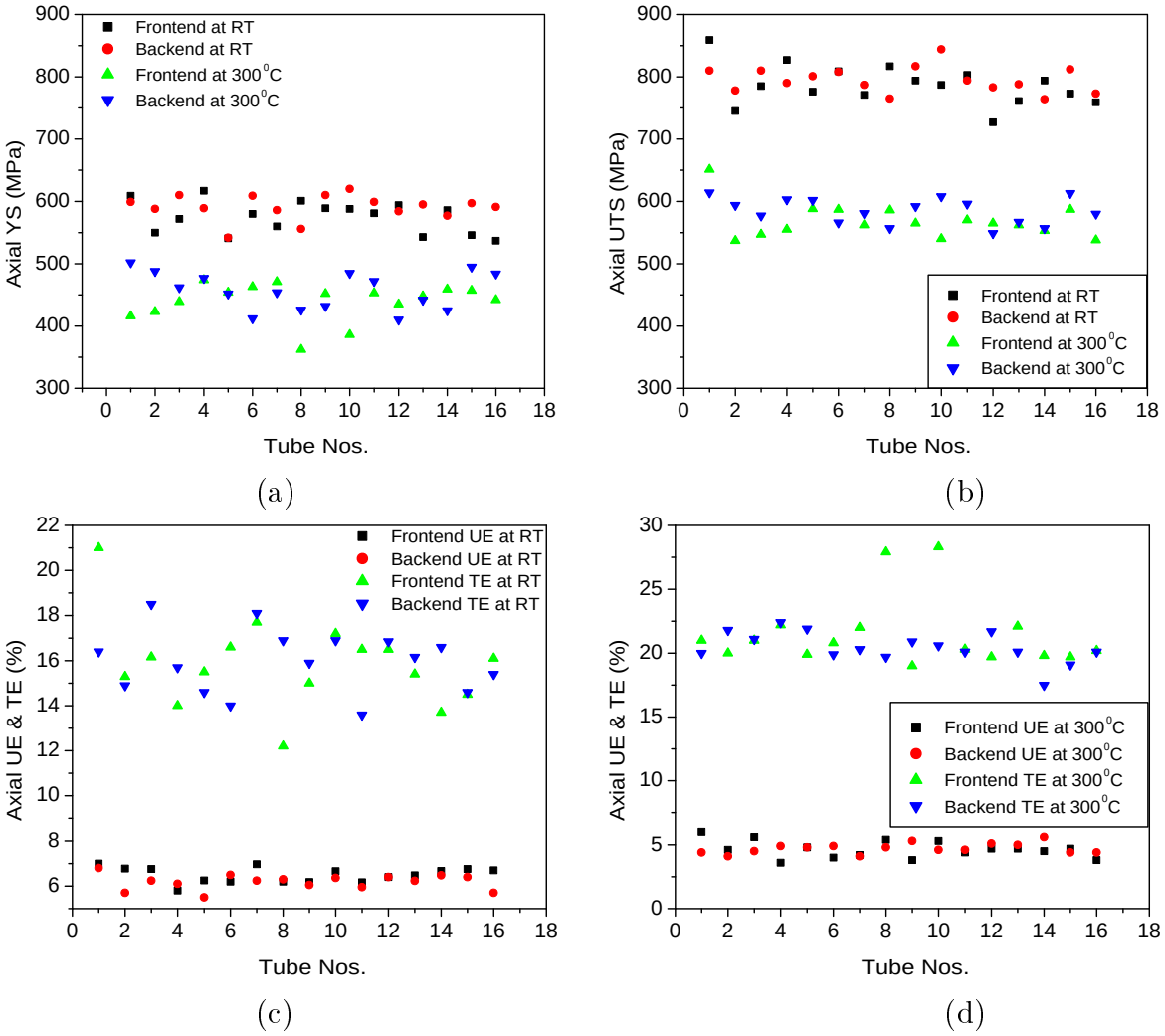

Figure 4.8: Frontend and backend tensile strength (a,b) and elongation (c,d) properties in longitudinal direction of the pressure tubes at room temperature and 300 $^{\circ}C$.

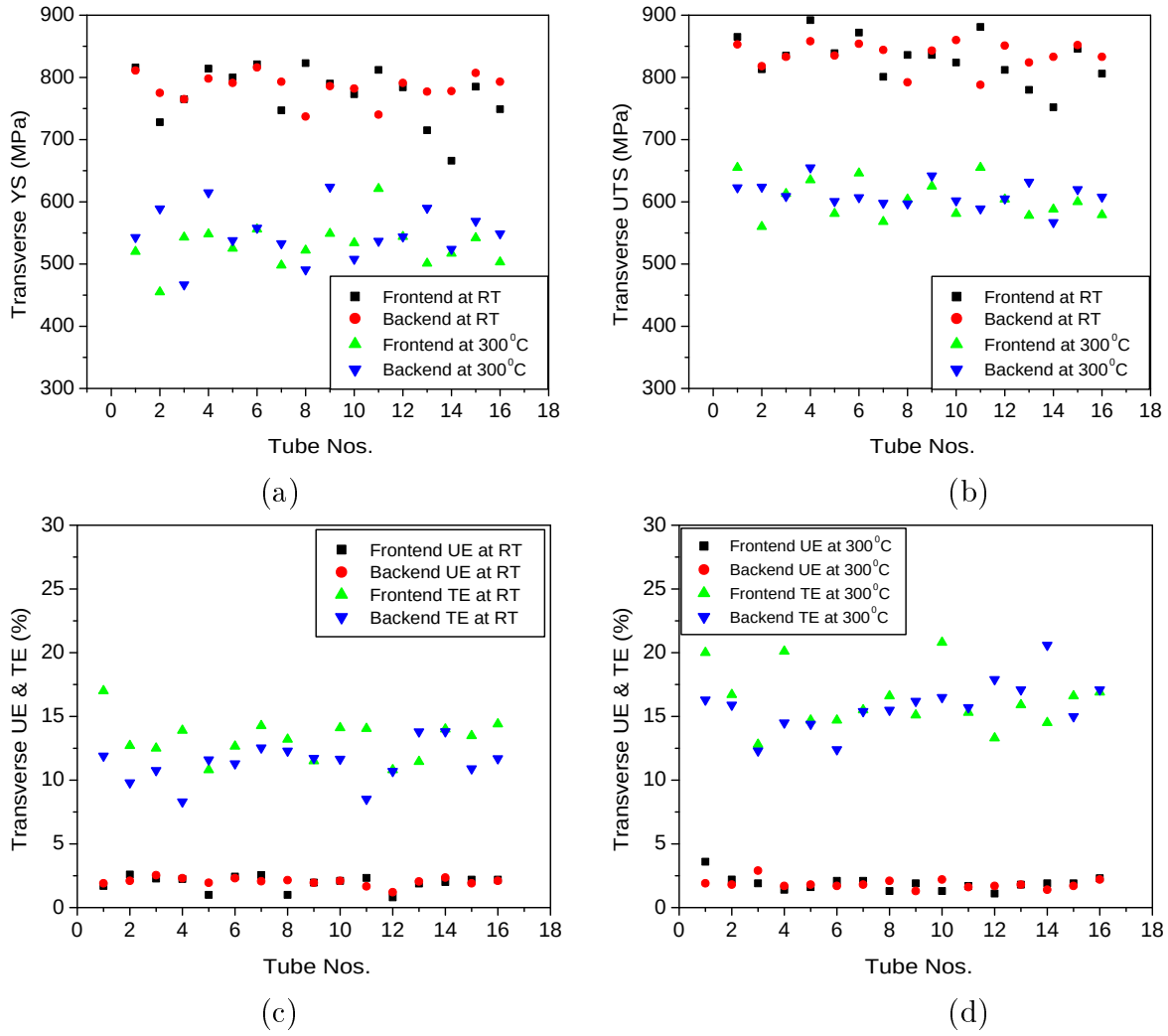

Figure 4.9: Frontend and backend tensile strength (a,b) and elongation (c,d) properties in transverse direction for the quadruple melted pressure tubes at room temperature and 300 $^{\circ}C$.

Table 4.3: Tensile properties of the front and back end of quadruple melted pressure tube off-cuts at room temperature.

Tensile properties	Longitudinal				Transverse			
	Front end		Back end		Front end		Back end	
	Mean	Std. Dev.	Mean	Std. Dev.	Mean	Std. Dev.	Mean	Std. Dev.
YS (MPa)	575	26	591	19	774	44	784	21.5
UTS (MPa)	787	33	795	21	831	37	836	20.9
UE (%)	6.5	0.34	6.2	0.3	2.0	0.56	2.0	0.3
TE (%)	15.8	1.97	15.9	1.3	13.2	1.6	11.3	1.5

Table 4.4: Tensile properties of the front and back end of quadruple melted pressure tube off-cuts at 300 °C.

Tensile properties	Longitudinal				Transverse			
	Front end		Back end		Front end		Back end	
	Mean	Std. Dev.	Mean	Std. Dev.	Mean	Std. Dev.	Mean	Std. Dev.
YS (MPa)	440	29.3	457	29.3	530	34.2	549	40.9
UTS (MPa)	568	27.3	585	20.4	605	29.9	611	20.6
UE (%)	4.6	0.7	4.7	0.4	1.9	0.6	1.9	0.4
TE (%)	21.5	2.7	20.5	1.2	16.2	2.3	15.8	1.9

Extrusion temperature variation between the leading and the trailing ends of the blank affects microstructure and texture and therefore mechanical properties and flow behavior vary along the length of the pressure tube. The grain size varies along the length of the tube because the billets continuously cool down during the extrusion process. Back-end of the tube has a smaller α-grain size and a higher dislocation density than the front-end of the tube, and these result in higher tensile strength at the back-end of the pressure tube.

The statistical variation in tensile properties for the front-end and back-end of the quadruple-melted pressure tubes is shown by box-plot in Figure 4.10 & Figure 4.11. The quadruple-melted pressure tubes studied in the present case did not show much difference between front-end and back-end off-cuts at room temperature except for total elongation in the transverse direction as seen in Figure 4.10 and Figure 4.11. Slightly higher axial yield strength is seen for the back end of the pressure tubes. However, along the transverse direction, strengths at both ends of the tube are nearly same. The front end of the pressure tubes have higher transverse basal pole texture, but this gets compensated by higher dislocation density at the back end that gets extruded at slightly lower temperatures during fabrication. Thus when tested along the transverse direction the tensile strength has been found to be nearly similar.

Total elongation in the transverse direction is lower for the back-end off-cuts as

compared to the front-end off-cuts. It is also clear from the figures that the scatter band is relatively higher for front-end off-cuts as compared to the back-end off-cuts.

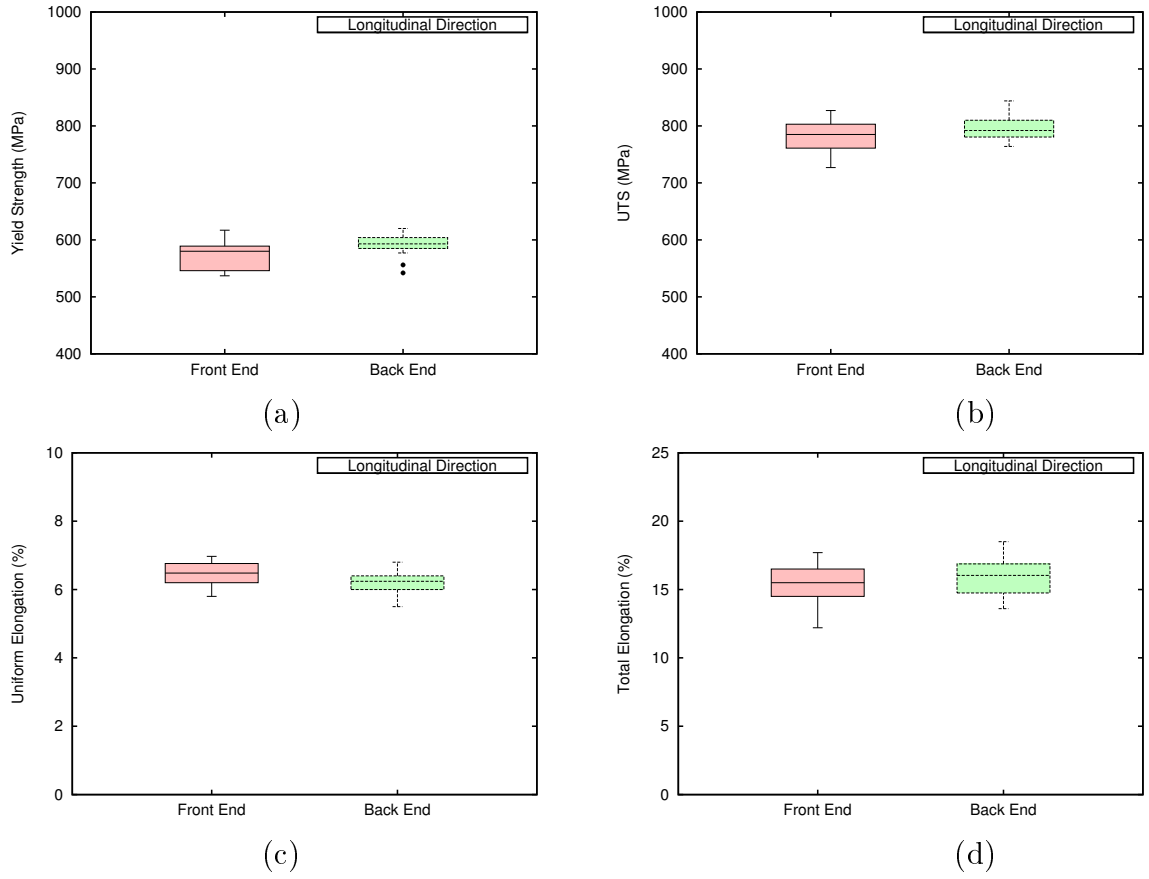

Figure 4.10: Box plot of room temperature strength (a & b) and elongation (c & d) in axial direction of front-end and back-end of quadruple melted pressure tube off-cuts.

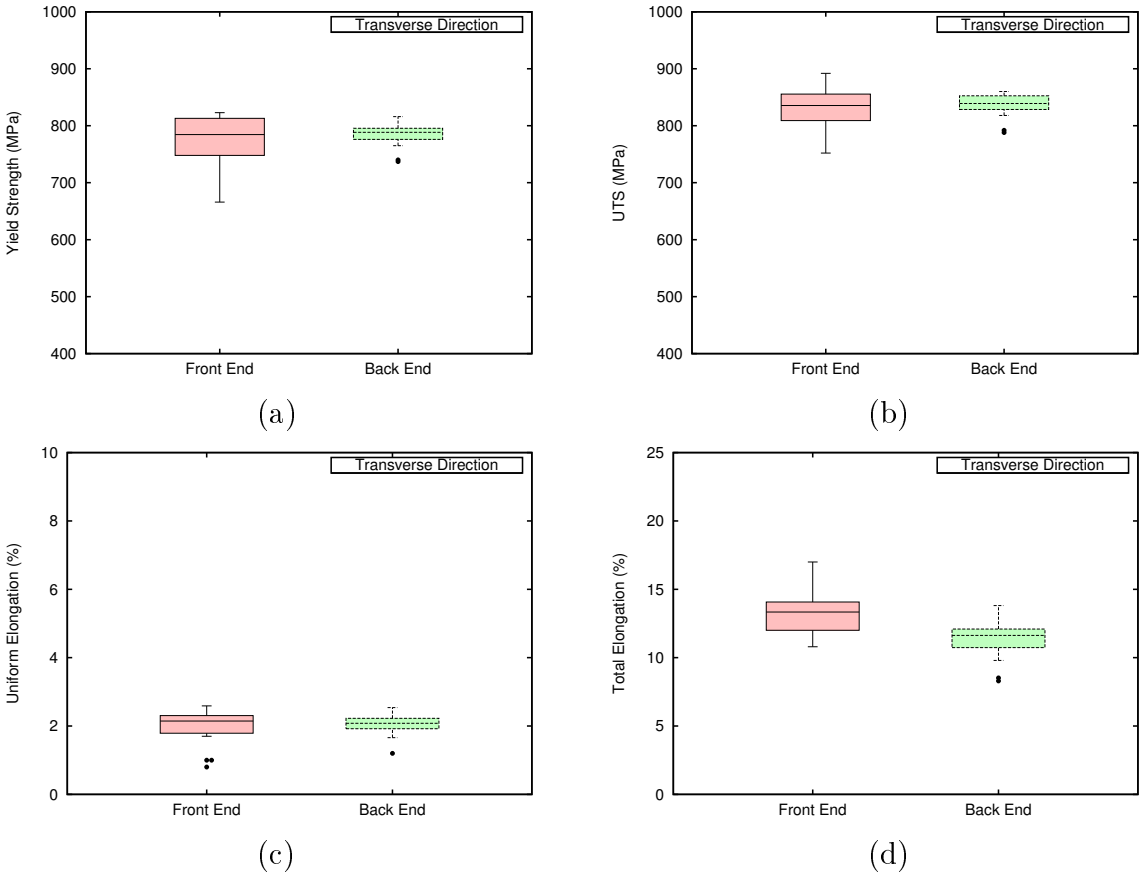

Figure 4.11: Box plot of room temperature strength (a & b) and elongation (c & d) in transverse direction of front-end and back-end of quadruple melted pressure tube off-cuts.

4.3.4 Scatter in fracture toughness

Typical plot of load, DCPD versus load line displacement (LLD) obtained in fracture toughness test of a double melted pressure tube is shown in Figure 4.12. The load, DCPD and load line displacement data along with the measured crack growth obtained for each of the tested specimens were analysed to get J versus $\triangle a$ for each of the specimen. One such plot, for double melted pressure tube offcuts is shown in Figure 4.13. Out of six DM pressure tubes, two pressure tubes have shown good crack growth resistance, $\frac{dJ}{da}$, as compared to the other four pressure tubes. The average value of $\frac{dJ}{da}$ for the tougher offcuts was 406 MPa as compared to 136 MPa for relatively less tough tubes. Open literature [2, 5, 28, 64] on fracture toughness of double melted pressure tubes of Indian origin have reported $\frac{dJ}{da}$ values of 35 to 87 MPa and

that for CANDU type tubes have also shown large tube to variations ranging from 60 MPa to 448 MPa, with most of them being around 150 MPa. This shows wide variability in the fracture toughness values of the double melted pressure tubes.

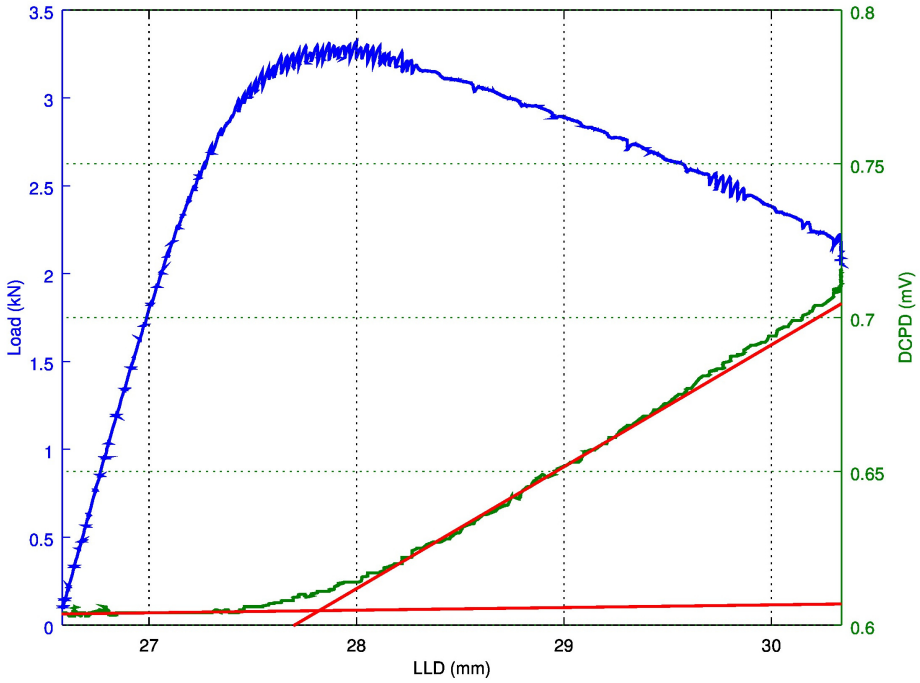

Figure 4.12: Typical plot of load, DCPD voltage drop versus load line displacement (LLD) obtained in fracture toughness test of a double melted pressure tube.

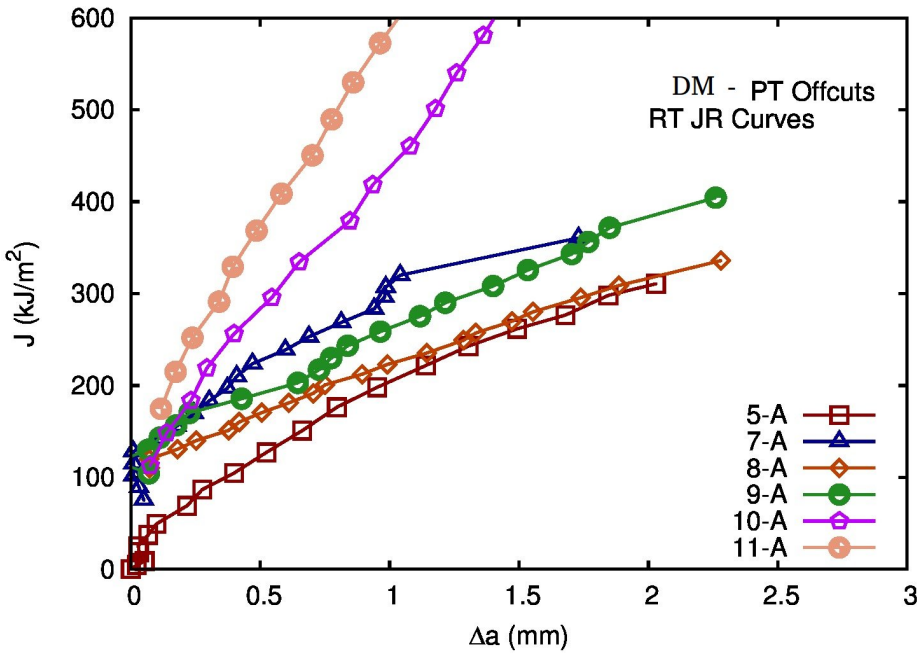

Figure 4.13: Typical J versus $\triangle a$ plots obtained in fracture toughness tests of various double melted (DM) pressure tube offcuts (5A, 7A-10A indicate specimens from different pressure tubes).

Total twenty three offcuts from quadruple melted pressure tubes of Indian origin were tested. All other offcuts, except three tubes, have shown crack growth resistance $\frac{dJ}{da}$ greater than 200 MPa with an average value being around 300 MPa. All the tubes, except one, have shown the fracture toughness corresponding to maximum load, J_{max} greater than 125 kJ/m^2. The average crack growth resistance and maximum load fracture toughness for the QM tubes are around 280 MPa and 187 kJ/m^2 including all the tested specimen results. Figure 4.14 shows the variation in fracture toughness between front end and back end of some of the QM pressure tubes. Except two tubes, other tubes had marginal variation in fracture toughness from one end of the tube to the other end. There was no clear trend in fracture toughness, whether it was more at the front end or back end offcuts and the difference in fracture toughness between the two ends were marginal. However, in general the front end seem to be relatively tougher. The average $\frac{dJ}{da}$ for these front end and back end offcuts is 314 MPa. Open literature [2, 11, 28] on fracture toughness of quadruple melted pressure tubes of Indian origin have reported values of 204 MPa, 227 MPa, 287 MPa and that for CANDU

type tubes shown dJ/da values in the range of 350 - 420 MPa.

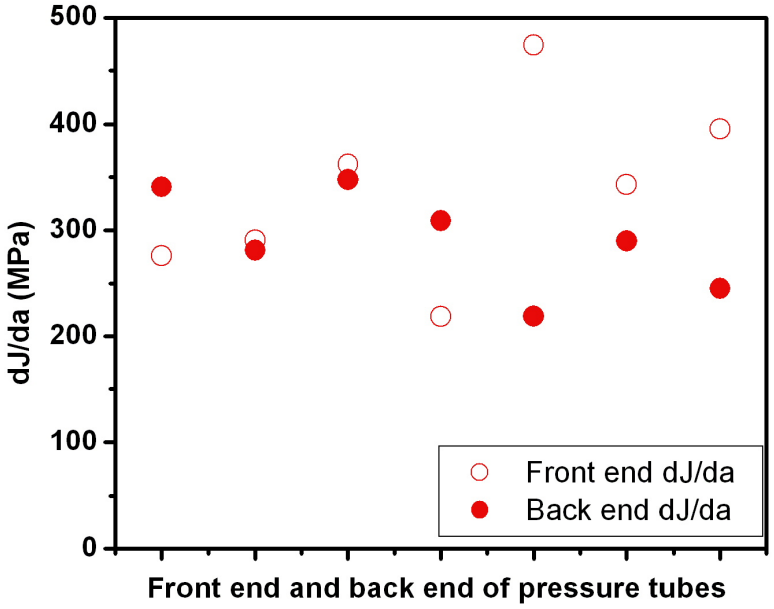

Figure 4.14: Fracture toughness of front-end and back-end of quadruple melted pressure tubes at room temperature.

The distribution of $\frac{dJ}{da}$ and J_{max} for double melted and quadruple melted pressure tube offcuts are shown in Figure 4.15 and Figure 4.16. In general, the QM pressure tubes showed much higher fracture toughness values as compared to DM tubes. Only three out of 23 QM pressure tube offcuts did show lower toughness that was similar to DM pressure tubes.

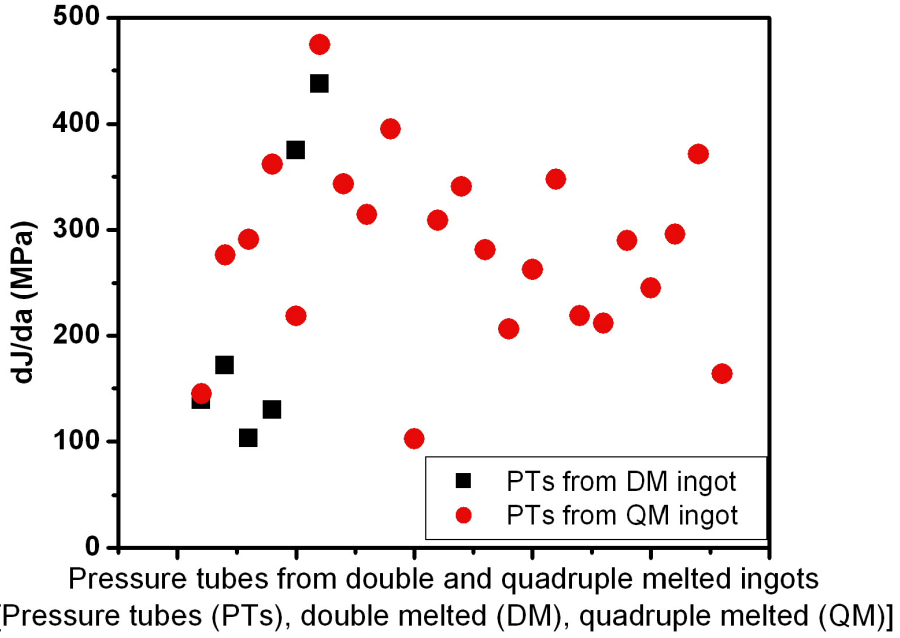

Figure 4.15: Crack growth fracture toughness (dJ/da) of pressure tubes from double melted and quadruple melted ingots.

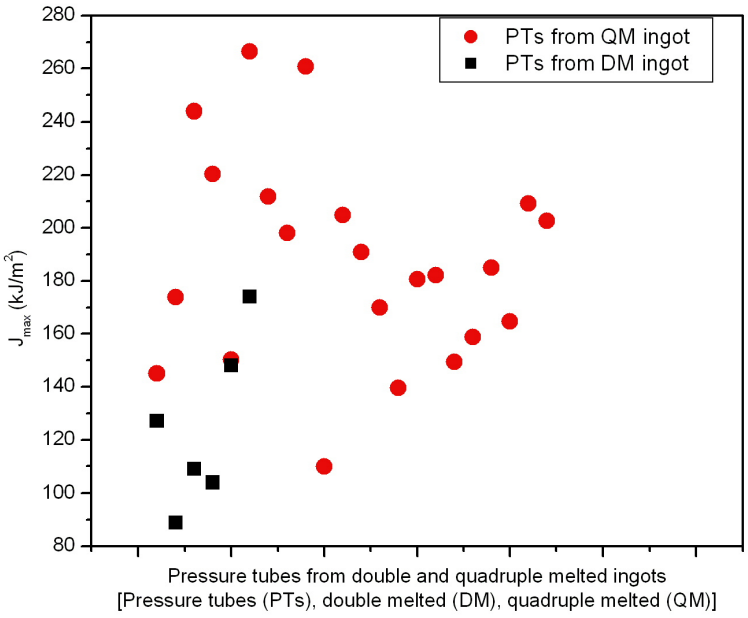

Figure 4.16: Fracture toughness (J_{max}) of pressure tubes from double melted and quadruple melted ingots.

The SEM observation of the fracture surfaces of both double melted and quadruple

melted pressure tubes having relatively low and high fracture toughness are shown in Figures 4.17-4.20. Fissure like long axial feature on the fracture surface were seen in low toughness tube specimens and no fissures were found in high toughness material for both DM and QM material. It is clearly seen that the low fracture toughness specimens had relatively high numbers of long fissures. The average fissure spacing was around 135 to 175 μm for specimens having dJ/da of around 145 MPa in both QM and DM tubes. It shows that irrespective of quadruple melting, presence of fissure like features result in low toughness. Other studies have also shown that the fissure density is correlated with the variations in the concentration of chlorine, phosphorus and carbon in the pressure tubes [64]. Thus this variability in fracture toughness of pressure tubes is mainly due to variations in these trace elements in as-fabricated pressure tubes, though, exact chemical composition analysis of the tested pressure tubes could not be carried out due to limited size of offcut rings available for study. It is well established from the ingot chemistry at manufacturing stage that quadruple melting in general leads to lower concentration of trace element impurities that results in higher toughness. Its the presence of fissure like features, i.e. trace impurities that affect the toughness, which can be lower even for QM tubes, if it is not well controlled.

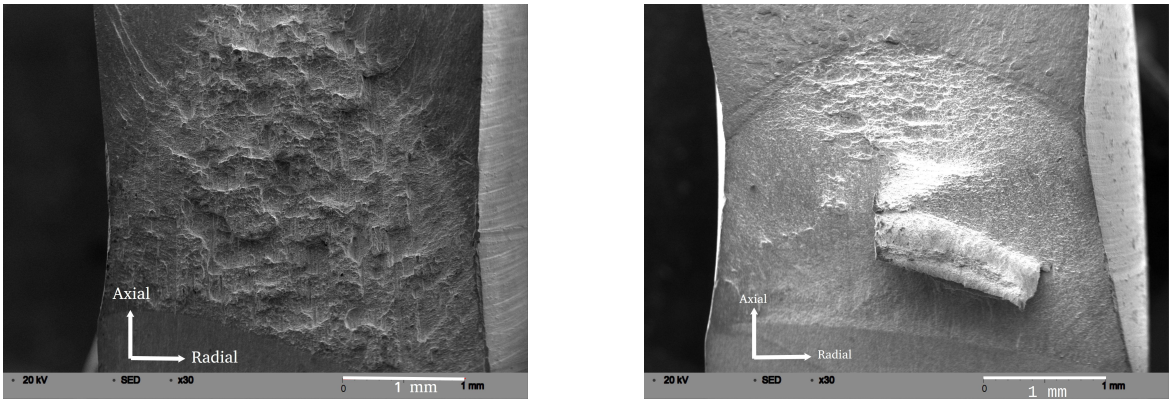

(a) (b)

Figure 4.17: Fracture surfaces of fracture toughness tested specimens of DM pressure tube off-cuts having relatively (a) lower toughness and (b) higher toughness.

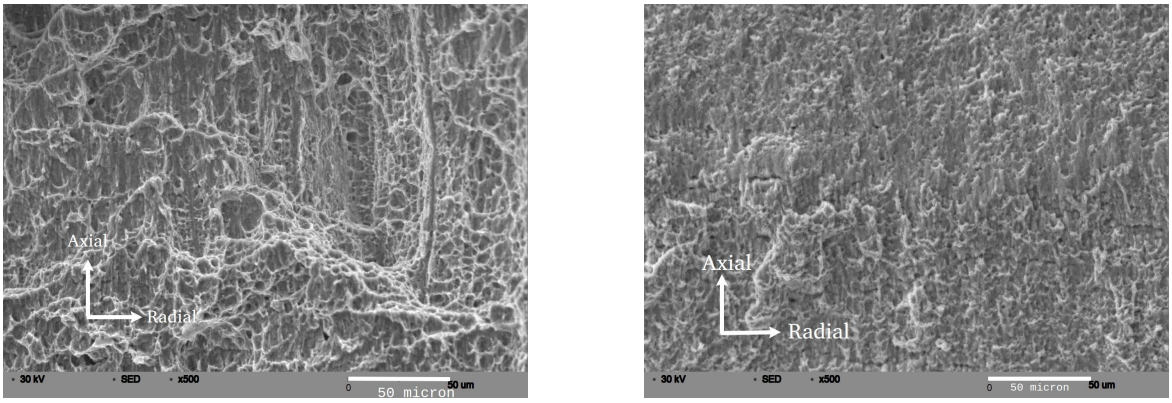

(a) (b)

Figure 4.18: Higher magnification view of fracture surfaces of fracture toughness tested specimens of DM pressure tube off-cuts having relatively (a) lower toughness showing higher fissure density and (b) higher toughness.

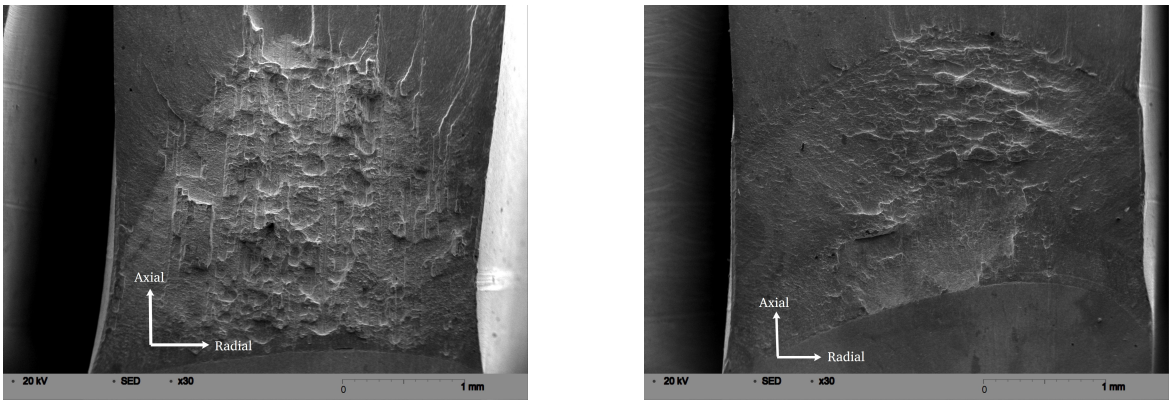

(a) (b)

Figure 4.19: Fracture surfaces of fracture toughness tested specimens of QM pressure tube off-cuts having relatively (a) lower toughness and (b) higher toughness.

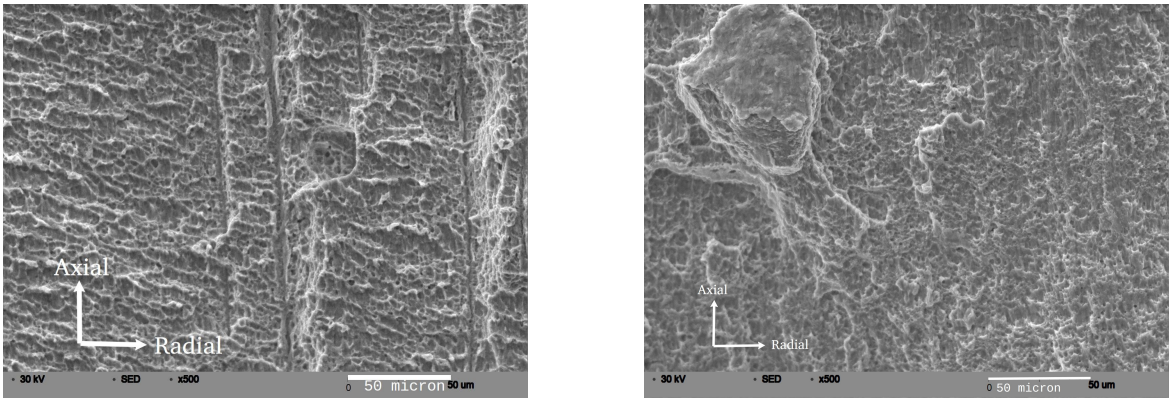

(a) (b)

Figure 4.20: Higher magnification view of fracture surfaces of fracture toughness tested specimens of QM pressure tube off-cuts having relatively (a) lower toughness showing higher fissure density and (b) higher toughness.

4.4 Conclusions

Tension tests were carried out on specimens of both axial and transverse orientation and from both front-end and back-end off-cuts of several pressure tubes fabricated from double and quadruple melted pressure tubes. The tensile properties have been evaluated at room temperature and $300\,^{\circ}C$ using miniature flat tensile specimens.

In general, the transverse specimens showed higher yield strength (YS) and ultimate tensile strength (UTS) as compared to the longitudinal specimens. Transverse specimens also showed less strain hardening as compared to the longitudinal specimens. The axial specimens showed higher uniform (UE) and total elongation (TE) as compared to the transverse specimens. This difference in axial and transverse properties has been explained on the basis of slip and twinning systems of the α-zirconium phase and the pdominant transverse basal pole texture in the pressure tubes.

Mean values of tensile properties showed that back-end off-cuts were relatively stronger and less ductile as compared to the front-end off-cuts. This is mainly due to the higher dislocation density and finer grain size at back end, otherwise the front ends have stronger transverse basal pole texture.

Double-melted pressure tubes showed relatively higher strength and lower elongation and larger standard deviation compared to the quadruple melted pressure tubes. This difference in double-melted and quadruple melted pressure tube properties indicates that the variability in minor trace element impurities, which lead to differences in second phase precipitates, such as carbides, phosphides as well as microsegregation of Cl-C complex also have role in larger scatter for DM pressure tubes. The tubes made from quadruple melted ingots having lower trace element impurities show lower scatter in mechanical properties.

The double melted pressure tubes have shown wide variations in fracture toughness. The average value of $\frac{dJ}{da}$ for the tougher offcuts was 406 MPa compared to 136 MPa for relatively less tough tubes. Total twenty three offcuts from quadruple melted pressure tubes of Indian origin were tested and except three offcuts, all other offcuts

have shown fracture toughness greater than 200 MPa with an average value of around 300 MPa. The average crack growth resistance is around 280 MPa including all the tested specimen results. Fracture toughness of front end and back end of six quadruple melted pressure tubes were evaluated. Except two tubes, other tubes had marginal variation in fracture toughness from one end of the tube to the other end. There was no clear trend in fracture toughness, whether it was more at the front end or back end offcuts when the difference in fracture toughness between the two ends were marginal. However, when there was relatively large difference in front end and back end fracture toughness, the front end seem to be relatively tougher compared to that of back end offcuts. The average $\frac{dJ}{da}$ for these front end and back end offcuts is 314 MPa.

Chapter 5

Impact behavior of Zr-2.5Nb pressure tube alloy

5.1 Objective

In this work, impact behavior of Zr-2.5Nb pressure tube material was characterized by impact tests using specimens to get crack growth along axial and transverse directions of the tubes. Both as-received and hydrogen charged materials were used for this investigation. The objective of this investigation was to study the effect of crack growth direction, hydrogen concentration and specimen geometry on the impact property of Zr-2.5Nb pressure tube over a range of temperature. Fracture morphology for specimens having axial notch and notch in transverse directions were also compared. An attempt has been made in this work to rationalize the observation in terms of microstructure, influence of sample holding device, sample geometry, hydrogen concentration and test temperature. Zr-2.5Nb pressure tubes are simple tubular component fabricated to have dominant tangential basal pole texture mainly to have lower in-reactor diametral creep deformation rate, without adversely affecting its axial irradiation growth or hydride embrittlement related properties. This texture leads to significant differences in the properties along the axial and circumferential direction of the tube. This difference was clearly seen in the studies carried out on the tensile and

fracture toughness of the pressure tubes offcuts in this work. The pressure tubes do not experience dynamic loading under normal operating conditions. The impact behaviour of pressure tubes was studied with following three broad motivations. Tensile and fracture properties were observed to have significant differences along two major direction of the tube and the amount of this difference changed with test temperature. It was of interest to see how high strain rates would affect the relative differences in the properties along these two directions. Also such studies are limited in open literature and could be of use in modelling the dynamic behaviour of this material in future works. Finally, there could be situations where the pressure tubes could be subjected to shock loads or dynamic loads and this work may be of use. Under the postulated condition of guillotine failure of pressure tube toughness along transverse direction becomes important and that is why these results are technologically important.

5.2 Experimental

5.2.1 Material

Zr-2.5Nb tube piece used in this investigation was from a pressure tube of 82.5 mm average internal diameter and 3.5 mm thickness. The fabrication route of the pressure tube, that imparted about 20% cold work in the finished product, included double vacuum arc melting, extrusion and two stages of cold pilgering with an intermediate annealing as given in Section 2.2. Spools of 150 mm length were cut from the pressure tube. Two spool pieces were used for hydriding them. Before hydriding the inner and outer surfaces of the spools were polished using 1200 grit abrasive paper to obtain a fresh and oxide free surface. The polished spools were gaseously charged at 363 $^{\circ}C$ to the desired concentration of hydrogen in a modified Sievert's apparatus [108]. The spools after hydrogen charging were furnace cooled to room temperature. The actual hydrogen concentration in the samples were estimated by inert gas fusion technique.

One as-received spool piece and one hydrided spool piece were axially cut into four pieces and then cold flattened. The flattened pressure tube pieces were stress relieved

by vacuum annealing at 400 $^{\circ}C$ for 24 hours.

Impact specimens were prepared from both as-received and hydrided pressure tubes in both as-fabricated and flattened conditions.

5.2.2 Drop tower impact test

Impact tests on pressure tube specimens, as shown in Section 3.7, were carried out from room temperature to up to 300 $^{\circ}C$. The basic data generated during the test was the load–time plot. These load and time data were then used to calculate load-displacement values during the impact test. The area under the load–displacement plot provides the total energy to fracture. The conversion of load-time into load displacement and calculation of corresponding energy was done by the software that was used for the impact testing and was associated with the impact testing machine. Typical load-time and load-displacement plots obtained for the room temperature impact tests are shown in Figure 5.1 and Figure 5.2 for axial and transverse specimens respectively. Similar plots for 300 $^{\circ}C$ tests are given in Figure 5.3 and Figure 5.4.

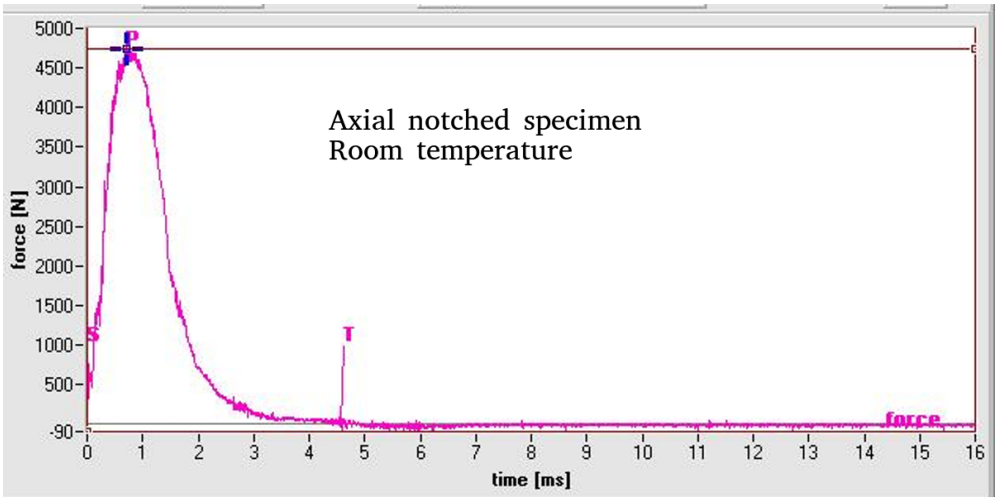

(a)

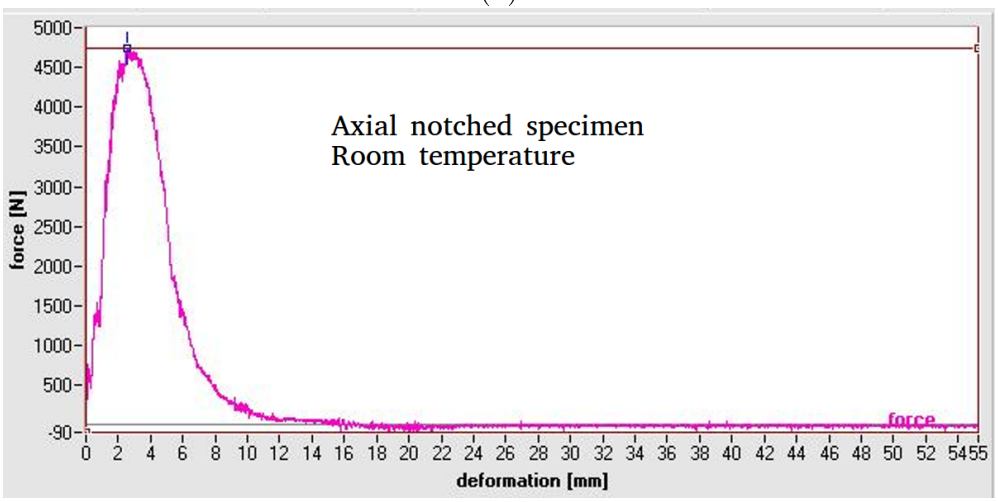

(b)

Figure 5.1: Typical online (a) load-time and (b) load-displacement plots obtained during impact test of axial specimens at room temperature.

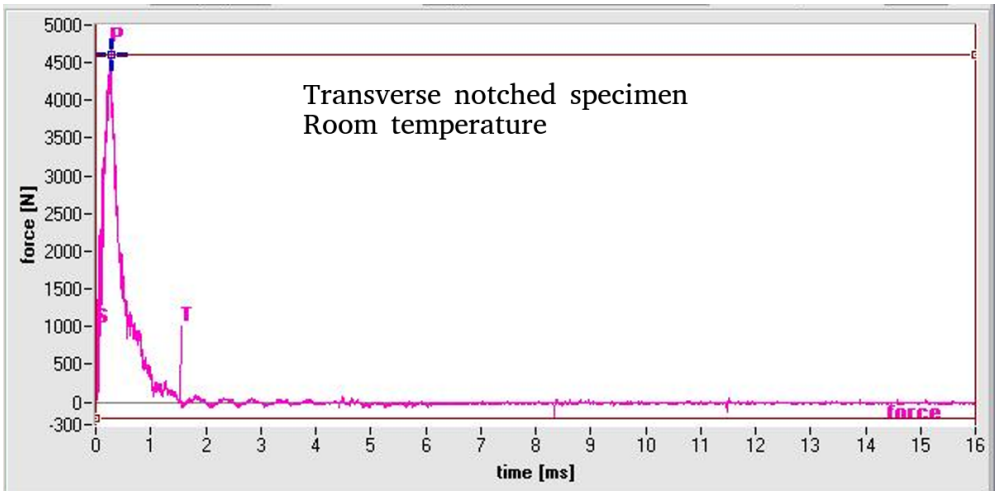

(a)

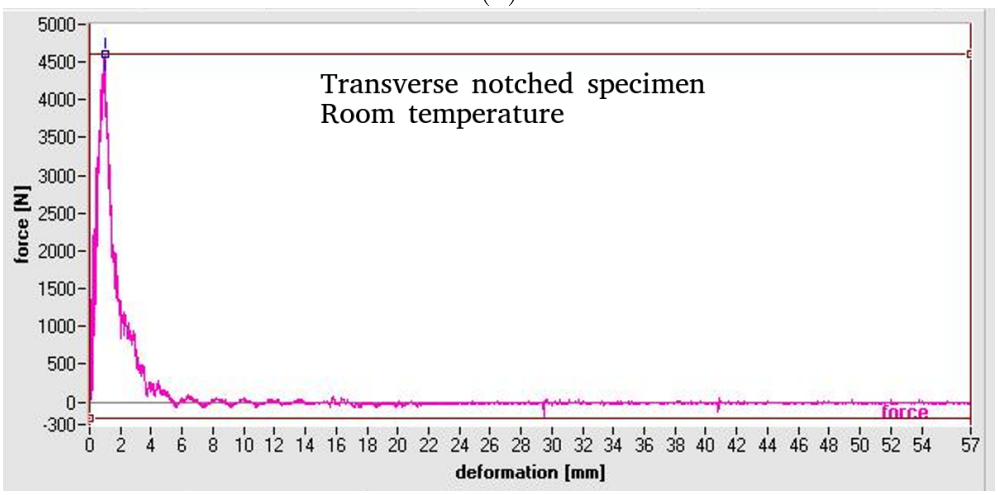

(b)

Figure 5.2: Typical online (a) load-time and (b) load-displacement plots obtained during impact test of transverse specimens at room temperature.

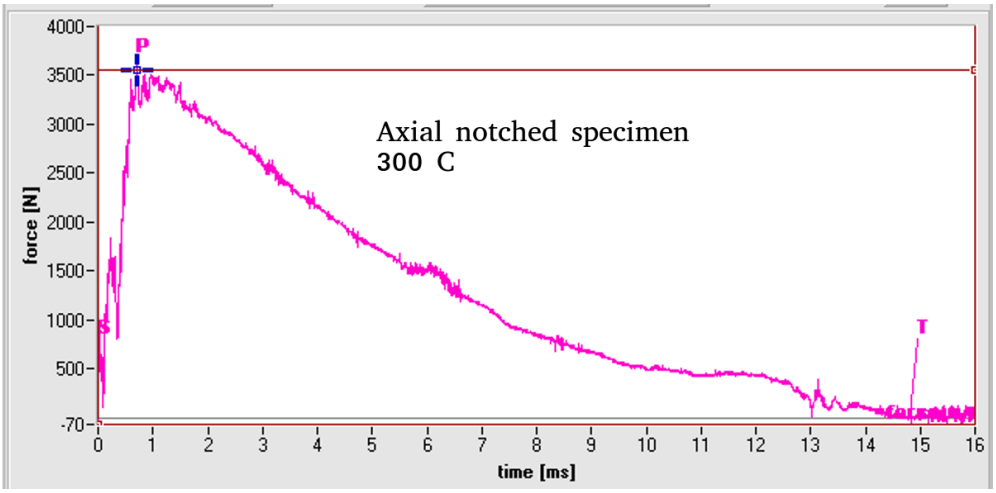

(a)

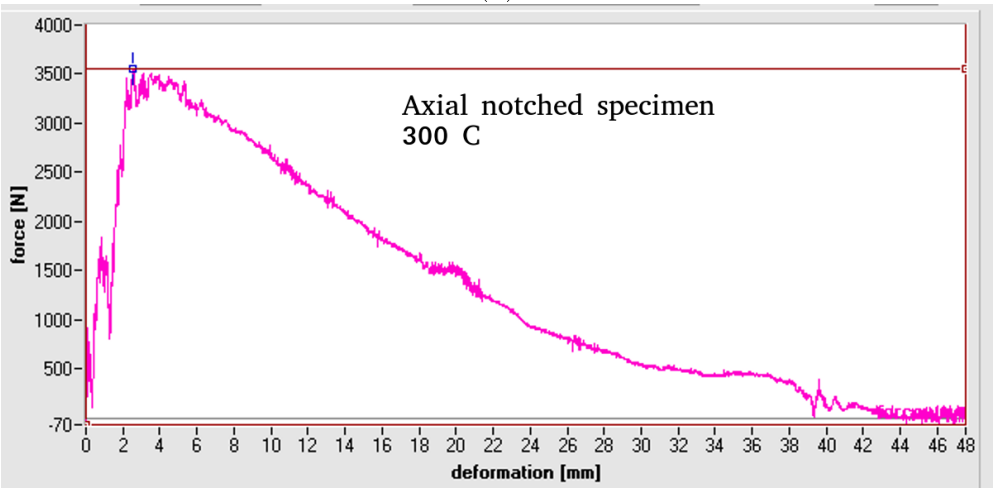

(b)

Figure 5.3: Typical online (a) load-time and (b) load-displacement plots obtained during impact test of axial specimens at 300$^{\circ}C$.

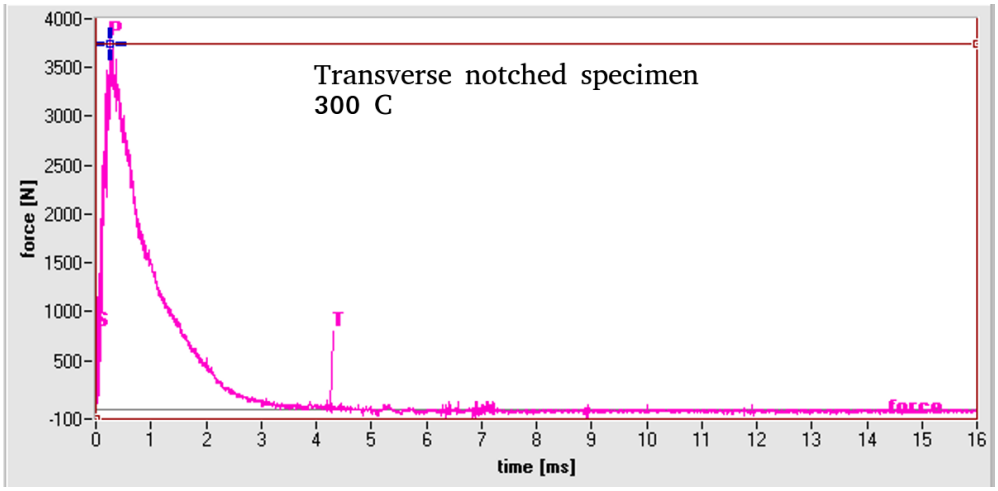

(a)

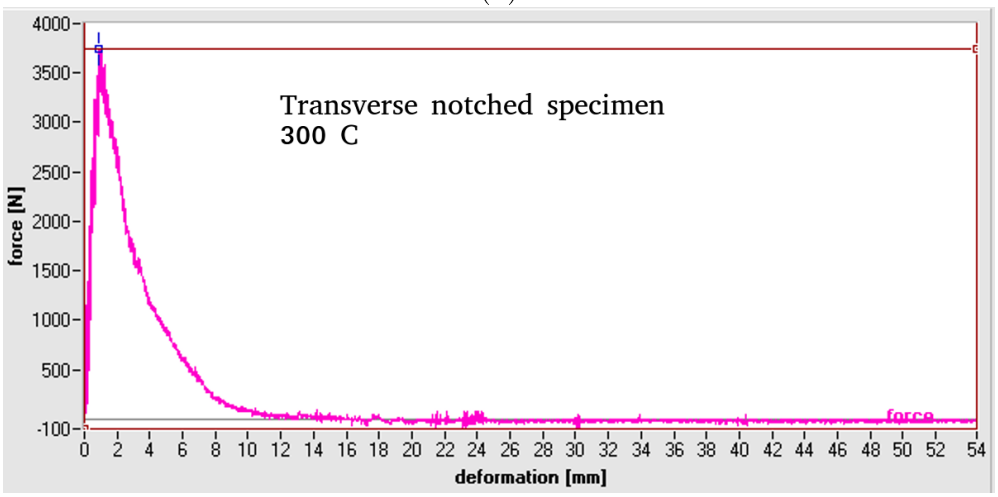

(b)

Figure 5.4: Typical online (a) load-time and (b) load-displacement plots obtained during impact test of transverse specimens at 300 °C.

5.2.3 Metallography and Fractography

Specimens from the undeformed end of the impact-tested samples were sectioned along axial–radial (longitudinal direction of the tube) and radial–circumferential (transverse direction of the tube) planes of the hydrided pressure tube. Standard metallographic techniques were used to prepare the samples. Hydrides were revealed after swabbing for few seconds with an etchant of 10%HF, 45% HNO_3 and 45% lactic acid. Fracture surfaces of broken Charpy specimens were examined under scanning electron microscope (SEM).

5.3 Results and Discussion

Hydrogen concentration (by weight) in the as received material was 10 *wppm* and in the hydrided pressure tube it was 84 *wppm*. Hydrogen charging was fairly uniform in the spools. Figure 5.5 shows the micrograph of the Zr-2.5Nb pressure tube material charged with 84 *wppm* of hydrogen along transverse-radial and axial-radial plane of the tube. Dark lines in these micrographs are the traces of hydride platelets. As is evident from this figure, the hydride platelets are uniformly distributed across the thickness of the tube. The hydride platelets along axial direction appear to be straighter and longer as compared to those along transverse direction and this is expected because the longer α-phase grain dimension along axial direction of the pressure tube provides for uninterrupted growth of hydride platelets along axial direction. The branching of the trace of the hydride on the radial–circumferential plane is due to shorter grain dimension along the circumferential direction of the pressure tube and also due to the lower density of basal pole along the radial direction[12, 108].

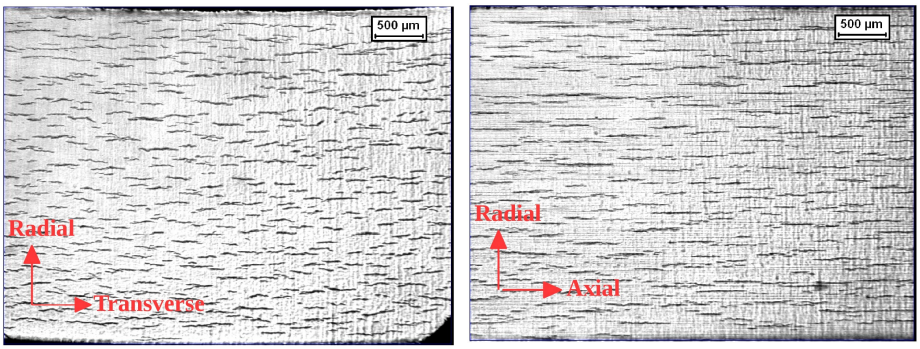

Figure 5.5: Hydride distribution along transverse-radial and axial-radial plane of the hydrided pressure tube spool.

Figure 5.6 shows the variation in impact energy as a function of temperature for axial and transverse samples for both the as-received as well as hydrided specimens of as-fabricated type (i.e of as-fabricated curvature). In case of as-received material, impact energy for the axial samples was observed to increase with increase in temperature nearly linearly up to about 180 $^{\circ}C$ after which it tapered off towards a saturation level. Such a behavior has also been reported [118] for Zircaloy-2 pressure tube material and

has been attributed to enhanced ductility of matrix with increase in temperature. The impact energy values for the samples having crack growth along transverse direction showed much weaker temperature dependence and its values were much lower as compared to those for axial notched samples. Such a drastic reduction in impact energy of the transverse specimens as compared to the axial specimens has been attributed to the combined effect of microstructural and crystallographic anisotropy.

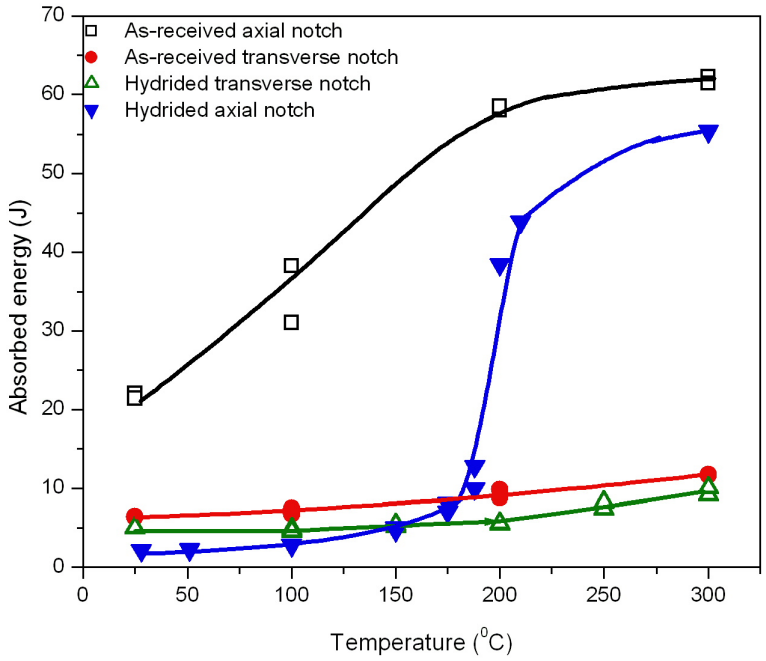

Figure 5.6: Absorbed energy for as-received and hydrided Zr-2.5Nb pressure tube in axial and transverse orientations obtained using specimens having curvature same as that of as-fabricated pressure tube.

The variation in the impact energy value of the hydrided samples of as-fabricated pressure tube curvature type is also shown in Figure 5.6 and the energy values were observed to be lower than as-received material for both types of sample orientation. For the samples facilitating crack growth along axial direction, the hydrided samples showed a remarkable change, as compared to as-received material, in its temperature dependence by exhibiting distinct lower and upper shelf regimes. The temperature dependence of impact energy values for hydrided samples facilitating crack growth along transverse direction showed weak temperature dependence similar to the as-received

material. It may be noted that pressure tubes have predominantly circumferential hydride orientation. The hydrides are like thin pancakes with longer axis along axial direction and shorter axis along the transverse direction. At lower test temperatures brittle hydride platelets act as cracks ahead of the notch and brings about substantial reduction in toughness. The reduction in impact energy for axial specimens due to hydrides is clearly seen Figure 5.6. However, this effect is not very evident in transverse notched specimens as their impact energies are already low.

A comparison of impact energy values of as-fabricated curvature specimens and flattened pressure tube specimens are shown in Figure 5.7 and Figure 5.8 for axial notch and transverse notch specimens of as-received pressure tube. Similar type of plots for the hydrided pressure tube are shown in Figure 5.9 and Figure 5.10. As seen in these figures its clear that the absorbed energy has increased with increase in test temperature for both as-fabricated and flattened impact specimens but the extent of increase is smaller for transverse specimens as compared to that of axial specimens. The as-fabricated axial specimens have shown higher absorbed energy compared to that of flattened axial specimens at all test temperatures as seen in Figure 5.7 whereas Figure 5.8 shows that the transverse specimens of both as-fabricated and flattened type have similar absorbed energy in that test temperature range. In case of hydrided material, the absorbed energy for as-fabricated and flattened specimen type is same over the entire test temperature range for transverse specimens and upto 100 $^{\circ}C$ for axial specimens as seen in Figures 5.9 and 5.10.

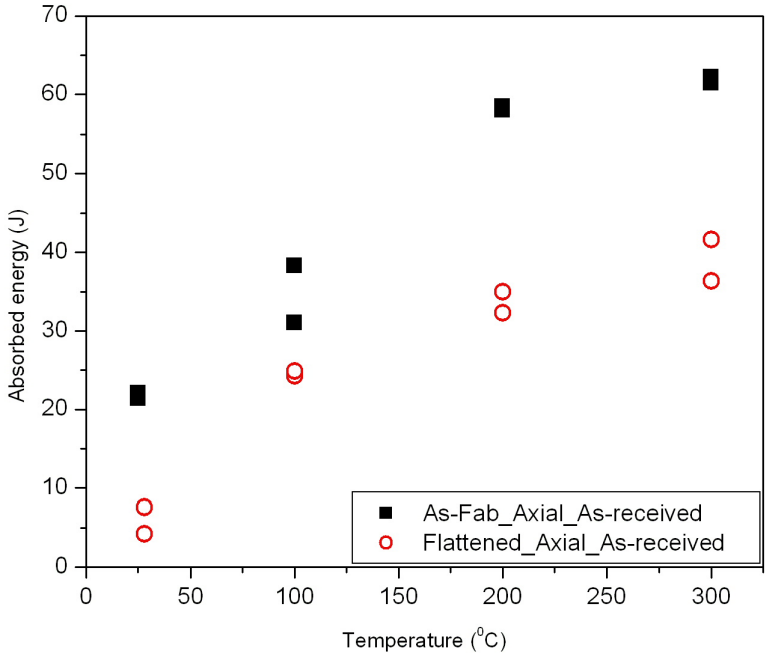

Figure 5.7: Absorbed energies for as-fabricated and flattened pressure tube impact specimens in axial directions.

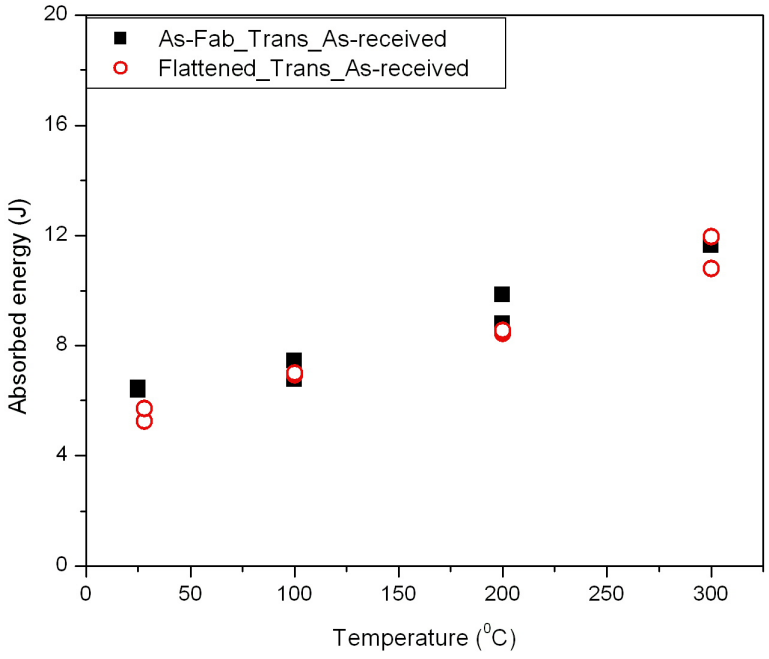

Figure 5.8: Absorbed energies for as-fabricated and flattened pressure tube impact specimens in transverse directions.

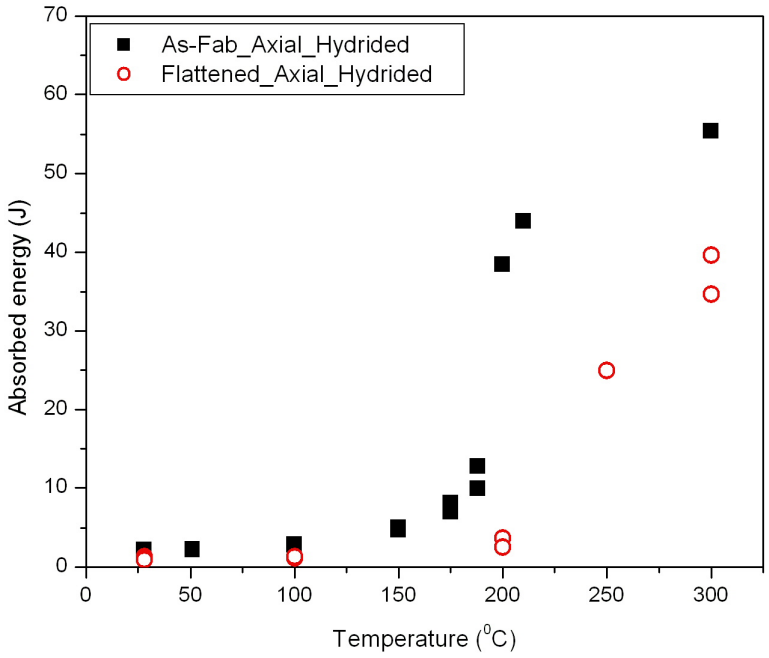

Figure 5.9: Absorbed energies for hydrided pressure tube, as-fabricated and flattened pressure tube impact specimens in axial directions.

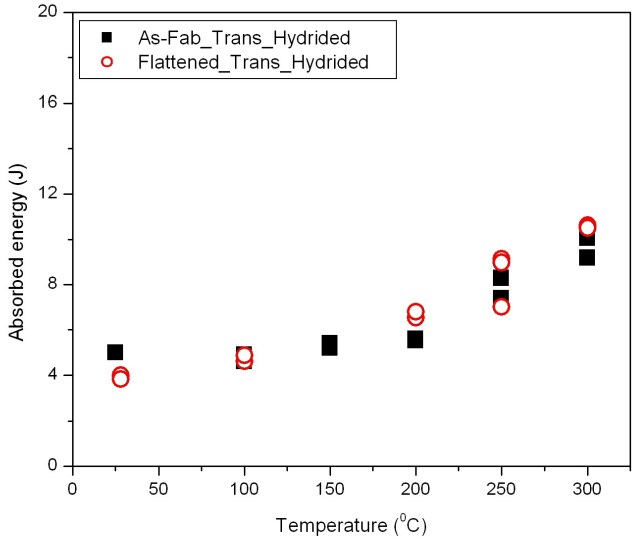

Figure 5.10: Absorbed energies for hydrided pressure tube, as-fabricated and flattened pressure tube impact specimens in transverse directions.

The impact energy data for flattened pressure tube in axial and transverse orientation is plotted in Figure 5.11. From this figure it can be noted that at room temperature

the impact energy is almost same for both axial and transverse orientation and with increasing temperature, the difference in absorbed impact energy between these two orientation increases.

Similar comparison for the hydride flattened pressure tube in axial and transverse orientation is shown in Figure 5.12. It shows that the hydrided pressure tubes have nearly same impact energy at room temperature and different impact energy at 250 $^{\circ}C$ in axial and transverse orientation.

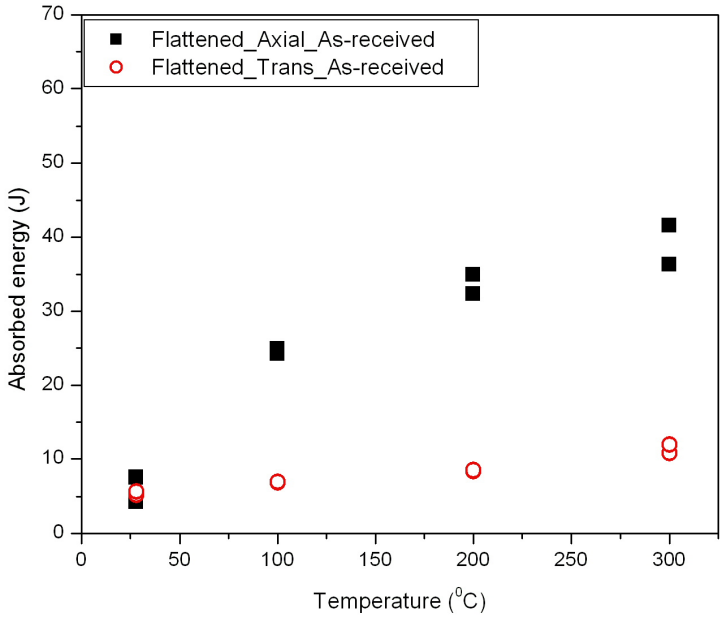

Figure 5.11: Absorbed energies for flattened as-fabricated pressure tube impact specimens in axial and transverse directions.

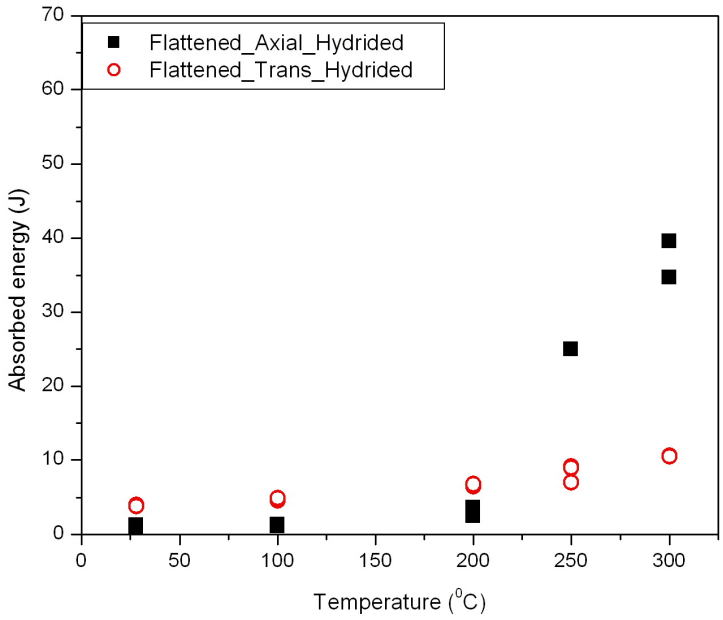

Figure 5.12: Absorbed energies for flattened hydrided pressure tube impact specimens in axial and transverse directions.

The difference in axial and transverse orientation impact energy at high temperature is lower for the flattened pressure tube compared to that of the as-fabricated curvature pressure tube. Due to the nature of curvature in axial specimens, it may be possible that some amount of interaction takes place with test anvil support when material becomes ductile. This may result in higher absorbed energy for axial specimen in addition to what is seen in the flattened specimens, which increases with increase in ductility at higher test temperatures, as seen in Figure. 5.7. The effect of specimen curvature is minimal for transverse specimens, as they are straight along the length direction, with very small curvature in the width direction, as seen in Figure. 5.8.

It is well known that high strength materials show low energy ductile fracture and are temperature insensitive. The low impact energies indicate the ease with which fracture is initiated and propagated in high strength materials. Zr-2.5Nb pressure tube material has relatively high strength and it shows no change in fracture micro-mechanism, which is always ductile fracture, in the range of test temperature under this study. The total absorbed energy in impact test corresponds to the crack initiation

energy plus propagation energy or total amount of plastic work done during fracture. The crack initiation energy, corresponding to peak load in instrumented impact tests, has been found to be more or less same for axial and transverse orientations at all test temperatures. The primary difference is in the propagation energy wherever difference in impact energy is observed.

At room temperature and under impact loading, Zr-2.5Nb absorb low energy in both axial and transverse notched specimens. The axial notched specimens, where loading ahead of the crack tip is in transverse direction that contains around 60% of the basal poles, material is able to deform more with increase in temperature due to activation of more slip and twin systems, and therefore the amount of plastic work energy increases with temperature. Much more extensive zone of deformation ahead of the notch tip can be seen in Figure 5.13(b) at $300\,^{\circ}C$ as compared to that seen in Figure 5.13(a) at room temperature.

At room temperature, the axial notched impact specimens showed relatively wider and shallower deformed zone ahead of the notch as compared to thin and slightly raised portion ahead of transverse notch. The transverse specimens showed relatively steeper and larger slanted region on both sides of fracture surface as compared to axial notch.

In case of transverse notched specimens, where crack tip gets loaded along axial direction that has around 10% of the basal pole, deformation is expected to be easier and similar at all test temperatures and this is supported by the relatively small change in impact energy with test temperature, as seen in Figure 5.11. The nature of zone of deformation ahead of notch tips as seen in Figure 5.14 also shows little change between room temperature and $300\,^{\circ}C$. Surprisingly, absorbed energies for this orientation has been found to be lower than the axial notch specimens at elevated temperatures. The reason for this needs further investigations to find out the reasons for smaller amount of plastic work for crack propagation in this direction.

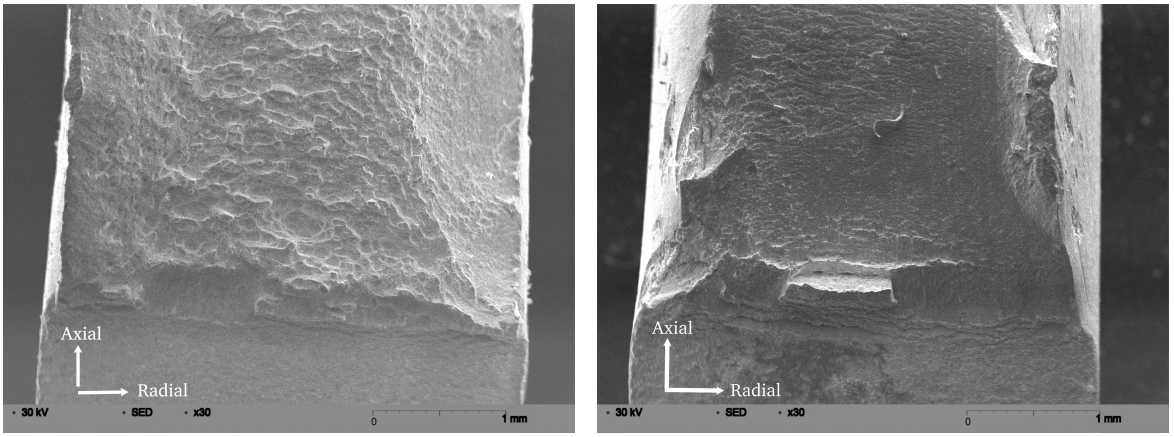

(a) (b)

Figure 5.13: Fracture surfaces of as-received flattened axial impact specimens tested at (a) room temperature and (b) 300 °C, showing larger deformed zone ahead of notch tip at elevated temperature.

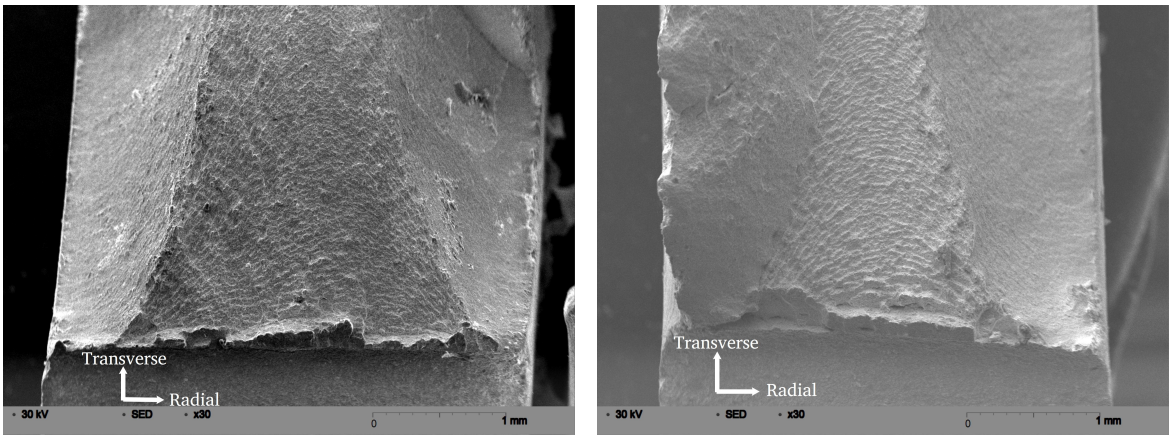

(a) (b)

Figure 5.14: Fracture surfaces of as-received flattened transverse impact specimens tested at (a) room temperature and (b) 300 °C, showing nearly similar deformed zone ahead of notch tip.

In hydrided material, brittle hydride platelets are present in the matrix at room temperature. As even unhydrided material fractured with low total absorbed energy at room temperature, the presence of hydrides did not make significant difference. Only the fracture surface showed presence of small splits associated with brittle hydride presence, as seen in Figure 5.15(a).

At 300 °C, most of the hydrides platelets will undergo dissolution in the Zr matrix. The matrix itself becomes softer and ductile and very little hydride crackings are seen, as seen in Figure 5.15(b) . Due to hydride dissolution and matrix getting softter, tran-

sition in absorbed energy with temperature is seen in axial hydrided impact specimen. The transverse specimens, however, continue to have low absorbed energy. Fracture surfaces of hydrided flattened transverse impact specimens tested at room temperature and 300 $^{\circ}C$ are shown in Figure 5.16.

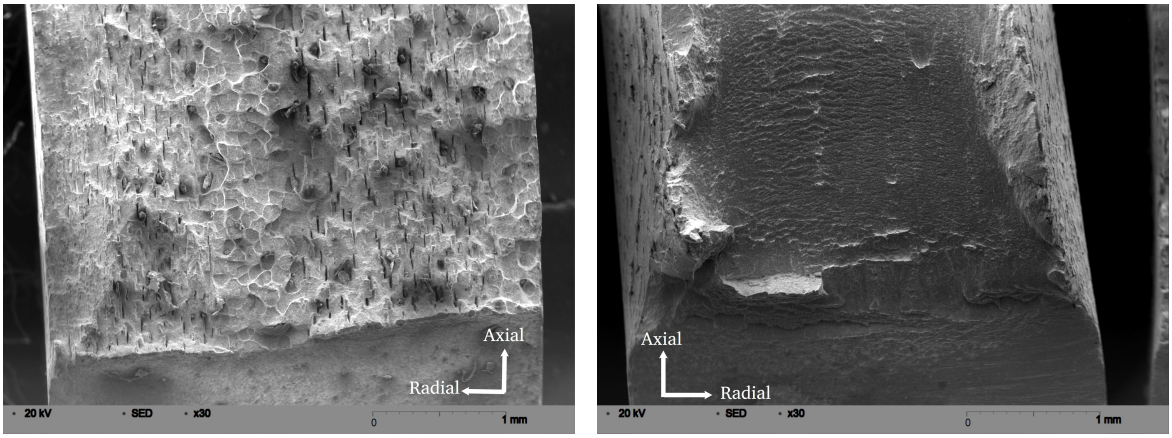

(a) (b)

Figure 5.15: Fracture surfaces of hydrided flattened axial impact specimens tested at (a) room temperature showing shallow ductile rupture and hydride platelet cracks and (b) 300 $^{\circ}C$ having larger deformed zone ahead of notch tip and no hydride cracking.

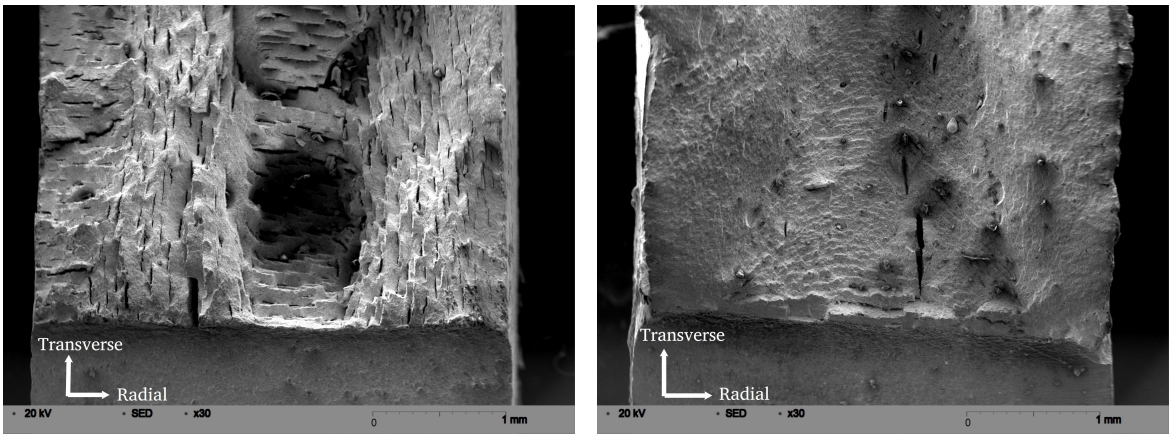

(a) (b)

Figure 5.16: Fracture surfaces of hydrided flattened transverse impact specimens tested at (a) room temperature and (b) 300 $^{\circ}C$.

5.4 Conclusions

The following conclusions could be drawn from this work:

- Zr-2.5Nb pressure tube showed near similar impact energy at room temperature in axial and transverse orientation in the flattened and stress relieved condition. At higher temperatures crack growth along axial direction absorbs more energy.
- Ductile-to-brittle-transition at around $200\,^{\circ}C$ was also clearly exhibited by hydrided Zr-2.5Nb pressure tube alloy, when crack growth occurs along axial direction on the radial-axial plane, under dynamic loading.
- Fractographic examination revealed distinct features when crack growth occurs in axial and transverse direction. The change in absorbed energy could be correlated with the nature of deformation ahead of the notch tip, as seen by SEM examinations.

Chapter 6

Fracture toughness and DHC behavior of irradiated Zr-2.5Nb pressure tubes from Indian PHWR

6.1 Objective

The primary objective of this study was to study the fracture toughness and DHC behavior of Indian irradiated Zr-2.5Nb pressure tube material.

Fracture toughness of irradiated pressure tubes and rolled joint regions, after different fluence and hydrogen concentrations, were characterized in detail. The rolled joint portion of the tube has significant amount of residual tensile stresses and higher hydrogen/deuterium concentration than the pressure tube main body. This tensile residual stress, in combination with the normal operating hoop stress, may lead to varying degree of hydride reorientation in radial-axial plane in the rolled portion. Thus effects of a) different neutron fluence b) hydrogen concentration as it occurs in actual service have been studied. The objective of the present investigation is to assess the fracture toughness of the irradiated pressure tubes using single specimen J-integral test method and compare it with the data available in the open literature. Two different pressure tubes having slightly different alloy chemistry and operating time have been studied

to assess the effect of small change in alloy chemistry and trace element impurities that is manifested in form of tube to tube variability in fracture properties.

DHC velocity measurements have been carried out on the irradiated Indian pressure tube material.

The main idea has been to get an estimate of End of Life (EOL) properties for the irradiated pressure tubes, that are currently used in Indian PHWRs, and to study their fracture toughness and DHC behavior. The results from this study would enable safety assessment including leak before break analysis for PHWR coolant channels over its operating life.

6.2 Experimental

The experimental setup for fracture toughness test consisted of a servo hydraulic universal testing machine located inside a lead-cell and a DCPD system. A resistance heated furnace was attached to the testing machine for carrying out the test at high temperatures with a temperature control within $\pm 4^{o}C$. The machine, with movable lower crosshead, had computerized test control and data acquisition systems.

The experimental setup for DHC test consisted of the servo hydraulic universal testing machine, constant load test set up with a furnace located inside lead-cell and a DCPD system consisting of a constant current source and a nano-voltmeter.

The experimental details have been given in Section 3.8.

6.2.1 Material

The materials used for fracture toughness study were double melted, cold worked and stress relieved (CWSR) Zr-2.5Nb pressure tubes from KAPS-2 PHWR. The channel locations were S-7 and Q-10 of the reactor, as shown in Fig. 3.4 on page 41 and they had respectively experienced about 8 and 12 EFPY of reactor operation. DHC velocity measurement was carried out on specimens prepared from irradiated S-7 pressure tube. In absence of sufficient S-7 pressure tube offcut material, DHC tests were carried out

on other as-fabricated pressure tube of similar specification.

The pressure tubes were fabricated at Nuclear Fuels Complex (NFC), Hyderabad, India using two stage hot extrusion followed by two stage cold pilgering with an intermediate stress relief annealing and autoclaving i.e. double melted PT fabrication route as described in Section 2.2. These two tubes, S-7 and Q-10, had different ingot origin and thus had minor variation in alloy chemistry and mainly impurity concentration. Tube S-7 was made from foreign billet and Q10 was made from indigenous ingot.

Typical microstructure of the as-fabricated and irradiated tube (S-7) as seen under Transmission Electron microscope (TEM) are shown respectively in Figure 2.6(b) and Figure 6.1 [39, 105]. The irradiated TEM specimen location was at the 3.38 m from the inlet end with $\approx 3.6 \times 10^{25}\ n/m^2$ fluence and operated at the temperature of around $283\,^{\circ}C$ as shown in Figure 3.7. Microstructural observation of unirradiated off-cuts of S-7 [39] showed the lamellar morphology of the α -Zr along with the β -phase present as stringers between two α-laths as well as fine and coarse β globules. The size of α -Zr lamellae was found to be in the range from 0.17 to 0.2 μm, 1.8 to 2.4 μm and 1.7 to 2.8 μm in the radial, circumferential and axial direction respectively (aspect ratio of 1:7:8). The irradiated S-7 pressure tube had average α-grain size 0.17-0.27 μm, 1.7-2.3 μm in radial and axial directions respectively [44]. The aspect ratio of α-grains remain same even after irradiation. The grain morphology of α-Zr phase in the Zr-2.5Nb alloy pressure tube did not change appreciably after irradiation. The grain size in terms of length and aspect ratio and the size distribution were nearly similar to that seen in the unirradiated sample [39]. Extensive modification in β morphology was seen at the high flux and high temperature regions of the pressure tubes [44]. The β phase was observed to have globulised completely in many regions. They were present at the interface of α-Zr laths as well as within the lath. The Nb concentration of the β phase appeared to have increased and the volume fraction had reduced.

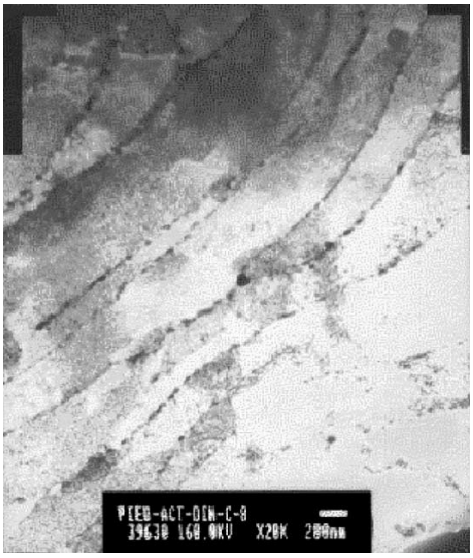

Figure 6.1: TEM microstructure of irradiated pressure tube S-7, at 3.38 m from the inlet end, as seen in transverse-radial plane showing discontinuous β-phase [105].

The profile of H_{eq} along the length of the irradiated pressure tube S-7 is shown in Figure 6.2 [105] .The irradiated pressure tube S-7 had maximum H_{eq} concentration of 16 *wppm* and small hydrides platelets were uniformly distributed across the tube cross-section (transverse-radial plane) as shown in Figure 6.3(a) [105]. The irradiated pressure tube Q-10 contained 10-14 *wppm* H_{eq} and hydrides were uniformly distributed throughout the pressure tube as shown in Figure 6.3(b).

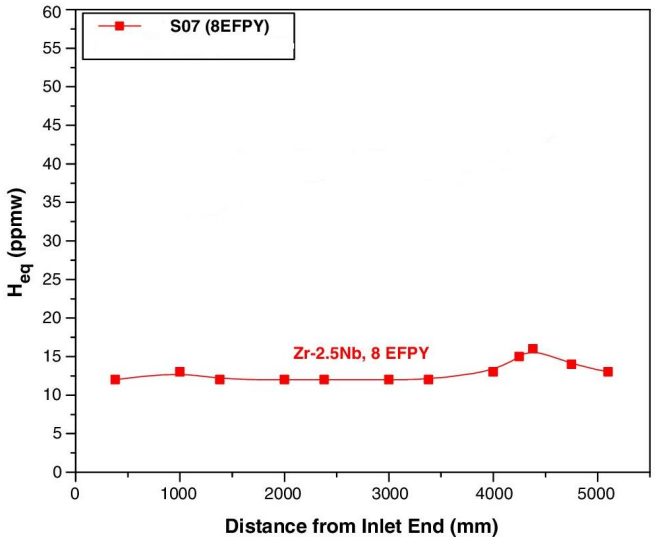

Figure 6.2: Measured H_{eq} along the length of the irradiated pressure tube S7 after 8 EFPY [105].

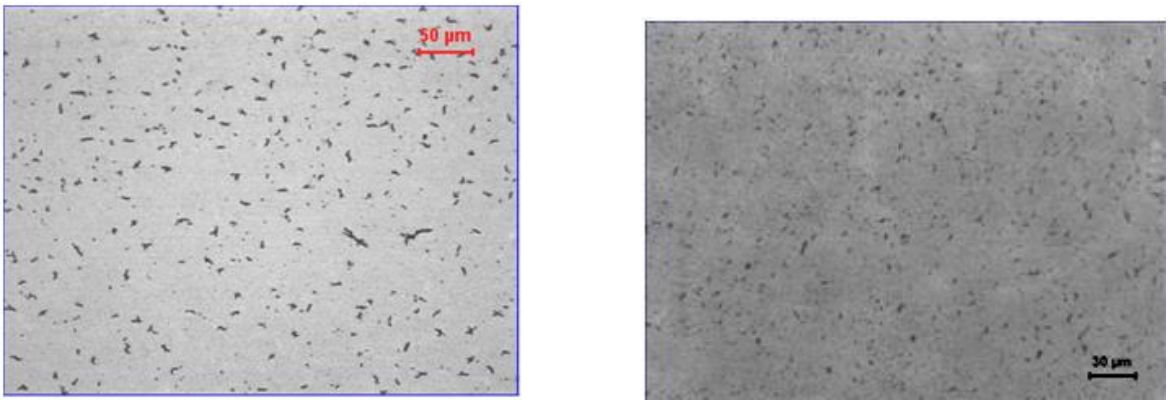

(a) (b)

Figure 6.3: Hydride distribution (dark phase) in the irradiated pressure tubes (a) S-7 and (b) Q-10 in transverse-radial-plane where radial direction is along the vertical axis [105].

S-7 and Q-10 both the pressure tubes were removed from reactor to serve as surveillance pressure tubes. The rolled joint region of the Q-10 pressure tube was received in the form of strips of 185 to 200 mm lengths. One such roll joint strip is shown in Figure 6.4. Fracture toughness properties have been evaluated for these tubes as well as for Q-10 rolled joint stub portion, which contained much more hydrogen than that of the pressure tube main body as seen in the Figure 6.5 in profile of H_{eq} along the length of the irradiated pressure tube Q10 that include both pressure tube main body as well as roll joint portions at the cold end of the pressure tube.

Figure 6.4: Part of rolled joint stub piece from irradiated pressure tube Q10.

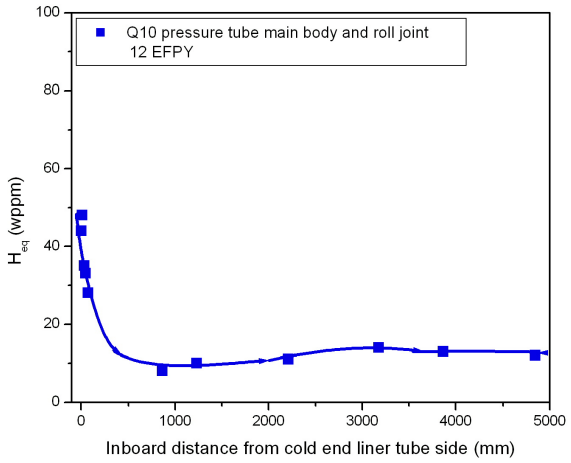

Figure 6.5: Measured H_{eq} in the cold end rolled joint and main body of the irradiated pressure tube Q10.

6.2.2 Specimen preparation

Specimen preparation for fracture toughness test

Circular disk coupons of 30 mm diameter were punched out or trepanned at a distance of around 1 meter from both inlet and outlet end of the irradiated pressure tubes. Specimens were also made from different portions of the roll joint stub. Then, the coupons were transferred to a custom made drilling and notching setup, inside the lead cells, to drill out two pin holes and a central slit with a sharp V-notch tip to get DCT specimens. For irradiated S-7 pressure tube specimens, four Zr-4 wires were spot welded,as explained in Chapter 3, at the slit mouth and at the top and bottom side of each of the DCT specimen to function as potential drop and current input leads as shown in Figure 6.6. The test specimen from the roll joint stub is shown in Figure 6.7.

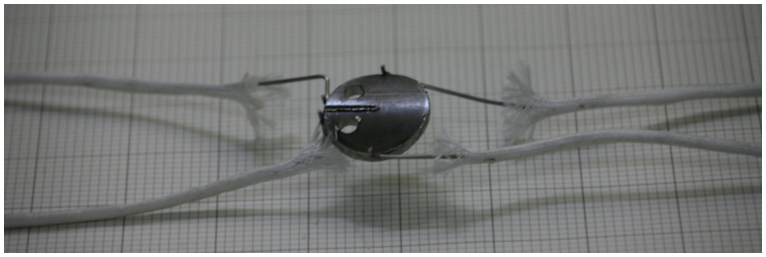

Figure 6.6: Irradiated DCT specimen with welded wires.

Figure 6.7: DCT specimen prepared from the roll joint stub.

Specimen preparation for DHC test

DCT specimens, just like used for irradiated pressure tube fracture toughness tests, with a radial-axial notch, were fabricated from the pressure tubes for DHC test. Irradiated specimens were taken from the hot-end (∼4.2 meter from the inlet end) of the irradiated pressure tube S-7. Fast neutron fluence (energy $> 1\ MeV$) and temperature seen by this portion of the pressure tube were around $2.76\,X\,10^{25}\ n/m^2$ and $291\,^{\circ}C$ respectively. Both as-fabricated pressure tube and irradiated S-7 pressure tube specimens were hydrided using electrolytic hydriding method to about100 $wppm$ hydrogen equivalent (H_{eq}) [109]. The actual H_{eq} concentration after charging was found to be ≈75 wppm by DSC technique.

6.2.3 Standardization of fracture toughness test procedures

The fracture toughness tests on more widely used 26 mm wide curved compact tension specimens and 30 mm diameter disk CT specimens used in present work (as shown in Figure 6.8) were carried out on an unirradiated double melted CWSR Zr-2.5Nb pressure tube. All the criteria for data qualification in fracture toughness tests as mentioned earlier in Chapter 3 could not be satisfied. But, since the specimen thickness was same as that of component thickness, the data are relevant. Data falling in between the two exclusion lines at 0.15 mm and 1.5 mm offset were fitted to a power law and straight line. The slope of the straight line gave dJ/da. The $J-value$ on the power law

curve corresponding to the crack initiation point (obtained from the DCPD output) is taken as J_q (i.e crack initiation toughness). The analysis process used for both the CCT and DCT specimens were exactly same and so the data obtained from the two types of specimens could be compared.

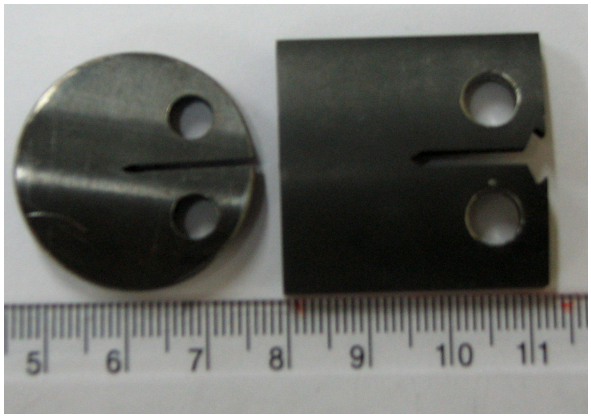

Figure 6.8: DCT, CCT specimens fabricated from pressure tube.

The $J-\Delta a$ curves obtained using the CCT and DCT specimens from unirradiated Zr-2.5Nb material were compared and is shown in Figure 6.9. The J-Δa curve from DCT specimens were only marginally lower than the $J-\Delta a$ curve obtained using the CCT specimens. Thus the$J-\Delta a$ curves generated using these two types of specimens can be considered equivalent. This equivalence implies that the Disk CT specimens can be used for estimating the $J-\Delta a$ curve of the material. DCT specimen is of use in the irradiated pressure tube studies, as punching out or trepanning a 30 mm disk from an irradiated pressure tube is easier than machining of a rectangular CCT specimen. This study also helped to standardize the test procedures to be used for irradiated pressure tube testing.

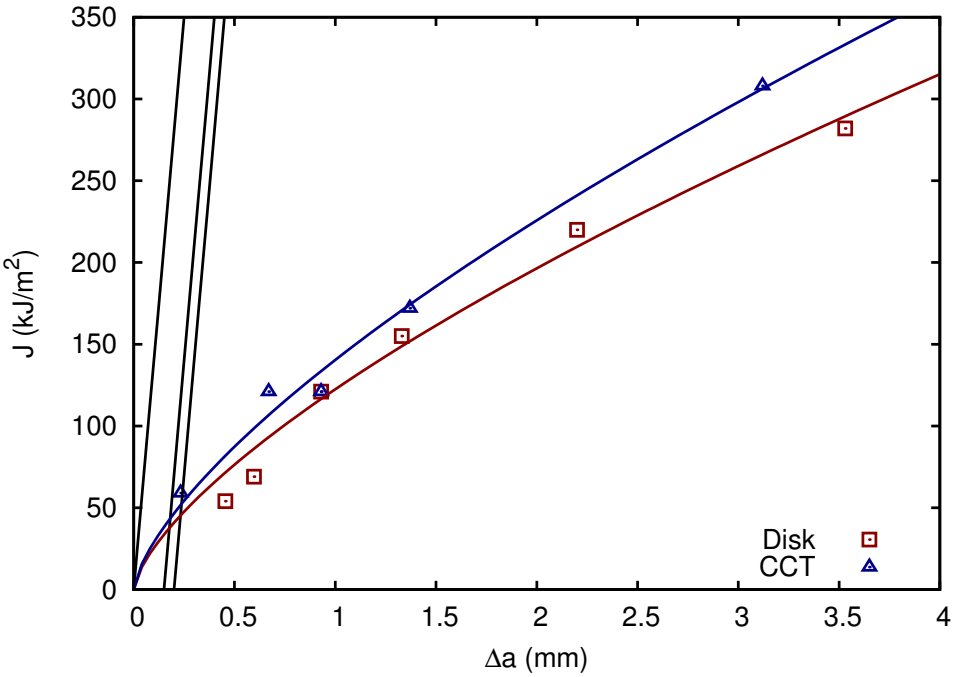

Figure 6.9: Comparison of $J - R$ curves obtained using DCT and CCT specimens for the as-fabricated pressure tube, showing their equivalence.

6.2.4 Fracture toughness test of irradiated pressure tubes

The important steps in experimental work involved fatigue precracking, loading of specimen, heat tinting, post fatigue fracture, crack length measurement by image analysis, load-displacement-DCPD voltage drop data analysis and J-integral calculation for each of the fracture toughness tested DCT specimen. Finally J versus $\triangle a$ plots were obtained for different test temperatures. Data analysis

For tests with DCPD system

For each of the tested specimens of S-7, the digital outputs from the machine and DCPD unit, i.e. load-displacement and DCPD voltage output, were analysed to get the crack lengths and corresponding area under the load-displacement plot. Crack growth initiation was detected from the intersection point of the two tangents drawn at the two slope regions in the voltage drop versus displacement output (Figures 6.10 and 6.11). First slope corresponds to the crack tip blunting and second one to the crack growth. Since the total crack extension was very limited (around 3 mm), a

linear relationship was assumed between measured voltage drop and measured crack length. The verification of linear relation is already given in Section 3.8.6. These data were then analysed as explained in Chapter 4, using the equations for DCT specimens instead of compact tension specimens, as per ASTM E 1820-11 [115] to get the J versus $\triangle a$ plot for each of the specimen tested.

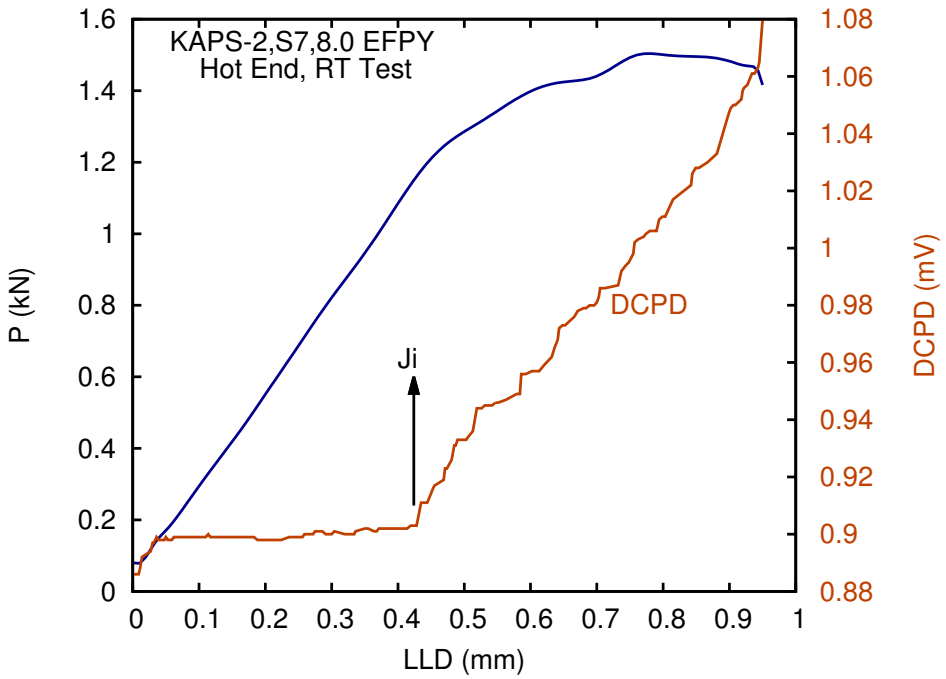

Figure 6.10: Typical load and DCPD voltage drop versus load line displacement (LLD) plot for fracture toughness test at 25 $^{\circ}C$ for irradiated pressure tube.

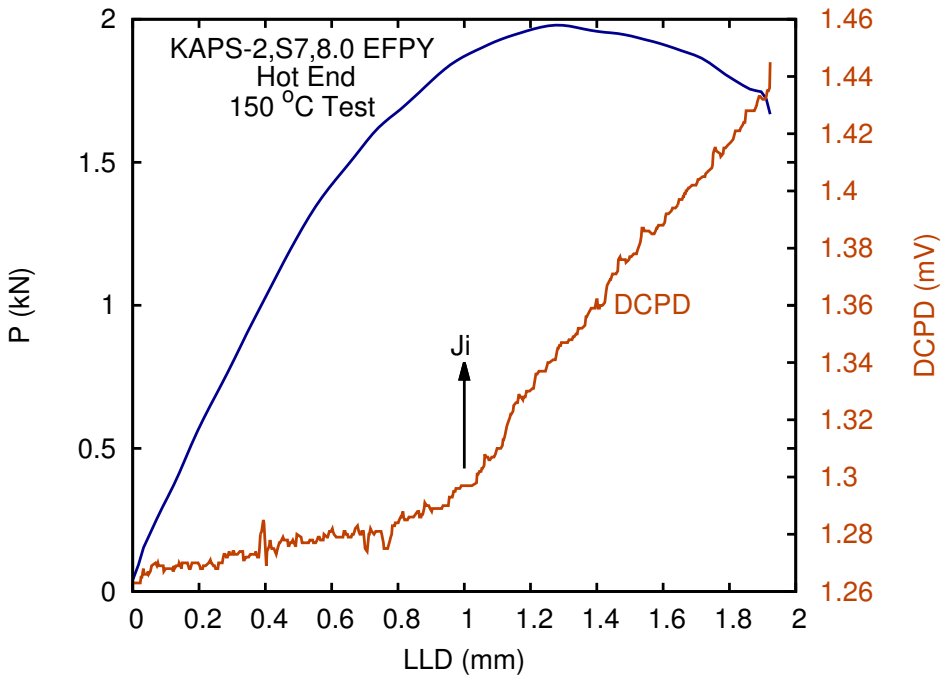

Figure 6.11: Typical load and DCPD voltage drop versus load line displacement (LLD) plot for high temperature fracture toughness test.

For test analysis as per load normalisation method

The load-displacement plots obtained from the tests of Q-10 pressure tube and its roll joint stub were analysed as per load normalization method [83, 115] as explained in Chapter 3. DHC test

The details of the DHC test parameters are given in Section 3.8.5 in Chapter 3. One of the plots of temperature and voltage drop versus time for the test at 250^{o}C is shown in Figure 6.12. The time at which the specimen was loaded after attaining the constant test temperature was manually noted down. After loading, since temperature is constant, the change in voltage is due to crack growth only. The time when the voltage started increasing after loading of the specimen could be calculated. The difference in time, between the time of loading the test specimen at the constant test temperature and the time of start of increase in DCPD at that constant test temperature, gives the incubation period (T_i). This (T_i) is then used in Equation 3.17 to get the actual time in which crack has grown by DHC, which then can give DHC velocity once we know the extent of crack growth $\triangle a_{DHC}$.

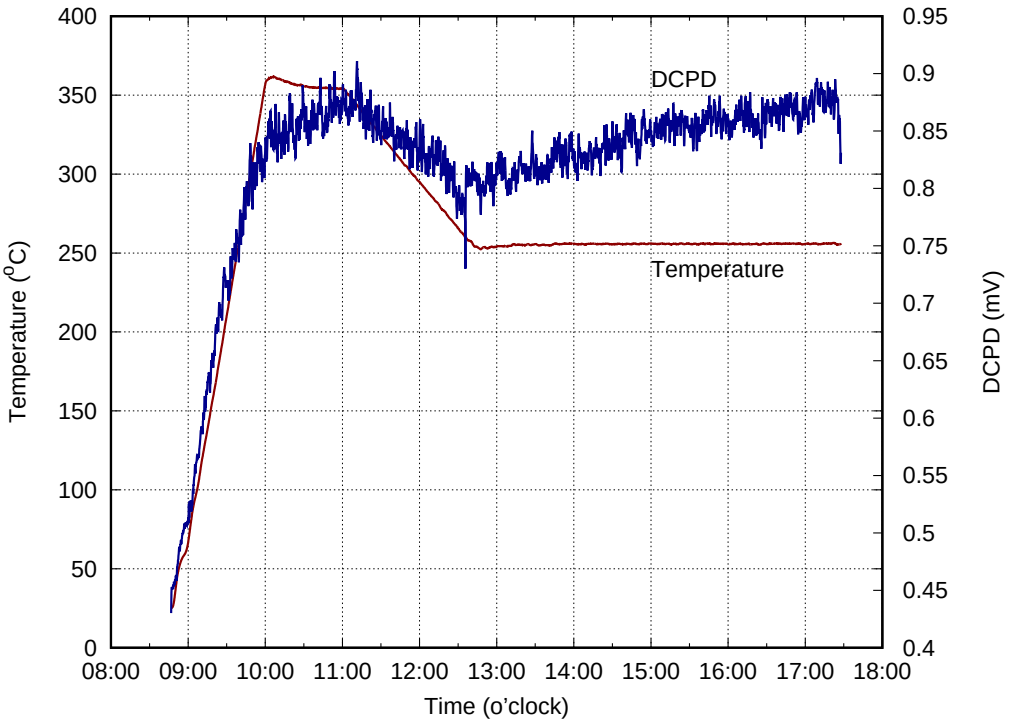

Figure 6.12: Typical plots of temperature and voltage drop versus time for DHC test at 250 $^{\circ}C$.

The incubation period was found to vary from 10 minutes to 225 minutes. It was also found to vary from specimen to specimen even for tests at same temperature. Incubation period was 95 minutes and 225 minutes for two specimens tested at 210^{o}C. For specimens tested at 250^{o}C and 290^{o}C it was slightly lower and varied from 15 to 60 minutes.

After the test, specimens were fractured by applying fatigue load. The fractured specimen surfaces were photographed using high resolution digital camera and these photographs were used for initial and final crack length measurement. Different regions on the fracture surface are shown in Figure 6.13.

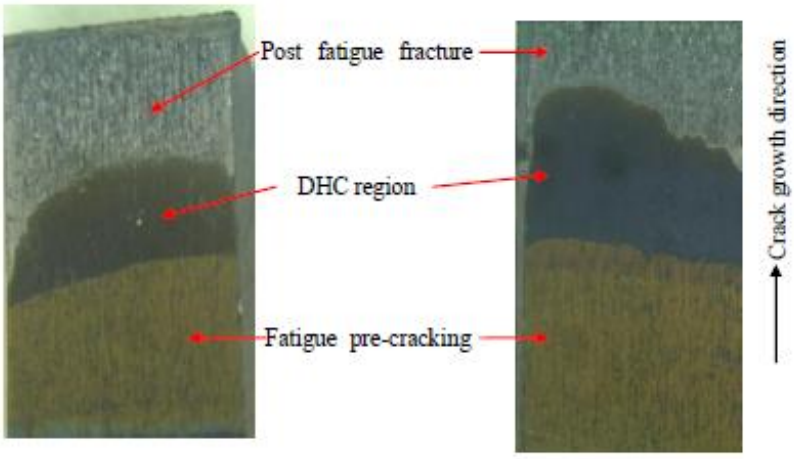

Figure 6.13: Fracture surface of the DHC tested specimens showing different regions.

6.2.5 Metallography, SEM and hydrogen equivalent concentration estimation

Small pieces, cut from the tested specimens, were used for metallography and determination of H_{eq} using the DSC technique. Fracture surfaces of some of the tested specimens were examined using SEM to study the fracture morphology.

6.3 Results and Discussion

It is reported that CWSR Zr-2.5Nb pressure tube material shows saturation in irradiation damage due to fast neutron flux at fluence of about 1.6×10^{25} n/m^2 that is equivalent to 3 to 4 EFPY of operation [5, 17, 41]. The pressure tubes S-7 and Q-10, which were in service for about 8 and 12 EFPY respectively, would thus be expected to have attained limiting reduction of fracture properties so far as the contribution from neutron irradiation is concerned.

6.3.1 Fracture toughness of Indian irradiated pressure tubes

6.3.1.1 Test results of irradiated S-7 pressure tube

Typical load-load line displacement-DCPD voltage drop plots for room temperature and high temperature tests are shown respectively in Figures 6.10 and 6.11. These figures show that the nature of increase in the DCPD value during the J-integral tests at 25 $^{\circ}C$ i.e. room temperature differs from that at higher test temperature. At 25 $^{\circ}C$ the DCPD increases abruptly at the initiation of crack growth, with absence of a slow rise in the DCPD values related to the crack tip blunting during the specimen loading and this is due to the low toughness of the irradiated material at 25 $^{\circ}C$. The J-integral tested specimen fracture surface for the specimen tested at 175 $^{\circ}C$ is shown in Figure 6.14. The J vs. $\triangle a$ plots obtained for irradiated Zr-2.5Nb pressure tube at different temperatures are shown in Figure 6.15. The crack growth at 25 $^{\circ}C$ starts at low load, corresponding to J-initiation (J_i) in the range 9 to 13 kJ/m^2. Sudden crack jumps have been observed at low temperature (25 to 100 $^{\circ}C$) tests. Table 6.1 gives the measured values of fracture toughness parameters for irradiated Zr-2.5Nb pressure tube S-7. For the irradiated pressure tube S-7 the values of the initiation fracture toughness J_i at room temperature was 9-13 kJ/m^2 and at 300 $^{\circ}C$ the corresponding value was 104 kJ/m^2. Some drops in fracture toughness at higher test temperatures as seen in Table 6.1 are basically due to scatter in toughness of irradiated pressure tube material.

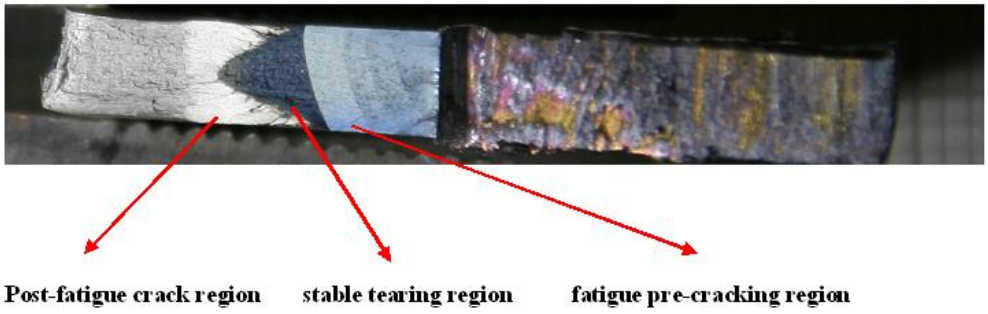

Figure 6.14: Fracture surface of the disk compact tension specimen tested at 175 $^{\circ}C$.

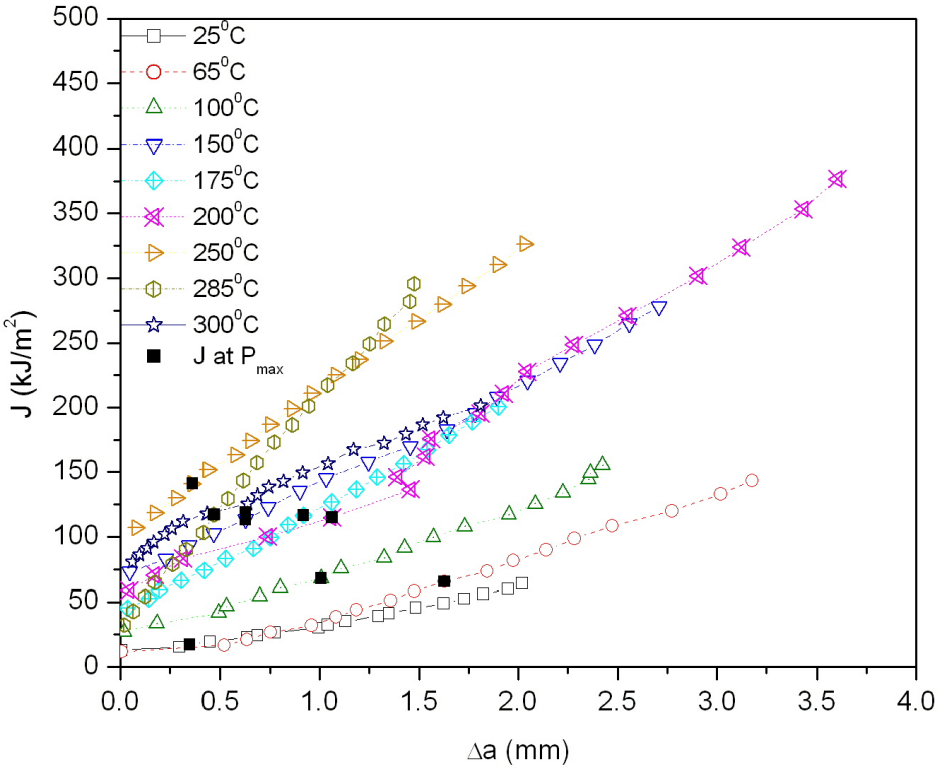

Figure 6.15: J **vs.** Δa **plots obtained for irradiated Zr-2.5Nb pressure tube S-7 at different test temperatures.**

Table 6.1: Fracture toughness parameters for irradiated S-7 pressure tube.

Temperature ($^{\circ}C$)	J_i (kJ/m^2)	J_{max} (kJ/m^2)	dJ/da (MPa)
25	9-13	17 - 35	16 - 28
65	12	65	47
100	27-46	70-116	54-83
150	50 - 70	100 - 110	60 - 80
175	60	116	85
200	59 - 78	120 - 140	80 - 95
250	104	125	112
285	80-100	115-130	100-175
300	104	127	110

The applied J values (J_{app}) due to coolant internal pressure for the pressure tubes can be calculated using several formula. One such relation is obtained by using the strip yield model [61] for a through wall axial crack in a tube, with the Folias correction factor for tube bulging:

$$J_{app} = \frac{8a\sigma_f^2}{\Pi E} ln \left[sec \frac{\Pi M \sigma_h}{2\sigma_f} \right] \tag{6.1}$$

$$M = \left\{ 1 + 1.125 \frac{a^2}{Rt} - 0.0135 \left(\frac{a^4}{R^2 t^2} \right) \right\}^{\frac{1}{2}} \tag{6.2}$$

where, σ_f is the flow stress, σ_h hoop stress corresponding to coolant pressure, a is the half crack length, M is Folias correction factor for tube bulging, E is Young's modulus, R is tube radius and t is the tube wall thickness.

After crack initiation, Zr-2.5Nb shows considerable slow, stable crack growth under rising load [129]. The value of J_i of the material has been used to estimate, in a conservative way, the critical pressure for the initiation of crack growth, for a through wall axial crack.

Table 6.2 shows the estimated values of the critical internal pressure, as per equation 6.1, based on the J_i values obtained for the irradiated pressure tube at different test temperatures. These were calculated for an inner diameter of 86 mm, assuming 5% creep on initial diameter of 82.5 mm (as the design allowance for the diametral expansion of pressure tubes is conservatively limited to 5% of the initial pressure tube diameter [8]), though the actual diametral creep of irradiated pressure tube S7 was much smaller than 5% as given in Reference [105], to get the conservative values of critical pressures. Wall thickness (t) of 3.5 mm and the flow strength of the irradiated pressure tube was taken as $\sigma_f = 888 - 0.745$T where σ_f is flow stress in MPa and T is temperature in $^{\circ}C$ based on the transverse ring tensile tests of the irradiated pressure tube at different temperatures [103]. The calculation was performed for a through wall axial flaw lengths of 4*t, 5.5*t, 7*t. In real-life case, crack shows stable crack growth during loading, and any unstable fracture is expected only after some amount

of crack extension, and at a higher J_{app} value that is closer to the J_{max} value. This would contribute to additional margin of safety on this calculated critical pressure.

Table 6.2: Estimated critical pressure based on the initiation fracture toughness.

Material (Zr-2.5Nb)	Temperature (^{o}C)	J_i (kJ/m^2)	Critical Pressure (MPa)		
			a/t=4	a/t=5.5	a/t=7
Irradiated pressure tube	25	9	11.96	10.27	9.1
(S7, KAPS-2) around	65	12	13.65	11.7	10.4
8 EFPY of operation	100	27	20.02	17.16	15.34
	150	50	25.09	22.1	19.76
	175	60	29.9	23.4	18.2
	200	59	26.52	22.62	21.06
	250	104	31.85	27.3	26.13
	285	80	31.3	24.8	19.9
	300	104	31.85	27.3	26.13

The pressure tube design is based on the leak before break (LBB) criterion, which is based on the detection of any leaking through thickness crack before it attains the critical crack length (CCL) that may lead to unstable tube rupture. The critical crack length values for the pressure tube at different temperatures expected during reactor operation is evaluated from the J_{max} values by iterative method as per equation 6.1 where the J_{max} value is put in place of J_{app}. Here credit is taken for the small amount of stable crack extension observed in the pressure tube alloy.

The CCL values were obtained for the irradiated pressure tube S-7, with an internal diameter of 86 mm and thickness 3.5 mm, for a 120 MPa hoop stress. The CCL values varied from 29 mm at 25 $^{\circ}C$ to 56 mm at 250 $^{\circ}C$. Figure 6.16 shows the plot of CCL values versus temperature. The J_{max} values from the pressure tube burst test have been found to be generally more than that from the compact tension specimens

[58]. Thus an additional margin of safety is introduced by using CCT specimens [61]. In experiments on unirradiated pressure tubes, it has been seen that DCT and CCT specimens give nearly same fracture toughness. Thus it can be concluded that the use of DCT specimens would also lead to additional margin of safety as compared to the burst tests. In short, the calculated critical pressure given here, represents a conservative estimate without taking credit for any stable crack extension and geometry effects found in the actual size pressure tube burst tests [61]. Since the critical pressure required for crack initiation is greater than the internal coolant pressure, any crack below length of 7 times wall thickness, is unlikely to grow under operating condition. Before any through wall crack reaches this size it shall give sufficient leakage of hot heavy water coolant in the annulus gas to get detected and reactor would be shutdown. However, for temperatures below $100\,^{\circ}C$, it is advisable to increase the coolant pressure slowly with increase in coolant temperature to have adequate margin of safety.

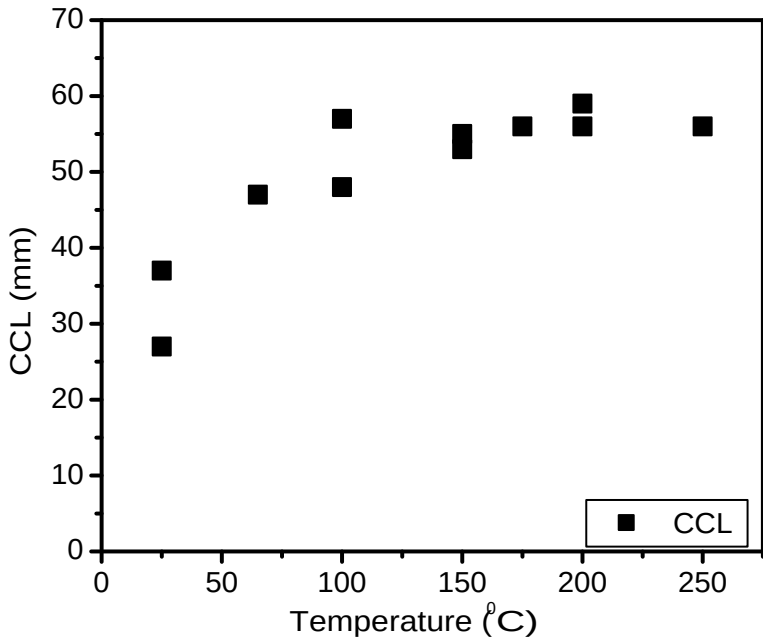

Figure 6.16: Plot of calculated critical crack length (CCL) for irradiated pressure tube S-7 at different temperatures corresponding to hoop stress of 120 MPa.

Figure 6.17 compares the irradiated Indian pressure tube data with irradiated pressure tube data available in the literature [4, 130]. The crack growth resistance of S-7 pressure tube falls near the mid range of the reported values. It may be noted

that the fabrication routes for these tubes are different from the Indian pressure tube. Also we can note here that dJ/da of irradiated S-7 that contained around 1.37 $wppm$ chlorine matches well with the dJ/da range shown in the Figure 2.10. It indicates that irrespective of the fabrication route the effect of chlorine on fracture toughness is similar.

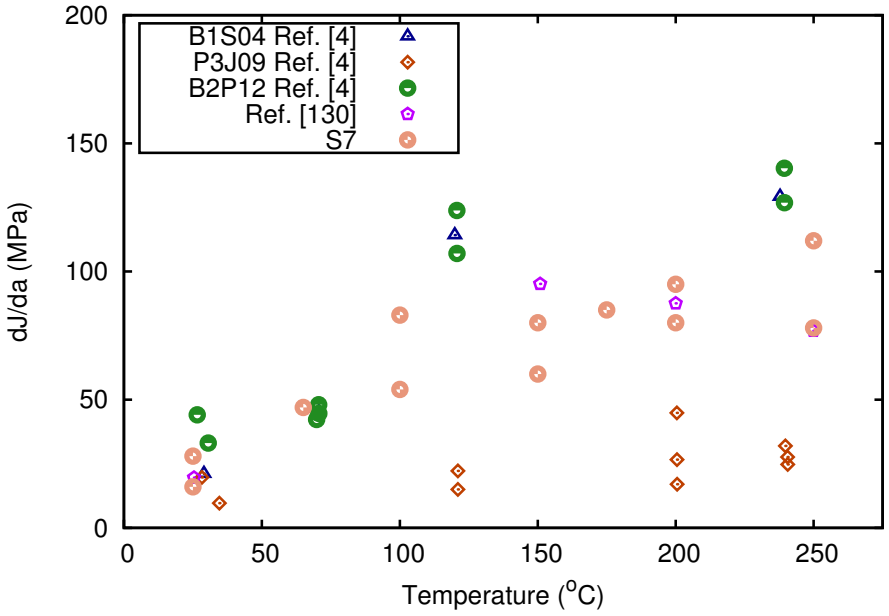

Figure 6.17: Comparison of fracture toughness parameter dJ/da for Indian irradiated double melted pressure tube S-7 with other irradiated pressure tubes data from literature [4,130].

The fracture surfaces of some of the tested and broken specimens were examined using scanning electron microscope (SEM). Figure 6.18 and Figure 6.19 show the fracture surfaces of the specimens tested at 150 $^{\circ}C$ and 200 $^{\circ}C$ respectively. Figure 6.18(b) and Figure 6.19(b) show the magnified view of the stable crack growth region of Figure 6.18(a) and Figure 6.19(a) respectively. In both the cases fracture surface was found to have a high density of fissure like features, with microvoid coalescence typically representative of ductile rupture in the region in between fissures, as shown in Figure 6.19(b). Figure 6.20 shows the region just ahead of fatigue crack front on the fracture surfaces of specimens tested at 65 $^{\circ}C$ and 200 $^{\circ}C$. The flat region ahead of the fatigue pre-crack region is the stretched zone width (SZW) for the two specimens tested and were measured to be around 23μm and 34μm respectively for specimens

tested at 65 $^{\circ}C$ and 200 $^{\circ}C$. Thus the SZW in specimen tested at 200 $^{\circ}C$ seems to be more than that at 65 $^{\circ}C$ and it indicates increase in toughness with increase in test temperature.

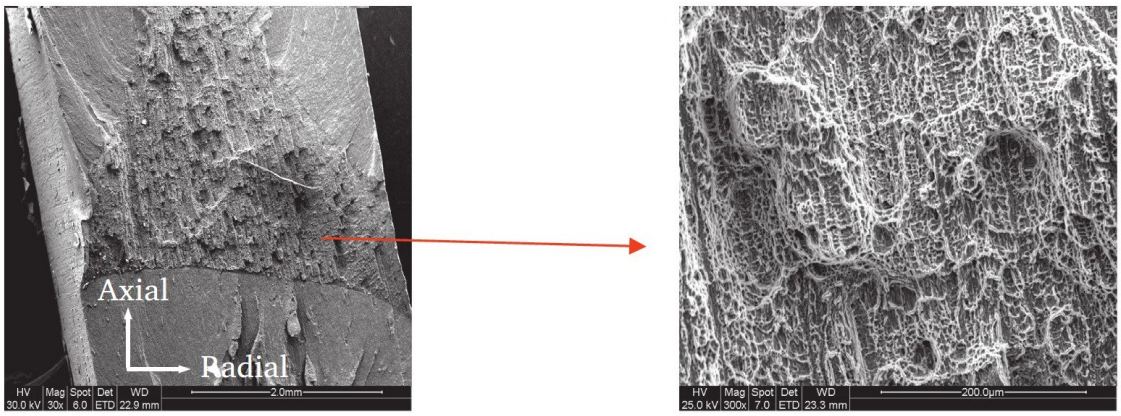

(a) (b)

Figure 6.18: SEM fractographs for the irradiated Zr-2.5Nb pressure tube (S7) tested at 150 $^{\circ}C$ showing large fissure density and ductile fracture of region in between fissures.

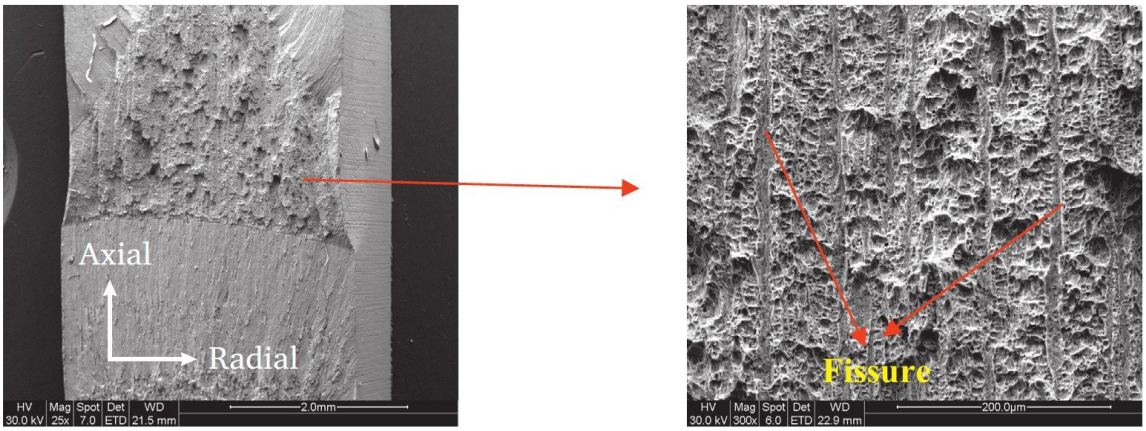

(a) (b)

Figure 6.19: SEM fractographs for the irradiated Zr-2.5Nb pressure tube (S7) tested at 200 $^{\circ}C$ showing magnified view of fissures.

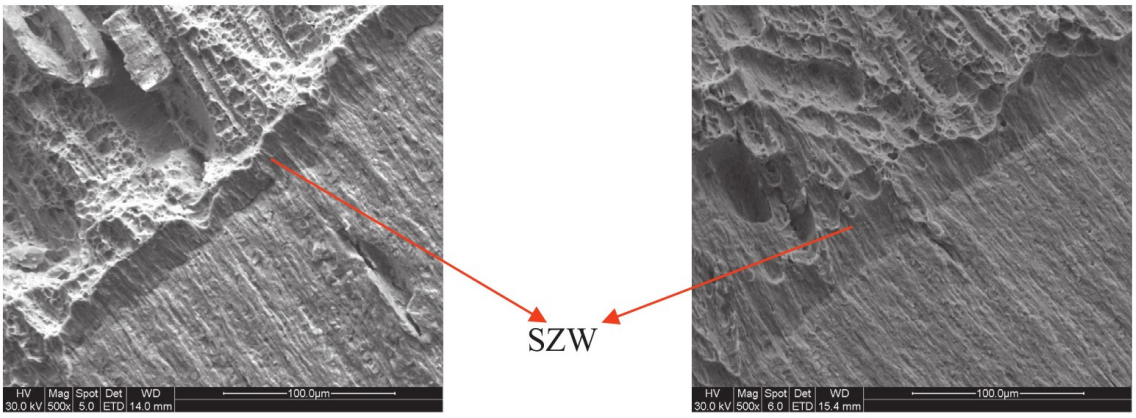

(a) (b)

Figure 6.20: Region near fatigue crack front of irradiated pressure tube (S7)specimens tested at (a) 65 $^{\circ}C$ and (b) 200 $^{\circ}C$ showing higher stretch zone width (SZW) at elevated temperature.

6.3.1.2 Test results of Q-10 pressure tube and roll joint stub

Q-10 pressure tube results Room temperature tests showed sharp load drops in the load-displacement plot as shown in Figure 6.21 indicating sudden advancement of crack front. Typical J-Δa curves for irradiated specimens from Zr-2.5Nb pressure tube, Q-10, tested at 150 $^{\circ}C$ and 200 $^{\circ}C$, are shown in Figure 6.22, which shows little increase in fracture toughness above 150 ^{o}C. The test specimens from irradiated pressure tube were tested at room temperature, 100 $^{\circ}C$, 150 $^{\circ}C$, 200 $^{\circ}C$ and 250 $^{\circ}C$. Table 6.3 gives the measured values of fracture toughness parameters for irradiated Zr-2.5Nb pressure tube Q-10. At room temperature the initiation fracture toughness of the irradiated pressure tube material is 13-37 kJ/m^2 and it increases with increase in test temperature and showed a value of 109-150 kJ/m^2 at 250 $^{\circ}C$. The crack growth resistance dJ/da at room temperature could not be measured as the specimens showed pop-in i.e. sudden load drop due to sudden crack growth at room temperature tests. The value of dJ/da improved with increase in temperature and was 65-170 MPa in the range of test temperatures.

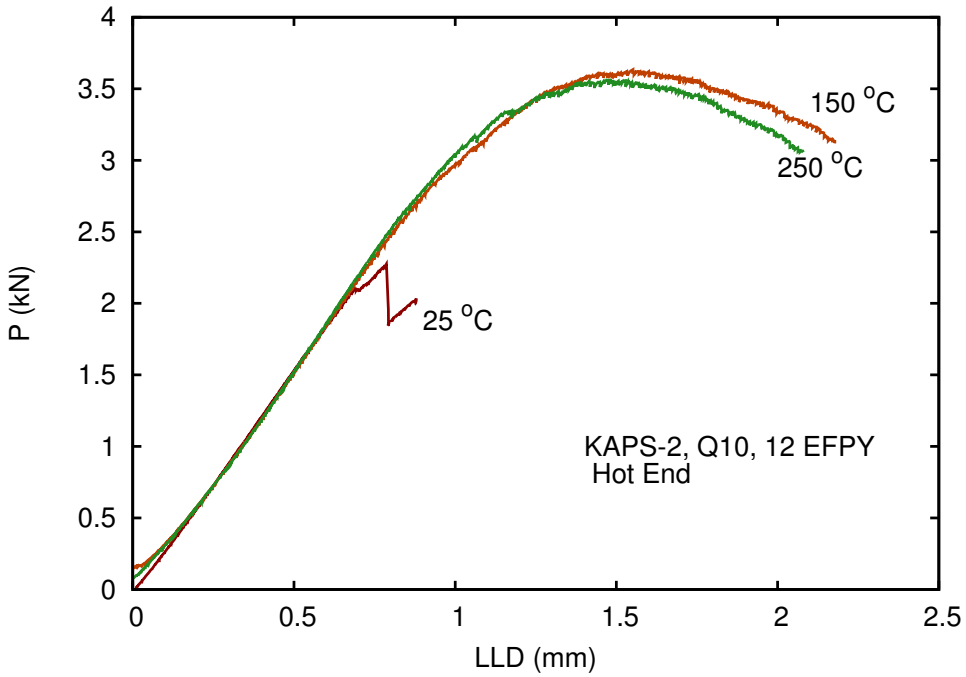

Figure 6.21: Load displacement plots for fracture toughness tests on irradiated Q10 specimens at different test temperatures.

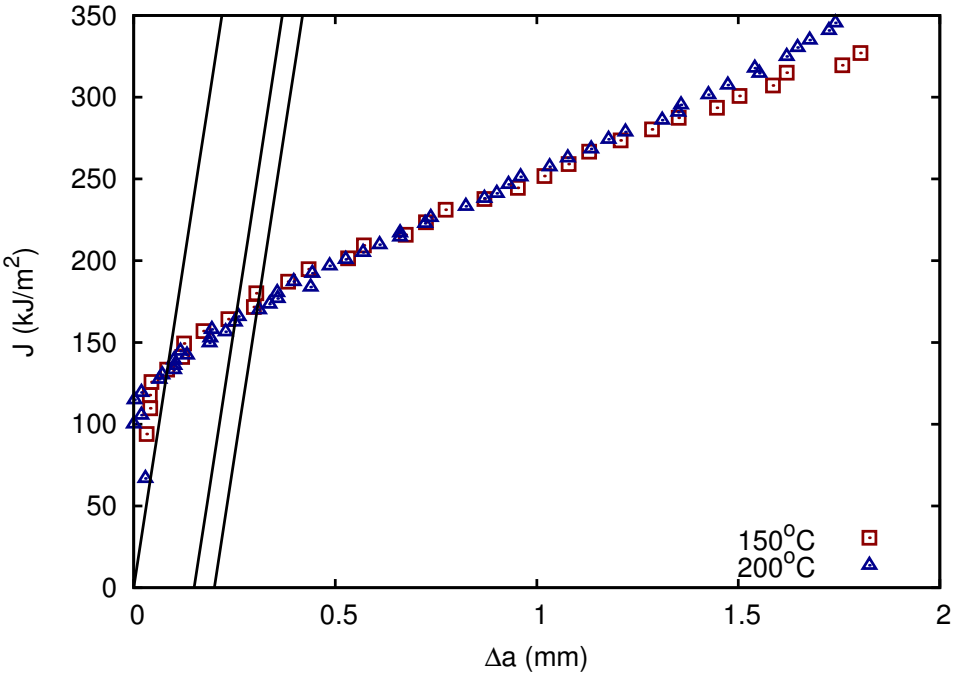

Figure 6.22: J versus $\triangle a$ plots for irradiated Q10 specimens tested at 150 $^{\circ}C$ and 200 $^{\circ}C$.

Table 6.3: Fracture toughness parameters for irradiated Q-10 pressure tube.

Temperature (^0C)	J_i (kJ/m^2)	J_{max} (kJ/m^2)	dJ/da (MPa)
25	13-37	-	-
100	85-165	105-215	85-144
150	118-180	146-235	76-170
200	112-165	136-202	70-117
250	109-150	144-164	65-111

Fracture toughness data generated from the unirradiated Q-10 pressure tube offcut using DCT test specimens gives an idea of the range of toughness of the unirradiated material [131]. Because of the limited amount of material available in the off-cut, the fracture toughness test on the unirradiated Q-10 was carried out only at room temperature and at 250 $^{\circ}C$ and the fracture toughness parameters evaluated is shown in Table 6.4 [131]. Comparison of the fracture toughness parameters of the unirradiated (i.e initial) and irradiated Q-10 pressure tubes show that the J_i reduced by about 80% at room temperature. Maximum reduction in J_i and dJ/da was about 50% at 250 $^{\circ}C$. Thus the results indicate that the degradation due to irradiation is severe at room temperature as compared to that at operating temperature regime.

Table 6.4: Fracture toughness parameters for unirradiated Q-10 pressure tube offcut.

Temperature (^0C)	J_i (kJ/m^2)	J_{max} (kJ/m^2)	dJ/da (MPa)
25	144	153	104
250	133	179	114
250	197	221	146

Q-10 rolled joint stub results The Q-10 rolled joint stub had limited number of specimens, as length of the rolled joint portion was small. So only five DCT specimens were tested four at room temperature and one specimen at 250 ^{o}C. Room temperature fracture toughness tests showed sharp load drops i.e. pop-in, as shown in the load-displacement plots in Figure 6.23. At 250 $^{\circ}C$ the specimens showed stable crack growth, as shown in Figure 6.23. The crack front of the specimens tested at room temperature and 250 ^{o}C are shown in Figure 6.24 and Figure 6.25 respectively. The roll joint stub specimens had different H_{eq} concentration ranging from 28 $wppm$ to 53 $wppm$ as there is generally sharp hydrogen concentration gradient in the the roll joint region along the axial direction and the DCT specimens were prepared from different axial location in the stubs. Table 6.5 gives the measured values of fracture toughness parameters for roll joint stub of irradiated Zr-2.5Nb pressure tube Q-10. The $J_{initiation}$ values ranged between 11-22 kJ/m^2 at room temperature and at 250 ^{o}C it was 87 kJ/m^2. Thus the rolled joint region, having higher amount of hydride and some amount of hydride reorientation along radial direction, showed fracture toughness in the lower band of the values found in main body of pressure tube.

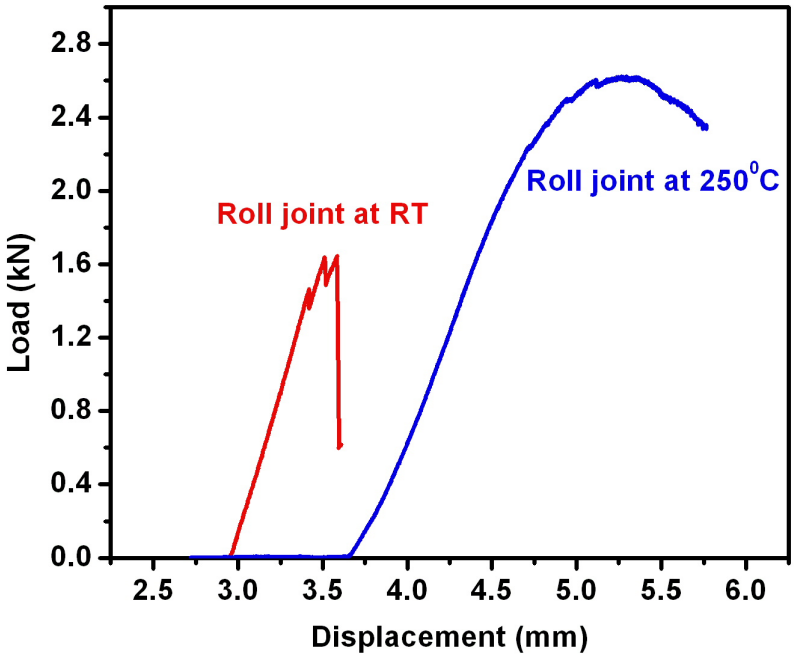

Figure 6.23: Load displacement plots for rolled joint stub specimens of irradiated Q10 pressure tube tested at room temperature (RT) and at 250$^{\circ}C$.

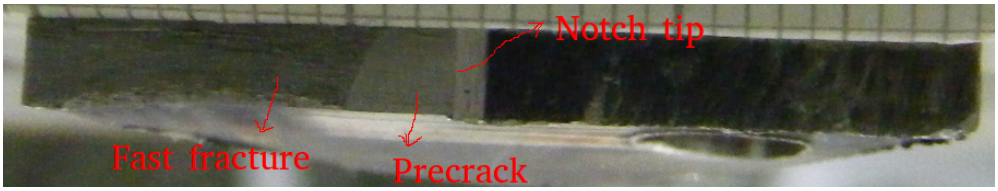

Figure 6.24: Crack front of the rolled joint stub specimen tested at room temperature.

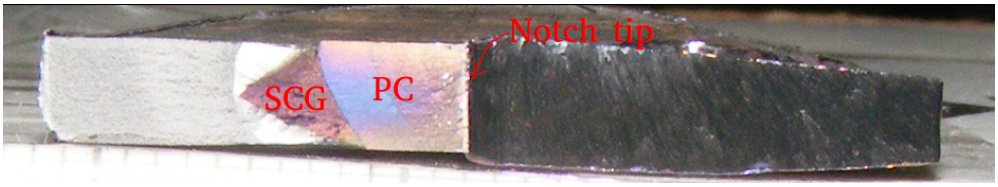

Figure 6.25: Crack front of the rolled joint stub specimen tested at 250$^{\circ}C$ (PC is precrack region and SCG is stable crack growth region).

Table 6.5: Fracture toughness parameters for rolled joint stub of irradiated Q-10 pressure tube.

Temperature ($^{\circ}C$)	J_i (kJ/m^2)	J_{max} (kJ/m^2)	dJ/da (MPa)
25	11-22	-	-
250	87	106	78

6.3.1.3 Comparison of fracture toughness of irradiated pressure tubes

The plots of fracture toughness parameters J_i, J_{max} and dJ/da versus temperature for the irradiated pressure tubes S-7 and Q-10 are shown in Figures 6.26-6.28, which show that at nearly all test temperatures the irradiated pressure tube Q10 had better fracture toughness as compared to that of irradiated S7 pressure tube. The fracture toughness was found to increase with the increase in test temperature till a temperature of around 150 to 200 ^{o}C.

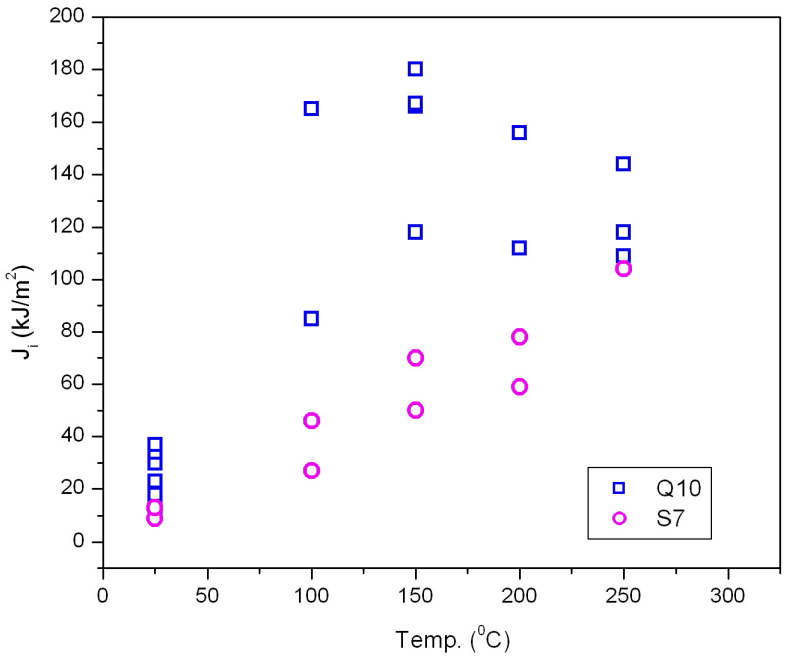

Figure 6.26: J_i versus temperature for irradiated pressure tubes S7 and Q10 .

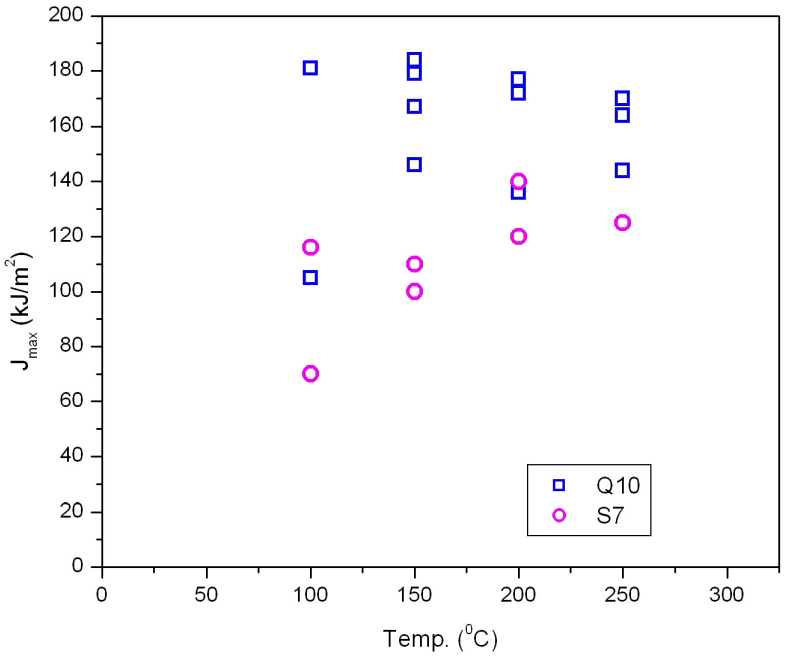

Figure 6.27: J_{max} **versus temperature for irradiated pressure tubes S7 and Q10.**

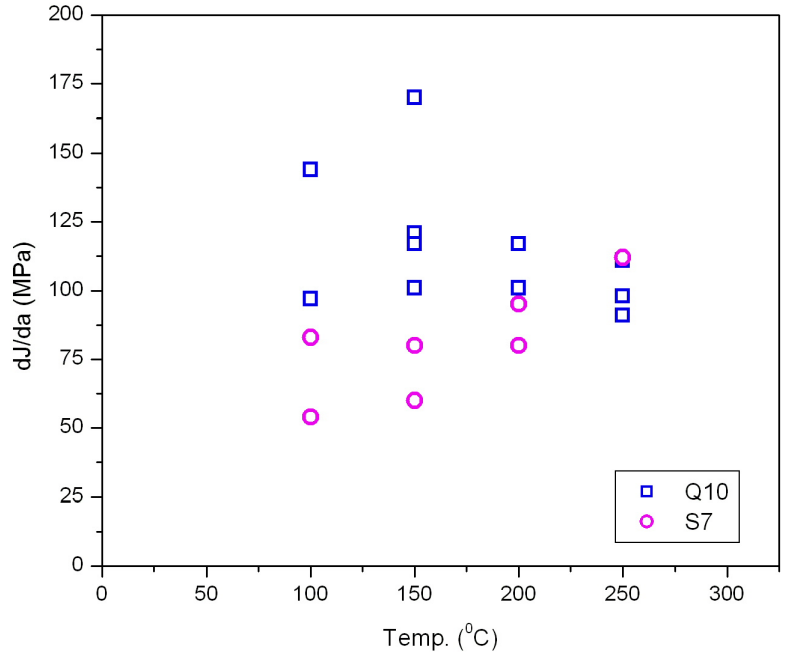

Figure 6.28: dJ/da **versus temperature for irradiated pressure tubes S7 and Q10.**

Initiation fracture toughness (J_i) versus temperature for the as-received irradiated pressure tubes S-7 (H_{eq}~20 *wppm*) and irradiated & hydrided S-7 (H_{eq}~75 *wppm*) pressure tube [132] is shown in Figure 6.29. It shows that the reduction in fracture toughness due to irradiation has almost saturated and further hydriding, even up to 75 *wppm* (H_{eq}), had no significant effect on the fracture toughness. So, from the available test data, fracture toughness of the irradiated pressure tube S-7 can be taken as the lower bound values of the fracture toughness for structural integrity analysis of the pressure tubes having chlorine concentration in the range of around 1.3 *wppm*.

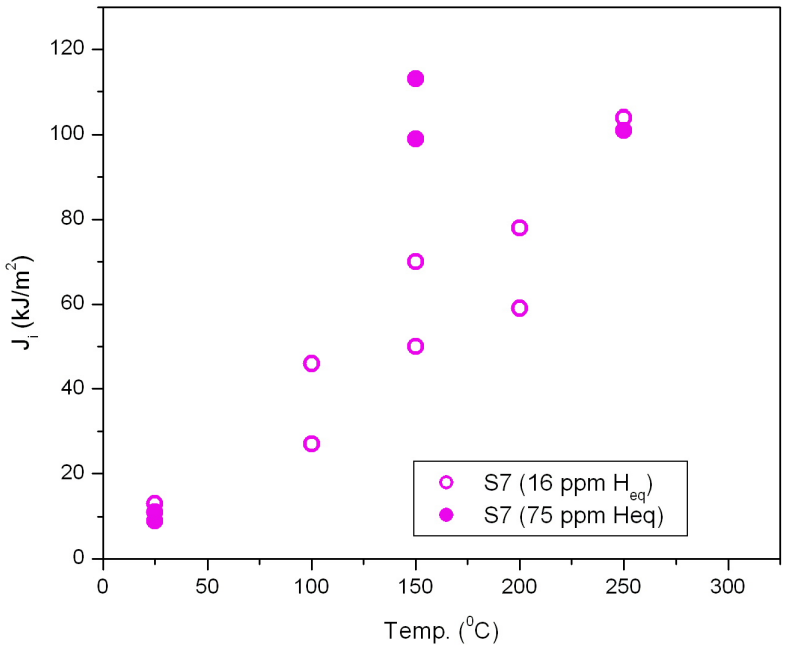

Figure 6.29: J_i **versus temperature for irradiated pressure tube S7 after additional hydrogen charging to 75** *wppm*.

The scanning electron microscopy of the fracture surface of specimens from S7 pressure tube, tested at room temperature, is shown in Fig. 6.30. The fracture surface showed central flat fracture region with negligible through thickness deformation, which is a sign of low energy fracture. The S7 tube, made from foreign ingot, had higher Cl, P, C and oxygen concentration as compared to Q10 PT, as given in Table 3.4, in as-fabricated condition. These trace element impurities like chlorine and

phosphorus have been shown to be responsible for the presence of fissure like features on the fracture surface of Zr-2.5Nb alloys. The S7 tube had large density of these fissures at all test temperatures as seen in one of the specimens tested at $150^{\circ}C$ in Fig. 6.31. The fissures were around $30 - 70\mu m$ apart running in axial direction on radial-axial fracture plane. Shallow dimpled fracture seen in the region in between fissures.

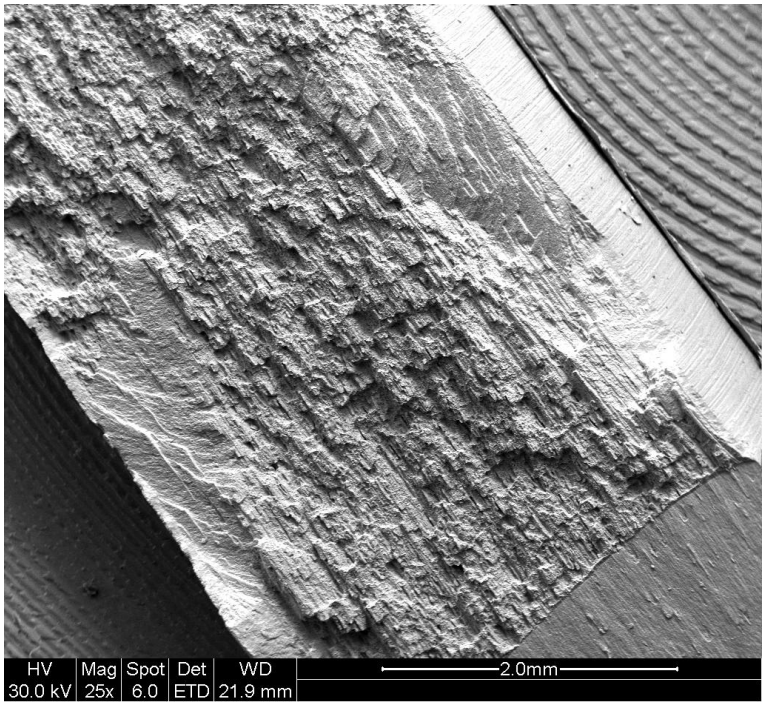

Figure 6.30: Fracture surface of irradiated S7 pressure tube tested at room temperature showing flat fracture in central region and negligible through thickness deformation.

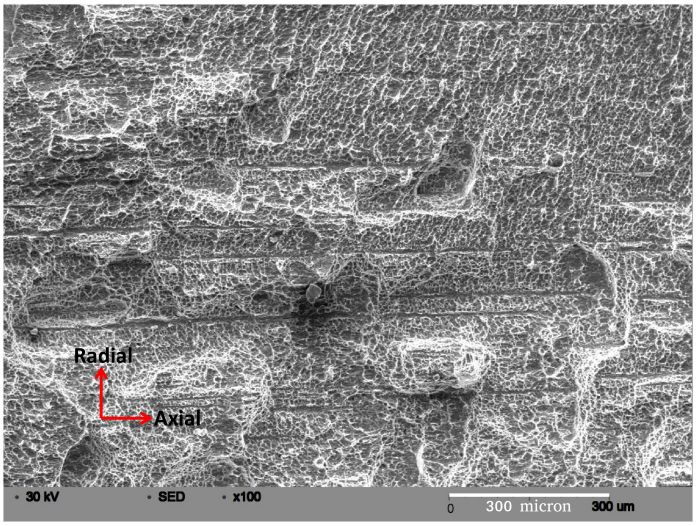

Figure 6.31: Fracture surface of irradiated S7 pressure tube tested at 150 $^{\circ}C$ showing high fissure density with intermediate regions of shallow dimpled fracture.

The irradiated Q10 tube, made from indigenous ingot having lower trace element impurities showed high stretched zone at room temperature, Fig. 6.32(a), which increased with test temperature, Fig. 6.33(b). The fracture surface had lower fissure density and more fibrous fracture as seen in Fig. 6.33(a). The SZW in Q10 fracture toughness test specimens, as shown in Fig. 6.32, were measured to be 33 μm and 45 μm at room temperature and 250 $^{\circ}C$ respectively. Thus the SZW values for Q10 pressure tubes were found to be higher than the irradiated S7 pressure tube . This increase in SZW values agrees well with the measured differences in the fracture toughness values.

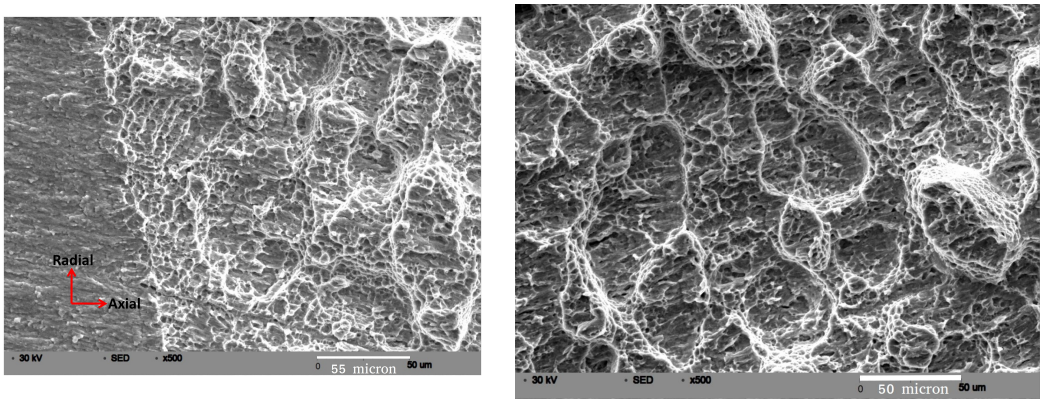

(a) (b)

Figure 6.32: Fracture surface of irradiated Q10 pressure tube tested at room temperature showing (a) stretched zone width ahead of fatigue crack front and fibrous fracture and (b) magnified view of ductile fracture region..

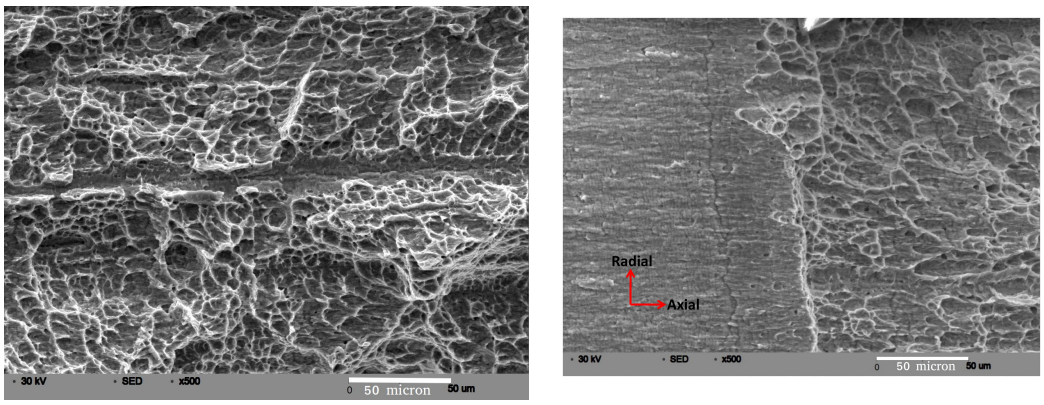

(a) (b)

Figure 6.33: Fracture surface of irradiated Q10 pressure tube tested at (a) 150 $^{\circ}C$ showing fibrous fracture and (b) tested at 250 $^{\circ}C$ showing large stretched zone width and ductile fracture.

6.3.2 DHC of unirradiated and irradiated pressure tubes

Delayed hydride cracking is a major sub-critical crack growth mechanism in the Zr-2.5Nb pressure tube alloy. DHC velocity is sensitive to the microstructure, texture and strength of the tube material. Due to irradiation during service, the pressure tube material undergoes significant changes in microstructure and irradiation hardening. The role of these changes have been evaluated in the irradiated material to obtain actual values that can be used for LBB analysis. DHC velocity measurements have

been carried out for irradiated Indian pressure tube.

The H_{eq} concentration in the irradiated and hydrogen charged specimen was around 100 $wppm$ and hydrides were seen to be uniformly distributed across the cross-section as shown in Figure 6.34. The intermittent propagation of DHC crack and its arrest creates ripple like lines on the fracture surface, which lie nearly parallel to the crack front and perpendicular to the direction of crack growth [133]. Each incremental advance of the crack front results in the formation of a striation on the fracture surface [134]. Figure 6.35 shows the striations, as seen on the fracture surface of the irradiated specimen tested, at 290 $^{\circ}C$. Figure 6.36 shows temperature dependence of striation spacing for as-fabricated and irradiated pressure tube. Decrease in striation spacing was observed with decrease in test temperature for both pressure tubes. This decrease in striation spacing has been attributed to increasing yield strength of the matrix with decreasing temperature [135]. At a given test temperature the striation spacing for as-fabricated pressure tube (dashed line) is relatively larger than that of the irradiated tube (solid line) due to the higher strength of irradiated material as compared to that of as-fabricated condition. At 250 $^{\circ}C$ the transverse yield strength of the as-fabricated and the irradiated pressure tube, measured by the ring tension test, were 554 MPa and 700 MPa respectively [The ring tension test of irradiated pressure tube S-7 was carried out using ring tension specimens (25 mm gauge length and 6.25 mm width) fabricated from 12.5 mm wide ring sections of the irradiated pressure tube [103]. The specimens were fabricated from inlet end, mid length and outlet end of the pressure tube and testing was carried out from room temperature to 300 $^{\circ}C$ using a remotised screw driven UTM. The tests were carried out at a crosshead speed of 0.1 mm/min . The load displacement data obtained were analysed to get stress-strain plot and tensile properties like yield strength, ultimate tensile strength and elongation values]. Higher strength of the material leads to higher crack tip stresses, which leads to lower critical size of the brittle hydride platelets that get formed at the crack tip prior to its cracking and leading to further crack growth. The crack again gets arrested in the Zr-2.5Nb alloy matrix and the cycle repeats.

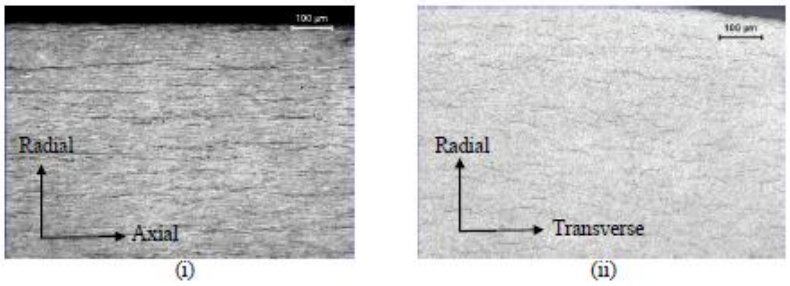

Figure 6.34: Hydride distribution in the irradiated and hydrided specimen in (i) axial-radial plane and (ii) transverse-radial plane, showing dark hydride platelets in the matrix.

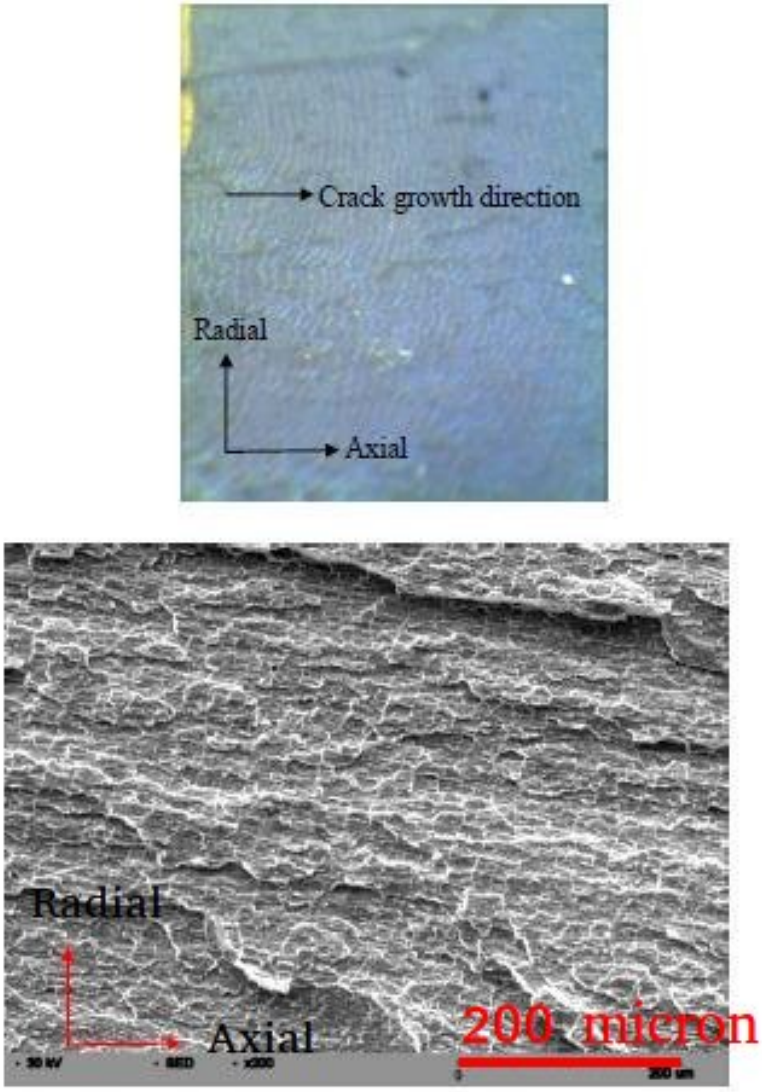

Figure 6.35: DHC striations as seen under (i) stereo microscope showing striations due to DHC and (ii) SEM for the irradiated pressure tube specimen tested at 290 °C.

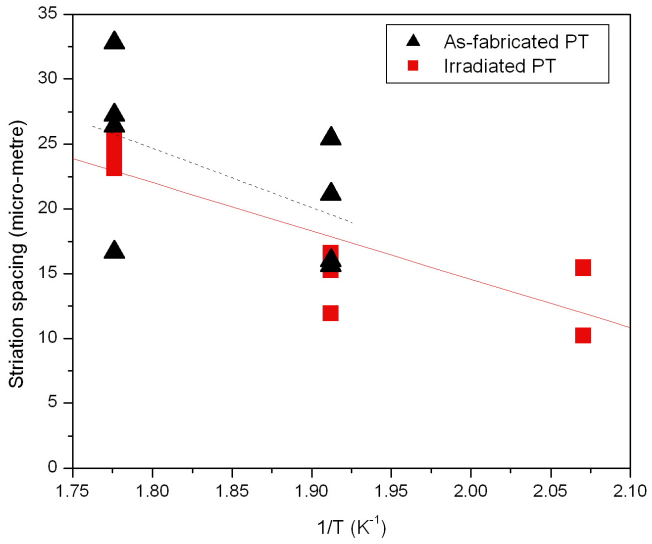

Figure 6.36: Temperature dependence of DHC striation spacing for as-fabricated pressure tube and irradiated Zr-2.5Nb pressure tube where crack was growing in the axial plane in the axial-radial plane.

DHC is a temperature-dependent mechanism, as the movement of hydrogen to the crack tip depends on the diffusion of hydrogen and its solubility limit, both of which are thermally activated processes [133]. DHC velocity increases with increase in temperature. DHC velocity in Zr-2.5Nb alloy has been found to be controlled primarily by its flow strength and microstructure, specifically the morphology of the β-phase, which affects hydrogen diffusivity [38, 136]. Table 6.6 gives the DHC test temperature and measured DHCV obtained for the irradiated and as-fabricated Zr-2.5Nb pressure tube. The influence of temperature on the DHCV in the as-fabricated and irradiated Zr-2.5Nb pressure tube is shown in Figure 6.37. At all the test temperatures DHCV of the irradiated pressure tube was more than that of the as-fabricated pressure tube. In the operating temperature range the DHCV for irradiated pressure tube has been found to be around 2 to 4 times the DHCV in the as-fabricated pressure tube. This increase is mainly attributed to the increase of the pressure tube yield strength due to irradiation as DHCV has been found to increase linearly with yield strength of zirconium alloys [15]. Delayed hydride cracking involves migration of hydrogen up the hydrostatic stress gradient to the region of stress concentration. Once the terminal

solubility is exceeded brittle hydride platelet nucleates perpendicular to tensile stress, grows to a critical size and crack grows by fracture of critical hydride and ductile tearing of matrix ligament between crack and hydride [29] and the whole sequence repeats. This gives rise to the appearance of striations on the fracture surface of the DHC tested specimens.

Table 6.6: DHC test temperature and DHC velocity of as-fabricated and irradiated Indian pressure tube.

Irradiated		As-fabricated	
Test Temp.	DHCV	Test Temp.	DHCV
(^{o}C)	m/sec	(^{o}C)	m/sec
210	4.83x10-8	200	6.66E-09
210	3.89x10-8	200	7.07E-09
250	1.29x10-7	250	4.21E-08
250	1.25x10-7	250	2.93E-08
265	1.17x10-7	250	3.45E-08
290	2.22x10-7	250	3.50E-08
		250	2.97E-08
		290	7.95E-08
		290	7.93E-08
		290	8.23E-08
		290	8.21E-08

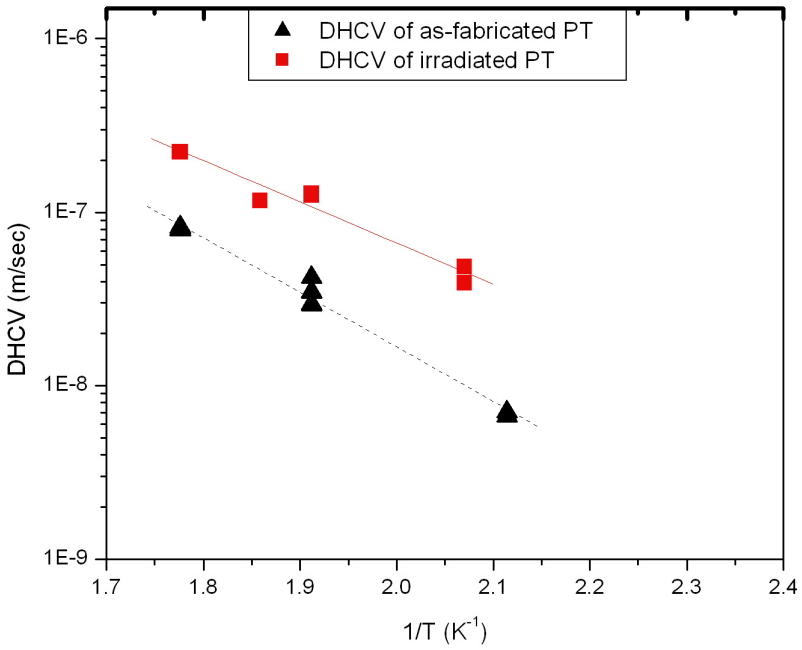

Figure 6.37: DHC velocity versus inverse of temperature for the as-fabricated and irradiated pressure tubes where crack was growing in the axial plane in the axial-radial plane.

The striation spacing represents the length of critical hydride, which forms in each DHC step [113, 137]. The decrease in striation spacing with increase in strength of alloy has been explained by the fact that the tensile stress normal to crack plane, at the crack tip, due to the far field applied stress is proportional to the strength of the material. At higher value of normal tensile stress even smaller hydride platelet fulfil the criteria for fracture and become critical hydride [77]. Higher the strength of material, higher is the value of normal stress and smaller is the critical hydride size and so smaller will be striation spacing. Therefore, it is said that as the strength of that material increases the striation spacing (critical hydride length) decreases.

The relationship between DHCV and temperature has been found to follow Arrhenius dependence, as shown in equation 6.3:

$$DHCV = Aexp\left(-\frac{Q}{RT}\right) \tag{6.3}$$

where, A = pre-exponential constant; Q = the activation energy (J/mol); T = test temperature (K); R (universal gas constant) = 8.314 J/mol/K. Values of A and Q, for the irradiated pressure tube, were found to be 3×10^{-3} m/sec and 45.5 kJ/mol respectively. Table 6.7 shows the A and Q values for both as-fabricated pressure tube and irradiated pressure tube. Similar results have also been reported for Canadian Zr-2.5 Nb pressure tubes [15, 138].

Table 6.7: Arrhenius relation parameters A and Q from DHC velocity versus temperature plot.

Source material	A (m/sec)	Q (kJ/mol)
As-fabricated PT	33×10^{-3}	60.2
Irradiated PT	3×10^{-3}	45.5

The temperature dependence of DHCV is due to combined effect of temperature on diffusion coefficient of hydrogen in α-Zr and terminal solid solubility of hydrogen in α-Zr, which has theoretical activation energy of 70 kJ/mol in unirradiated material [15]. A secondary effect comes from temperature dependence of yield strength, which reduces the total activation energy for DHC to about 60 kJ/mol [15]. Many other experimental studies on unirradiated materials have shown temperature dependencies in the range from 58 to 72 kJ/mol. The activation energy of 60.2 kJ/mol obtained in current study on as-fabricated Indian Zr-2.5Nb pressure tubes agrees well with above reported values.

The DHC velocity in irradiated pressure tubes is mainly governed by strength, with DHC velocity increasing with increasing flow stress. The continuity of β-phase, which are in thin filament form has also been reported to affect DHCV [138]. Hydrogen diffuses faster in the BCC β-phase than in the α-phase and diffusion coefficient for hydrogen in β-zirconium is nearly two orders of magnitude higher than that in α-zirconium [21]. Presence of β-phase greatly enhances the diffusion of hydrogen through a short-circuiting effect and hence the DHCV in as received Zr-2.5Nb materials with continuous β-Zr [139] has been found to be higher. With decomposition of the β-

phase, which may be due to thermal treatments during autoclaving in fabrication or during irradiation in service, the diffusivity of hydrogen is expected to decrease. This decomposition of the β-phase has been found to lower DHCV. The effect of β-phase decomposition in lowering of DHCV is also seen from the fact that the increase in DHCV after irradiation has been found to be more in Zr-2 (where only α-phase is present) than that in Zr-2.5Nb pressure tubes. Limited studies on irradiated Indian Zr-2 pressure tubes have shown increase in DHCV of around 8 times [101, 140] as compared to 2 to 4 times for irradiated Zr-2.5Nb pressure tube in present study.

Irradiation has been found to reduce the values of activation energy due to further decomposition of β - phase during irradiation, as the activation energy for diffusion in the β-phase is lower than that in the α-phase. This effect of β-phase decomposition is reflected in the reduction in activation energy for DHC after irradiation to 45.5 kJ/mol similar to the values reported in the literature [15, 141].

A comparison of unirradiated DHCV data generated in the present experiment with the mean DHCV data on the other Indian pressure tubes and CANDU pressure tubes available in open literature is shown in Figure 6.38. Its seen that the present material, in unirradiated condition, has relatively lower DHCV as compared to both data available in literature. This variation is within the tube to tube scatter observed in DHCV due to minor variations in parameters like tensile strength, microstructure and texture. Though the microstructure of Indian pressure tubes differ from CANDU tubes in terms of β-phase continuity and α-phase grain size and aspect ratio, the DHCV was found to be quite similar in irradiated condition and it shows that the minor variations in these microstructural features are overridden by irradiation hardening effect in the pressure tube.

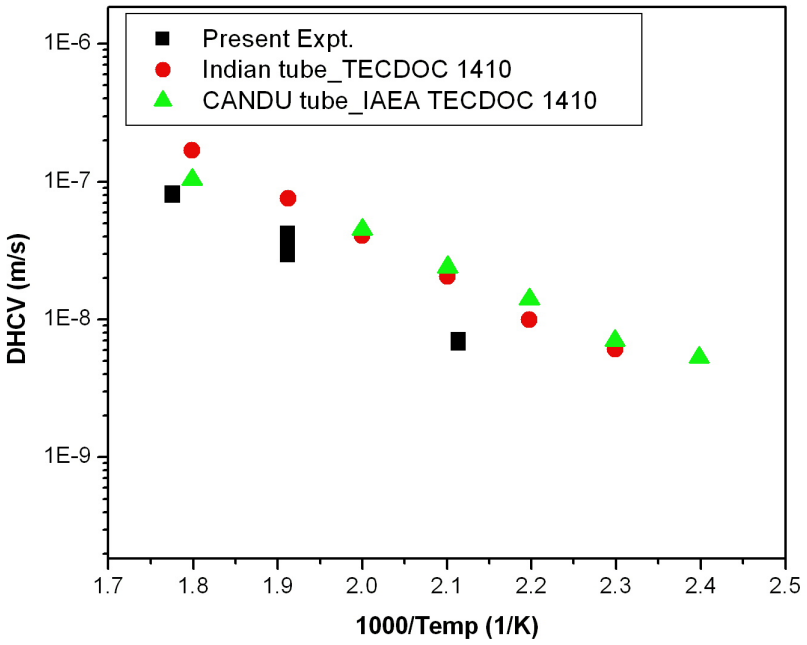

Figure 6.38: Comparison of DHC velocity versus inverse of temperature for the as-fabricated pressure tubes with other reported values, where crack was growing in the axial plane in the axial-radial plane [133].

6.3.3 Operator response time (ORT)

Fracture toughness and DHC velocity for the irradiated pressure tubes have been evaluated. These data can be used to evaluate the operator response time once a crack becomes through and through and is detected by the leak detection system. As a typical example, fracture toughness and DHCV at 250^{o}C (55 mm and $1.27\times10^{-7}m/s$ respectively for irradiated pressure tube S-7) has been used to get the idea of available ORT. Two different aspect ratios (4 and 7) of crack were taken for the through wall crack. The operator response time (t) is given by Equation 2.1 .

ORT has been found to be in the range of 33 to 45 hours at 250^{o}C for the irradiated pressure tube. The minimum required operator response time is around 13 hours. So the available ORT from the present experimental analysis is sufficient.

6.4 Conclusions

The fracture toughness parameters for irradiated Zr-2.5Nb pressure tubes, S-7 and Q-10, after 8.0 and 12 EFPY of operation have been evaluated using disk compact tension specimens, at different test temperatures. The irradiated pressure tubes had around 20 $wppm\ H_{eq}$ in the form of small hydride platelets uniformly distributed across the pressure tube thickness. DHC velocity has been measured for the irradiated Indian Zr-2.5Nb pressure tube S-7. DCT specimens have been used for the fracture toughness and DHC tests.

The DCT specimens have been found to give conservative estimate of the fracture toughness as compared to rectangular compact tension specimens in the unirradiated condition. Test methodology for fracture toughness tests on irradiated pressure tubes was established.

At nearly all the test temperatures the irradiated pressure tube Q-10 showed better fracture toughness as compared to that of irradiated S-7 pressure tube. The fabrication route of both the tubes were same, however Q-10 had lower amount of carbon, chlorine, phosphorus and initial hydrogen concentration. This small variation in trace element impurities had significant effect on the fracture behavior. Fractographic examination showed larger presence of fissure like features on the fracture surface of S-7 pressure tube.

Initiation fracture toughness (J_i) values for the irradiated pressure tube, roll joint stub and irradiated & hydrided pressure tube have shown that the reduction in fracture toughness due to irradiation & hydriding had almost saturated, during in-reactor service of around 8 years, and further hydriding, even up to 75 $wppm\ H_{eq}$, had no significant effect on the fracture toughness. The reduction in fracture toughness is quite significant at 25 $^{\circ}C$, and the toughness improves at temperatures above 150 $^{\circ}C$ to 180 $^{\circ}C$.

The relationship between DHCV and temperature has been found to follow Arrhenius dependence with activation energy of 45 and 60 kJ/mol in irradiated and

as-fabricated material. This value corresponds to the activation energy of hydrogen/deuterium diffusion in the zirconium alloy matrix. DHCV in irradiated pressure tube was found to be around 2 to 4 times than that in as-fabricated pressure tube in the given test temperature range. The DHCV was found to be of similar order as reported for CANDU pressure tubes, which have differences in microstructure and texture from the Indian pressure tubes. Nearly similar DHCV in irradiated Indian and CANDU pressure tubes suggests that the minor variations in these microstructural features are overridden by irradiation hardening effect in pressure tube as far its effect on DHC velocity is concerned.

The intermittent propagation of DHC crack and its arrest created ripple like lines on the fracture surface, which lie nearly parallel to the crack front and perpendicular to the direction of crack growth. The striation spacing was observed to decrease with decrease in test temperature. Also at a given test temperature the striation spacing for as-fabricated pressure tube were larger than that of the irradiated tube. This reduction in striation spacing has been attributed to the increasing yield strength of the matrix in both cases.

Chapter 7

Summary

The fracture toughness and delayed hydride cracking behaviour of irradiated Indian Zr-2.5Nb pressure tubes and its rolled joint regions have been studied and compared with the data available in open literature. These two parameters are important for assurance of Leak before Break in the tube. The main idea has been to study and understand the End of Life properties for irradiated pressure tubes, that are currently in use in Indian PHWRs, with respect to its fracture toughness and DHC behaviour. Inherent variability in the mechanical properties of the pressure tubes and the effect of specimen orientation in this textured material, have been evaluated using tensile tests on the as-fabricated off-cuts of the pressure tubes. Effect of hydrogen concentration and higher strain rate effects in two major possible crack orientations, have been studied using impact tests using unirradiated alloy to make experimental work feasible. These studies have important role in understanding the deformation and fracture behaviour of the Zr-2.5Nb pressure tube made from indigenous route.

7.1 Study on variability in mechanical properties of as-fabricated pressure tubes

The Zr-2.5Nb alloy pressure tubes have been found to have significant tube to tube variability in mechanical properties in as-fabricated and irradiated conditions. Ten-

sile properties of the pressure tube also showed significant differences along axial and transverse directions. The transverse tensile specimens showed higher yield strength and ultimate tensile strength as compared to the longitudinal specimens. Transverse specimens also showed lower strain hardening as compared to the longitudinal specimens. The axial specimens showed higher uniform and total elongation compared to the transverse specimens. All these changes have been attributed to the anisotropy in the pressure tubes as they have dominant transverse basal pole texture (f_t = 0.55-0.6, f_r = 0.3-0.35). The axial loading direction results in easier activation of slip systems on prismatic planes and higher work hardening.

Pressure tubes, which are around 5.5m long showed differences in its front and back end tensile properties, mainly due to drop in temperature during extrusion from front end to back. Mean values of tensile properties showed that the back-end of the pressure tubes, end which came out last during extrusion, were relatively stronger and less ductile as compared to the front-end of the tube in most of the cases.

Effect of alloy chemistry was also observed in form of difference in tensile and fracture properties of double melted and quadruple melted pressure tubes. Double-melted pressure tubes showed relatively higher strength and lower elongation and larger standard deviation compared to the quadruple melted pressure tubes. This indicates that the variability in minor trace element impurities, which lead to differences in second phase precipitates, such as carbides, phosphides as well as microsegregation of Cl-C complex also have role in larger scatter for double melted pressure tubes. The tubes made from quadruple melted ingots having lower trace element impurities show lower scatter in mechanical properties.

The double melted pressure tubes have shown wide variations in fracture toughness. The average value of $\frac{dJ}{da}$ for the tougher offcuts was 406 MPa as compared to 136 MPa for relatively less tough tubes. Twenty three offcuts from quadruple melted pressure tubes of Indian origin were tested and except three offcuts, all other offcuts have shown fracture toughness greater than 200 MPa with an average value being around 300 MPa. The average crack growth resistance is around 280 MPa including all the

tested specimen results. Fracture toughness of front end and back end of six quadruple melted pressure tubes were also compared. Except two tubes, other tubes had marginal variation in fracture toughness from one end of the tube to the other end. There was no clear trend in fracture toughness, whether it was more at the front end or back end offcuts when the difference in fracture toughness between the two ends were marginal. However, when there was relatively large difference in front end and back end fracture toughness, the front end seem to be relatively tougher compared to that of back end offcuts. The average $\frac{dJ}{da}$ for these front end and back end offcuts was found to be 314 MPa.

7.2 Impact toughness of as-received and hydrided Zr-2.5Nb pressure tube

Zr-2.5Nb pressure tube showed near similar impact energy at room temperature in axial and transverse orientation. However, at higher temperatures crack growth along axial direction absorbs significantly more energy. Fractographic examinations revealed distinct features when crack growth occurs in axial and transverse direction. The change in absorbed energy could be correlated with the nature of deformation ahead of the notch in impact specimens, as seen by SEM examinations. Use of curved impact specimen was found to result in higher absorbed energy due to specimen anvil interaction when specimens deformed and was prominently seen in axial impact specimens, which absorbed higher energies.

Ductile-to-brittle-transition at around 200 $^{\circ}C$ was also clearly exhibited by hydrided Zr-2.5Nb pressure tube alloy, when crack growth occurs along axial direction on the radial-axial plane, under dynamic loading.

The effect of hydrogen, which is present in form of hydride platelets, is marginal in transverse notch direction as compared to the axial notch. In hydrided material, brittle hydride platelets are present in the matrix at room temperature. Even unhydrided material fractured with low total absorbed energy at room temperature, which show

that the presence of hydrides did not make significant difference. Only the fracture surface showed presence of small splits associated with brittle hydride phase. At 300 $^{\circ}C$, most of the hydride platelets will undergo dissolution in the Zr matrix. The matrix itself becomes softer and ductile and very few hydride cracks were observed. Due to above two factors, transition in absorbed energy with temperature is seen in axial hydrided impact specimen. The transverse specimens continue to have low absorbed energy.

7.3 Effect of irradiation on fracture toughness

Fracture toughness of two irradiated pressure tubes, with different ingot chemistry, after different fluence, was characterized in detail. This included portions of the pressure tubes, which form part of the mechanical rolled joints with the end fittings. The rolled joint portion of the tube, has significant amount of residual tensile stresses, which in combination with the normal operating hoop stress, lead to varying degree of hydride reorientation in the radial-axial plane in the rolled portion. Thus effects of a) different neutron fluence b) alloy chemistry and c) hydrogen concentration on the fracture toughness of irradiated pressure tubes have been studied. At nearly all the test temperatures the irradiated pressure tube Q10 showed better fracture toughness as compared to that of irradiated S7 pressure tube. The fabrication route of both the tubes were same, however Q10 had lower amount of carbon, phosphorus, chlorine and initial hydrogen concentration. This small variation in trace element impurities had significant effect on the fracture behavior.

Initiation fracture toughness (J_i) values for the irradiated pressure tube and irradiated and hydrided pressure tube have shown that the reduction in fracture toughness due to irradiation and hydriding had almost saturated, during in-reactor service of around 8 years, and further hydriding, even up to 75 $wppm$ H_{eq}, had no significant effect on the fracture toughness. The fracture toughness was found to increase with the increase in test temperature till a temperature of around 150 to 200 $^{\circ}C$.

7.4 Effect of irradiation on DHC behaviour

Delayed hydride cracking is a major sub-critical crack growth mechanism in the Zr-2.5Nb pressure tube alloy. DHC velocity is sensitive to the microstructure, texture and strength of the tube material. Due to irradiation during service, the pressure tube material undergoes significant changes in microstructure and irradiation hardening. The role of these changes have been evaluated in the irradiated material to obtain actual values for indigenous pressure tubes that can be used for LBB analysis. It also gave an idea of the performance of the tubes made by indigenous fabrication route with respect to international experience. The DHCV being a sensitive property reflects the changes occurring in material over its operating life.

The relationship between DHCV and temperature has been found to follow Arrhenius dependence with an activation energy of 45 and 60 kJ/mol in irradiated and as-fabricated material, which agrees well with the values reported in the literature. This activation energy or temperature dependence of DHCV is due to the combined effect of temperature on diffusion coefficient of hydrogen in α-Zr and terminal solid solubility of hydrogen in α-Zr.

DHCV in irradiated pressure tube was found to be around 2 to 4 times higher than that in the as-fabricated pressure tube in the given test temperature range. The DHCV was also found to be of similar order as reported for CANDU pressure tubes, which show that the minor variations in the microstructural features between these two fabrication routes are overridden by the irradiation hardening effect in the pressure tubes and the DHCV is governed mainly by the strength of the material.

The intermittent propagation of DHC crack and its arrest created ripple like lines on the fracture surface, which lie nearly parallel to the crack front and perpendicular to the direction of crack growth. The striation spacing was observed to decrease with decrease in test temperature. Also at a given test temperature the striation spacing for as-fabricated pressure tube were larger than that of the irradiated tube. This has been attributed to the increasing yield strength of the matrix.

The results generated serve a valuable role in LBB based safety analysis of coolant channels. At cold end operating temperature of 250^{o}C the critical crack length and DHCV was estimated to be 55 mm and $1.27 \times 10^{-7} m/s$ respectively for irradiated pressure tube. These were used to calculate available operator response time for two different crack aspect ratios (4 and 7). Operator response times were found to be in the range of 33 to 45 hours at 250^{o}C. The minimum required operator response time, to take corrective actions in case of any event of coolant leakage, is around 13 hours. So the available time, as estimated from the present experimental analysis, is sufficient and irradiated pressure tubes meet leak before break criteria.

7.5 Scope for future research

Present thesis has emphasised on fracture studies of double melted pressure tube.

- As the present route of pressure tube fabrication is quadruple melted route, the studies carried out in the present thesis can be extended to the irradiated quadruple melted pressure tubes.
- Lower impact energies observed in transverse notch orientation as compared to axial one, under impact loading, need further careful investigations to study its deformation mode and fracture micro-mechanism.
- The as-received irradiated pressure tubes and roll joint stub studies in the present thesis had mainly circumferentially oriented hydrides. It is of interest to see how the distribution of radial hydrides affect the fracture toughness and DHC velocity in the as-fabricated as well as irradiated material.

Bibliography

[1] D. K. Rodgers, C. E. Coleman, M. Griffith, G. A. Bickel, J. R. Theaker, I. Muir, A. A. Bahurmuz, S. St. Lawrence, and M. R. Levi. In-Reactor Performance of Pressure Tubes in CANDU Reactors. *Journal of Nuclear Materials*, 383:22–27, 2008.

[2] J. R. Theaker, R. Choubey, G. D. Moan, S. A. Aldridge, L. Davies, R. A. Graham, and C. E. Coleman. Fabrication of Zr-2.5Nb Pressure Tubes to Minimize the Harmful Effects of Trace Elements. In Garde A.M., Bradley E.R., editor, *Zirconium in the Nuclear Industry: Tenth International Symposium*, number 1245 in ASTM STP, pages 221–242, Philadelphia, 1994. ASTM.

[3] G. A. Bickel and M. Griffith. Manufacturing Variability, Microstructure and Deformation of Zr-2.5Nb Pressure Tubes. *Journal of ASTM International*, 4(10):529–540, 2007.

[4] C.K. Chow, C.E. Coleman, R.R. Hosbons, P.H. Davies, M. Griffiths, and R. Choubey. Fracture Toughness of Irradiated Zr-2.5Nb Pressure Tubes from CANDU Reactors. ASTM STP 1132:246–275, 1991.

[5] P. H. Davies, R. R. Hosbons, M. Griffiths, and C. K. Chow. Correlation Between Irradiated and Unirradiated Fracture Toughness of Zr-2.5Nb Pressure Tubes. In Garde A.M., Bradley E.R., editor, *Zirconium in the Nuclear Industry: Tenth International Symposium*, number 1245 in ASTM STP, pages 135–167, Philadelphia, 1994. ASTM.

[6] M. Trelinski. Application of Ultrasonic Testing Methods for Volumetric and Surface Inspection of CANDU Pressure Tubes. *NDT net*, 4(2), 1999.

[7] Y. W. Park and Y. K. Chung. Leak-Before-Break Assessment of CANDU Pressure Tube Considering Leak Detection Capability. *Nuclear Engineering & Design*, 191:205–216, 1999.

[8] IAEA TECDOC 1037. *Assessment and Management of Ageing of Major Nuclear Power Plant Components Important to Safety: CANDU Pressure Tubes*, 1998.

[9] S. K. Sinha. Indian R & D Programme Related to Life Management of Coolant Channels of Indian PHWRs : An Overview. *BARC News letter - Founder's day special issue*, pages 112–121, 2015.

[10] B. A. Cheadle, C. E. Coleman, and H. Licht. CANDU-PHWR Pressure Tubes: Their Manufacture, Inspection and Properties. *Nuclear Technology*, 57:413–425, 1982.

[11] R. G. Fleck, E. G. Price, and B. A. Cheadle. Pressure Tube Development For CANDU Reactors. In *Zirconium in the Nuclear Industry: Sixth International Symposium, ASTM STP 824*, pages 88–105, 1984.

[12] D. Srivastava, G. K. Dey, and S. Banerjee. Evolution of Microstructure During Fabrication of Zr-2.5 Wt Pct Nb Alloy Pressure Tubes. *Metall. Mater. Trans. A*, 26A:2707–2718, 1995.

[13] B. A. Cheadle. Fabrication of Zirconium Alloys into Components for Nuclear Reactors. *ASTM STP 633*, pages 457–485, 1977.

[14] N. Saibaba, S. K. Jha, S. Tonpe, K. Vaibhaw, V. Deshmukh, S. V. Ramana Rao, K. V. Mani Krishna, S. Neogy, D. Srivastava, G. K. Dey, R. V. Kulkarni, B. B. Rath, E. Ramadasan, and S. A. Anantharaman. Microstructural Studies of Heat Treated Zr-2.5Nb Alloy for Pressure Tube Applications. *Journal of ASTM International*, 8(6):1–15, 2011.

[15] S. Sagat, C. E. Coleman, M. Griffiths, and B. J. S. Wilkins. The Effect of Fluence and Irradiation Temperature on Delayed Hydride Cracking in Zr-2.5Nb. In Garde A.M., Bradley E.R., editor, *Zirconium in the Nuclear Industry: Tenth International Symposium*, number 1245 in ASTM STP, pages 35–61, Philadelphia,

1994. ASTM.

[16] R. N. Singh, R. Kishore, T. K. Sinha, and S. Banerjee. Tensile Properties of Zr-2.5Nb Pressure Tube Alloy between 25 and 800 °C. Technical Report BARC/2000/E/029, BARC, 2000.

[17] B. A. Cheadle. The Development of Zr-2.5Nb Pressure Tubes for CANDU Reactors. *Journal of ASTM International*, 7(8):1–15, 2010.

[18] D. Rodgers, M. Griffiths, G. Bickel, A. Buyers, C. Coleman, H. Nordin, and S. St. Lawrence. Irradiation Effects on Zr-2.5Nb in Power Reactors. *CNL Nuclear review*, 5(1):1–15, 2016.

[19] B. A. Cheadle and E. G. Price. Operating Performance of CANDU Pressure Tubes. Technical Report AECL-9939, AECL, 1989.

[20] N. Saibaba, K. Vaibhaw, S. Neogy, K. V. Mani Krishna, S. K. Jha, C. Phani Babu, S. V. Ramana Rao, D. Srivastava, and G. K. Dey. Study of Microstructure, Texture and Mechanical Properties of Zr-2.5Nb Alloy Pressure Tubes Fabricated with Different Processing Routes. *Journal of Nuclear Materials*, 440:319–331, 2013.

[21] L. A. Simpson and C. D. Cann. The Effect of Microstructure on Rates of Delayed Hydride Cracking in Zr-2.5Nb Alloy. *Journal of Nuclear Materials*, 126:70–73, 1984.

[22] S. A. Bharadwaj. Design Criterion For Zirconium Alloy Components in NPPs. In *Proc. of the symposium Zirconium-2002, ZIRC-2002*, pages 66–72. BARC, September 2002.

[23] R. N. Singh, S. Mukherjee, R. Kishore, and B. P. Kashyap. Flow Behaviour of A Modified Zr-2.5Nb Pressure Tube Alloy. 345(2-3):146–161, 2005.

[24] C. Coleman, M. Griffiths, V. Grigoriev, V. Kiseliov, B. Rodchenkov, and V. Markelov. Mechanical Properties of Zr-2.5Nb Pressure Tubes Made from Electrolytic Powder. *Journal of ASTM International*, 4(10):1–23, 2007.

[25] M. Koike and T. Asada. Irradiation Creep and Growth of Pressure Tubes in

HWR Fugen. *Journal of Nuclear Materials*, 159:62–74, 1988.

[26] E. F. Ibrahim and R. A. Holt. Anisotropy of Irradiation Creep and Growth of Zirconium Alloy Pressure Tubes. *Journal of Nuclear Materials*, 91:311–321, 1980.

[27] C. K. Chow, C. E. Coleman, M. H. Koike, A. R. Causey, C. E. Ells, R. R. Hosbons, S. Sagat, V. F. Urbanic, and D. K. Rodgers. Properties of an Irradiated Heat-Treated Zr-2.5Nb Pressure Tube Removed from the NPD Reactor. *ASTMSTP 1295*, pages 469–491, 1996.

[28] H. K. Khandelwal, R. N. Singh, A. K. Bind, S. Sunil, J. K. Chakravartty, A. Ghosh, P. Dhandharia, D. Bhachawat, R. Shekhar, and S. J. Kumar. Tensile Properties and Fracture Toughness of Zr-2.5Nb Alloy Pressure Tubes of IPHWR220. *Nuclear Engineering & Design*, 293:138–149, 2015.

[29] R.N. Singh, P. Ståhle, J.K. Chakravartty, and A.A. Shmakov. Threshold Stress Intensity Factor For Delayed Hydride Cracking in Zr-2.5%Nb Pressure Tube Alloy. *Materials Science and Engineering A*, 523:112–117, 2009.

[30] A.K. Bind, R.N. Singh, S. Sunil, J.K. Chakravartty, A. Ghosh, P. Dhandharia, N. S. More, S. Vijayakumar, and A.G. Chhatre. Mechanical Properties of Zr-2.5Nb Pressure Tube Material Manufactured Employing Forging Routes For PHWR700 - Part 1: Tensile Behavior. Technical Report BARC/2012/E/002, BARC, 2012.

[31] C. Song. Irradiation Effects on Zr-2.5Nb in Power Reactors. *CNL Nuclear Review*, 5(1):17–36, 2016.

[32] B.A. Cheadle, C.E. Ells, E.F. Ibrahim, R.A. Holt, C.E. Coleman, R.W. Gilbert, D.O. Northwood, W.J. Langford, and R.R. Hosbons. The Physical Metallurgy of Zirconium Alloys. Technical Report CRNL-1208, Atomic Energy of Canada Limited, AECL, Canada, 1975.

[33] J.P. Abriata and J.C. Bolcich. The Nb-Zr System. *Bull. Alloy Phase Diagrams*, 3, no. 1:34–44, 1982.

[34] V.F. Urbanic and M. Griffiths. Microstructural Aspects of Corrosion and Hydrogen Ingress in Zr-2.5 Nb. *ASTM STP 1354*, pages 641–656, 2000.

[35] V. F. Urbanic, B. D. Warr, A. Manolescu, C. K. Chow, and M. W. Shanahan. Oxidation and Deuterium Uptake Rate of Zr-2.5Nb Pressure Tubes in CANDU-PHW Reactors. In L. F. P. Van Swam and C. M. Eucken, editors, *Zirconium in Nuclear Industry: Eighth Int. Symposium, ASTM STP 1023*, pages 20–34. ASTM, 1989.

[36] G. A. Bickel, M. Griffiths, A. Douchant, S. Douglas, O. T. Woo, and A. Buyers. Improved Zr-2.5Nb Pressure Tubes for Reduced Diametral Strain in Advanced CANDU Reactors. *Journal of ASTM International*, 8(2):1–14, 2011.

[37] M. Griffiths, J. F. Mecke, and J. E. Winegar. Evolution of Microstructure in Zirconium Alloys During Irradiation. *ASTM STP 1295*, pages 580–602, 1996.

[38] Z.L. Pan, S. St. Lawrence, P.H. Davies, M. Griffiths, and S. Sagat. Effect of Irradiation on the Fracture Properties of Zr-2.5Nb Pressure Tubes at the End of Design Life. In *ASTM STP 1467*, pages 759–782, 2006.

[39] D. Srivastava, S. Banerjee, S. Neogy, E. Ramdasan, S. Anantharaman, G. K. Dey, and N. Saibaba. Microstructural Studies of Zr-2.5Nb and Zircaloy-2 Pressure Tubes Irradiated in Indian Pressurised Heavy Water Reactors. *Advanced Materials Research*, 585:56–61, 2012.

[40] Y. S. Kim, S. B. Ahn, K. S. Im, S. S. Kim, and Y. M. Cheong. Microstructural Evoluation in Wolsong 1 Zr-2.5Nb Tube With Neutron Irradiation. In *Proceedings of the Korean Nuclear Society Autumn Meeting*, Yongpyong, Korea, 2003.

[41] R. R. Hosbons, P. H. Davies, M. Griffiths, S. Sagat, and C. E. Coleman. Effect of Long Term Irradiation on Fracture Properties of Zr-2.5Nb Pressure Tubes. *ASTM STP 1354*, pages 122–138, 2000.

[42] M. Griffiths, P. H. Davies, W. G. Davies, and S. Sagat. Predicting the in-Reactor Mechanical Behavior of Zr-2.5Nb Pressure Tubes from Post Irradiation

Microstructural Examination Data. *ASTM STP 1423*, pages 507–523, 2002.

[43] R. W. Gilbert, K. Farrell, and C. E. Coleman. Damage Structure in Zirconium Alloys Neutron Irradiated at 573-923 K. *Journal Nuclear Materials*, 84:137–148, 1979.

[44] D. Srivastava, S. Neogi, G. K. Dey, S. Banerjee, E. Ramdasan, and S. Anantharaman. Microstructural Examination of Zr-2.5Nb Pressure Tube S-07 from Kakrapar Atomic Power Station Unit-2. Technical Report BARC/2011/E/007, BARC, 2011.

[45] D. D. Himbeault, C. K. Chow, and M.P. Puls. Deformation Behaviour of Irradiated Zr-2.5Nb Pressure Tube Material. *Metallurgical and Materials Transactions*, 25A(1):135–142, 1994.

[46] R. A. Holt. In-reactor Deformation of Cold-Worked Zr-2.5Nb Pressure Tubes. *Journal of Nuclear Materials*, 372:182–214, 2008.

[47] M. Griffths, W. G. Davies, G. D. Moan, A. R. Causey, R. A. Holt, and S. A. Aldridge. Variability of in-Reactor Diametral Deformation For Zr-2.5Nb Pressure Tubing. *ASTM STP 1423*, pages 796–810, 2002.

[48] M. Griffths, N. Christodoulou, and S. Donohue. Damage Dependence of Radiation Deformation of Zr-2.5Nb Pressure Tubes. *ASTM STP 1467*, pages 783–801, 2006.

[49] P. H. Davies, I. Aitchison, D. D. Himbeault, A. K. Jarvine, and J. F. Watters. On the Fracture of Cold-Worked Zr-2.5Nb Pressure Tubes Fabricated from 100% Recycled Material. *Fatigue and Fracture of Engineering Materials and Structures*, pages 789–800, 1995.

[50] A. R. Causey, V. Fidleris, S. R. MacEwen, and C. W. Schulte. In-Reactor Deformation of Zr- 2.5Nb Pressure Tubes. *ASTM STP 956*, pages 54–68, 1987.

[51] A. R. Causey, J. E. Elder, R. A. Holt, and R. G. Fleck. On the Anisotropy of in-Reactor Creep of Zr-2.5Nb Tubes. *ASTM STP 1245*, pages 202–220, 1994.

[52] Atomic Energy of Canada Limited. *Canada Enters the Nuclear Age: A Technical*

History of Atomic Energy of Canada Limited. McGill-Queens University Press, 1997.

[53] A. K. Dureja, S. K. Sinha, A. Srivastava, R. K. Sinha, J. K. Chakravartty, P. Seshu, and D. N. Pawaskar. Flow Behavior of Autoclaved, 20% Cold Worked, Zr-2.5Nb Alloy Pressure Tube Material in the Temperature Range of Room Temperature to 800°C. *Journal of Nuclear Materials*, pages 22–29, 2011.

[54] R. N. Singh, S. Mukherjee, A. Gupta, and S. Banerjee. Terminal Solid Solubility of Hydrogen in Zr-alloy Pressure Tube Materials. *Journal of Alloys and Compounds*, 389:102–112, 2005.

[55] R. N. Singh, R. M. Lala, G. K. Dey, D. N. Sah, I. S. Batra, and P. Ståhle. Influence of Temperature on Threshold Stress For Reorientation of Hydrides and Residual Stress Variation Across Thickness of Zr-2.5Nb Alloy Pressure Tube. *Journal of Nuclear Materials*, 359:208–219, 2006.

[56] R. N. Singh, R. Kishore, S. S. Singh, T. K. Sinha, and B. P. Kashyap. Stress-Reorientation of Hydrides and Hydride Embrittlement of Zr-2.5 Wt. % Nb Pressure Tube Alloy. *Journal of Nuclear Materials*, 325:26–33, 2004.

[57] L. A. Simpson and C. K Chow. Effect of Metallurgical Variables and Temperature on Fracture Toughness of Zirconium Alloy Pressure Tubes. *ASTM STP 939*, pages 579–596, 1987.

[58] P.H. Davies, D.D. Himbeault, R.S.W. Shewfelt, and R.R. Hosbons. Crack Growth Resistance of Irradiated Zr-2.5Nb Pressure Tube Material at Low Hydrogen Levels. *ASTM STP 1405*, pages 846–868, 2001.

[59] R. Adamson and B. Cox. Impact of Irradiation on Material Performance. Technical report, ZIRAT-10 Special Topics Report, ANT International, 2005.

[60] H. R. Higgy and F. H. Hammad. Effect of Neutron Irradiation on The Tensile Properties of Zircaloy-2 and Zircaloy-4. *Journal of Nuclear Materials*, 44:215–227, 1972.

[61] P.H. Davies and R.S.W. Shewfelt. Link Between Results of Small and Large

Scale Toughness Tests on Irradiated Zr-2.5Nb Pressure Tube Material. *ASTM STP 1295*, pages 492–517, 1996.

[62] C. K. Chow and L. A. Simpson. Effect of Fracture Micromechanism on Crack Growth Resistance Curves of Irradiated Zr-2.5Nb Alloy. *ASTM STP 995*, pages 537–562, 1989.

[63] M. Griffiths. A Review of Microstructure Evolution in Zirconium Alloys During Irradiation. *Journal of Nuclear Materials*, 159:190–218, 1988.

[64] I. Aitchison and P. H. Davies. Role of Microsegregation in Fracture of Cold Worked Zr-2.5Nb Pressure Tubes. *Journal of Nuclear Materials*, 203:206–220, 1993.

[65] C. E. Coleman, B. A. Cheadle, C. D. Cann, and J. R. Theaker. Development of Pressure Tubes with Service Life Greater Than 30 Years. *ASTM STP 1295*, pages 884–898, 1996.

[66] C. E. Coleman, J. R. Theaker, and K. V. Kidd. Effect of Fabrication Variables on Irradiation Response of Crack Growth Resistance of Zr-2.5Nb. *Journal of ASTM International*, 1(7):783–801, 2004.

[67] L. A. Simpson, C. K. Chow, and P. H. Davies. Standard Test Method for Fracture Toughness of CANDU Pressure Tubes. Technical Report AECL Report COG-89-110-1, AECL, 1989.

[68] C.K. Chow and L.A. Simpson. Determination of the Fracture Toughness of Irradiated Reactor Pressure Tubes Using Curved Compact Specimens. *ASTM STP 945*, pages 419–439, 1988.

[69] K. Kapoor, N. Saibaba, B. P. Kashyap, and A. V. Ramana Rao. Tearing Crack Growth and Fracture Micro-Mechanisms Under Micro Segregation in Zr-2.5%Nb Pressure Tube Material. *Journal of ASTM International*, 5(7):1–18, 2008.

[70] P. H. Davies. Predicting Crack Instability Behaviour of Burst Tests from Small Specimens For Irradiated Zr-2.5Nb Pressure Tubes. *ASTM STP 1321*, pages 535–561, 1997.

[71] T. Asada, K. Kimoto, V. Chiba, and Y. Kasai. Fracture Toughness Evaluation of Heat Treated Zr-2.5Nb Pressure Tubes. *ASTM STP 1132*, pages 99–118, 1988.

[72] B. W. Leitch and S. St. Lawrence. Stress-Triaxiality in Zr-2.5Nb Pressure Tube Materials. *Journal of ASTM International*, 6(2):1–13, 2009.

[73] D.O. Northwood and U. Kosasih. Hydrides and Delayed Hydrogen Cracking in Zirconium and Its Alloys. *International Metals Reviews*, 28(2):92–121, 1983.

[74] R. N. Singh, R. Kishore, and T. K. Sinha. Studies on Stress Reorientation of Hydride in Zr-2.5Nb Pressure Tube Alloy. BARC/2002/E/036, BARC, 2002.

[75] L. A. Simpson. *Metallurgical and Materials Transactions*, 12A:2113, 1981.

[76] M. P. Puls. The Influence of Hydride Size and Matrix Strength on Fracture Initiation at Hydrides in Zirconium Alloys. *Metallurgical and Materials Transactions*, 19A:1507–1522, 1988.

[77] S. Q. Shi and M. P. Puls. Criteria for Fracture Initiation at Hydrides in Zirconium Alloys : I Sharp Crack Tip. *Journal of Nuclear Materials*, 208:232–242, 1994.

[78] K. S. Chan. A Fracture Model for Hydride-Induced Embrittlement. *Acta Metall. Mater.*, 43(2):4325–4335, 1995.

[79] L. G. Bell and R. G. Duncan. Hydride Orientation in Zr-2.5Nb: How It is Affected by Stress, Temperature and Heat Treatment. Technical Report AECL-5110, AECL, 1975.

[80] C. E. Coleman and H. Hardie. The Hydrogen Embrittlement of Alpha-Zirconium: A Review. *Journal of Less-Common Metals*, 11:168–185, 1966.

[81] M. Daunys, R. Dundulis, A. Grybenas, and P. Krasauskas. Hydrogen Influence on Mechanical and Fracture Mechanics Characteristics of Zirconium Zr-2.5Nb Alloy at Ambient and Elevated Temperatures. *Nuclear Engineering & Design*, 238(10):2536–2545, 2008.

[82] R.N. Singh, A.K. Bind, N.S. Srinivasan, and P. Ståhle. Influence of Hydrogen Content on Fracture Toughness of CWSR Zr-2.5Nb Pressure Tube Alloy. *Journal of Nuclear Materials*, 432:87–93, 2013.

[83] J. S. Dubey, S. L. Wadekar, R. N. Singh, T. K. Sinha, and J. K. Chakravartty. Assessment of Hydrogen Embrittlement of Zircaloy-2 Pressure Tubes Using Unloading Compliance and Load Normalization Techniques For Determining J-R Curves. *Journal of Nuclear Materials*, 264:20–28, 1999.

[84] A. C. Wallace, G. K. Shek, and O. E. Lepik. Effects of Hydride Morphology on Zr-2.5Nb Fracture Toughness. *ASTM STP-1023*, pages 66–88, 1989.

[85] R. Dutton, K. Nuttall, M. P. Puls, and L. A. Simpson. Mechanisms of Hydrogen Induced Delayed Cracking in Hydride Forming Materials. *Metallurgical and Materials Transactions*, 8A:1553–1562, 1977.

[86] S. Hanlon. The Effect of Testing Direction on DHC Growth Rate Using Zr-2.5Nb Plate. Masters thesis, Carleton University, 2013.

[87] A. H. Jackman and J. T. Dunn. Delayed Hydrogen Cracking of Zirconium Alloy Pressure Tubes. Technical Report AECL-5691, AECL, 1976.

[88] P. A. Ross-Ross, J. T. Dunn, A. B. Mitchell, G. R. Towgood, and R. Hunter. Some Engineering Aspects of the Investigation into the Cracking of Pressure Tubes in the Pickering Reactors. Technical Report AECL 5261, 1975.

[89] B. A. Cheadle, C. E. Coleman, and J. F. R. Ambler. Prevention of Delayed Hydride Cracking in Zirconiunn Alloys. *ASTM STP 939*, pages 224–240, 1987.

[90] A. R. Causey, V. F. Urbanic, and C.E. Coleman. In-Reactor Oxidation of Crevices and Cracks in Cold-Worked Zr-2.5Nb. *Journal of Nuclear Materials*, 71:25–35, 1977.

[91] G. D. Moan, C. E. Coleman, E. G. Price, D. K. Rodgers, and S. Sagat. Leak-Before-Break in pressure tubes of CANDU Reactors. *International Journal of Pressure Vessel and Piping*, 43:1–20, 1990.

[92] F. H. Huang and W. J. Mills. Delayed Hydride Cracking Behaviour for Zircaloy-2 Tubings. *Metallurgical and Materials Transactions*, 22A:2049–2060, 1991.

[93] G. K. Shek and D. B. Graham. Effects of Loading and Thermal Manoeuvres on Delayed Hydride Cracking in Zr-2.5Nb Alloys. *ASTM STP 1023*, pages 89–110,

1989.

[94] B. A. Cheadle, C. E. Coleman, D. K. Rodgers, P. H. Davies, C. K. Chow, and M. Griffiths. Examination of Core Components Removed from CANDU Reactors. Technical Report AECL-9710, AECL, 1988.

[95] E.G. Price, G.D. Moan, and C.E. Coleman. Leak Before Break Experience in CANDU Reactors. Technical Report AECL-9609, AECL, 1988.

[96] K. Kapoor, K. Murlidharan, and N. Saratchandran. Microstructure Evolution and Tensile Properties of Zr-2.5Nb Pressure Tubes Processed from Billets With Different Microstructures. *Journal of Materials Engineering and Performance*, 8(1):61–67, 1999.

[97] J.S. Dubey, J.K. Chakravartty, and S. Banerjee. Fracture Behaviour of Dilute Zirconium Alloys: Role of Hydrogen and Trace Impurities. *Proceedings of 13th. International Conference on Nuclear Engineering (ICONE-13, ASME), Bejing, China*, 2005.

[98] S. Chatterje, S. Anantharaman, K. S. Balakrishnan, and H. K. Sriharsha. Critical Crack Length Estimation of Irradiated Pressure Tube from the Ring Tension Test. Technical Report BARC/1999/E/027, BARC, 1999.

[99] S. Chatterje, H. K. Sriharsha, and K. S. Balakrishnan. Evaluation and Analysis of Critical Crack Length of Irradiated Pressure Tubes from Indian Pressurised Heavy Water Reactors. Technical Report BARC/2001/E/027, BARC, 2001.

[100] S. Chatterjee, K. S. Balakrishnan, and P. K. Shah. Measurement and Utility of Fracture Toughness Properties of Irradiated Pressure Tube from the Ring Tension Test. Technical Report BARC/2004/E/007, BARC, 2004.

[101] J. L. Singh, E. Ramadasan, J.S. Dubey, N. K. Mondal, P.B. Kondejkar, A. Bhandekar, M. P. Dhotre, H. N. Singh, K. M. Pamdit, B. N. Rath, U. Kumar, N. Kumawat, P. Mishra, V. D. Alur, R. S. Shriwastaw, A. Kumar, P. K. Shah, and S. Anantharaman. Post Irradiation Examination of Zr-2 Pressure Tubes from KAPS-1. Technical Report BARC/2015/I/001, BARC, 2015.

[102] S. Chatterje and H. K. Sriharsha. Conservative Estimation of Fracture Toughness of Reactor Operated Cold Worked Zr-2.5Nb Pressure Tubes. Technical Report BARC/1999/E/029, BARC, 1999.

[103] S. Chatterje, P.K. Shah, and J.S. Dubey. Measurement and Application of Fracture Toughness Properties of Zr-2.5Nb Pressure Tube Removed from KAPS-2. BARC External Report BARC/2008/E/008, BARC, 2008.

[104] S. Chatterje and P. K. Shah. Computation of Diametral Deformation of Irradiated Zr-2.5Nb Pressure Tube from RAPS-2. Technical Report BARC/2008/E/014, BARC, 2008.

[105] D.N. Sah, E. Ramadasan, K. Unnikrishnan, J.L. Singh, P.M. Ouseph, B.N. Rath, H.N. Singh, P.B. Kondejkar, V.D. Alur, S. Banerjee, R.S. Shriwastaw, P. Mishra, V.P. Jathar, N. Kumawat, and M.P. Dhotre. Post Irradiation Examination of Reactor Operated Pressure Tube S-07 of KAPS-2. *Journal of Nuclear Materials*, 383:128–131, 2008.

[106] C. Ganguly. Advances in Zirconium Technology For Nuclear Reactor Application. *Proc. Of the Symposium Zirconium-2002, ZIRC-2002*, pages 1–27, 2002.

[107] R. N. Singh, R. Kishore, S. Mukherjee, S. Roychowdhury, D. Srivastava, B. Gopalan, R. Kameswaran, Smita S. Sheelvantra, T. K. Sinha, P. K. De, and S. Banerjee. Hydrogen Charging, Hydrogen Content Analysis and Metallographic Examination of Hydride in Zr-Alloys. BARC External Report BARC/2003/E/034, BARC, 2003.

[108] R. N. Singh. *Flow Behavior and Hydrogen Embrittlement in Zr- 2.5Nb Pressure Tube Alloy.* PhD thesis, Indian Institute of Technology, Mumbai, India, 2003.

[109] A.D. Lepage, W.A. Ferris, and G.A. Ledoux. Procedure For Adding Hydrogen to Small Sections of Zirconium Alloys. FC-IAEA-03, T1.20.13-CAN-27363-03, 1998.

[110] V.D. Alur, R.V. Kulkarni, V.P. Jathar, E. Ramdasan, K. Unnikrishnan, and K.C. Sahoo. Evaluation of Hydrogen Content of Operating Pressure Tubes of

Indian PHWRs By Differential Scanning Calorimetry. In *Proc. of Intl. Workshop on Hydrogen Embrittlement of Metals-HEM 08*, pages 65–70, 2008.

[111] J.J. Kearns. Terminal Solubility and Partitioning of Hydrogen in the Alpha Phase of Zirconium, Zircaloy-2 and Zircaloy-4. *Journal of Nuclear Materials*, 22:292–303, 1967.

[112] B.N. Rath, H.N. Singh, J.L. Singh, P.M. Ouseph, and D.N. Sah. Measurement and Analysis of Diametral Deformation in Irradiated Zr-2.5Nb Pressure Tube. BARC Internal Report BARC/2006/I/014, BARC, 2006.

[113] M. P. Puls. Effects of Crack Tip Stress States and Hydride-Matrix Interaction Stresses on Delayed Hydride Cracking. *Metallurgical Transactions A*, 21A:2905–2917, 1990.

[114] Technical Requirements For in-Service Evaluation of Zirconium Alloy Pressure Tubes in CANDU Reactors. CSA N 285.8-05, 2005.

[115] *Standard Test Method For Measurement of Fracture Toughness, ASTM E1820-11*, 2011.

[116] J.J. Kearns. On the Relation Among 'f' Texture Factors for the Principal Planes of Zirconium, Hafnium and Titanium Alloys. *Journal of Nuclear Materials*, 299(2):171–174, 2001.

[117] S. Kumar, B.N. Rath, D. Bhachawat, and S. Anantharaman. Texture Analysis and Dislocation Density Determination on Offcuts of Pressure Tubes of PHWRs. BARC Internal Report BARC/2014/I/005, BARC, 2014.

[118] U.K. Viswanathan, R. N. Singh, C. B. Basak, S. Anantharaman, and K.C. Sahoo. Evaluation of Effect of Hydrogen on Toughness of Zircaloy-2 By Instrumented Drop Weight Impact Testing. *Journal of Nuclear Materials*, 350:310–319, 2006.

[119] W.J. Langford and L.E.J. Mooder. Fracture Behaviour of Zirconium Alloy Pressure Tubes for Canadian Nuclear Power Reactors. *Intl. J. of Pressure Vessel and Piping*, 6:275–310, 1978.

[120] A. Cowen and W.J. Langford. Effect of Hydrogen and Neutron Irradiation on

the Failure of Flawed Zircaloy-2 Pressure Tubes. *Journal of Nuclear Materials*, 301:271–281, 1969.

[121] B.J.S. Wilkins, J.N. Barrie, and R.J. Zink. Slit-Burst Testing of Cold-Worked Zr-2.5 Wt.% Nb Pressure Tubing for CANDU-PHW Reactors. Technical Report Report AECL-6195, AECL, 1978.

[122] M.H. Sharobeam and J.D. Landes. The Load Separation Criterion and Methodology in Ductile Fracture Mechanics. *International Journal of Fracture*, 47:81–104, 1991.

[123] E.D. Reese and K.H. Schwalbe. The Linear Normalization Technique - An Alternative Procedure for Determining J-R Curves from a Single Specimen Test Record Based on Landes Normalization Method. *Fatigue and Fracture of Engineering Materials and Structures*, 16(3):271–280, 1993.

[124] J. D. Landes, Z. Zhou, K. Lee, and R. Herrera. Normalization Method for Developing J-R Curves with LMN Function. *Joural of Testing and Evaluation*, 19:305–311, 1991.

[125] B. Bose and R. J. Klassen. Temperature Dependence of the Anisotropic Deformation of Zr-2.5Nb Pressure Tube Material During Micro-Indentation. *Journal of Nuclear Materials*, 419:235–240, 2011.

[126] Y.S. Kim. Role of Twinning and Slip in Deformation of Zr-2.5Nb Tube. *Journal of ASTM International*, 5(6):1–14, 2008.

[127] F. James. *Statistical Methods in Experimental Physics*. 2006.

[128] N. Christodoulou, P. A. Turner, E. T. C. Ho, C. K.Chow, and M. R. Levi. Anisotropy of Yielding in Zr-2.5Nb Pressure Tube Material. *Metallurgical and Materials Transactions A*, 31A:409–420, 2000.

[129] L.A . Simpson and C.F. Clarke. An Elastic-Plastic R-Curve Description of Fracture in Zr-2.5Nb Pressure Tube Alloy. (ASTM STP 668):643–662, 1979.

[130] S. J. Oh, I. S. Kim, Y.S. Kim, and S.B. Ahn. Fracture Toughness of Irradiated Zr-2.5Nb CANDU Pressure Tube Using Load Ratio Method. SMiRT18-C04-1,

18th International Conference on Structural Mechanics in Reactor Technology (SMiRT 18), 2005.

[131] A. Kumar. Fracture Toughness Study of Irradiated Indian Zr 2.5Nb Pressure Tube. Master's thesis, HBNI, Mumbai, India, 2015.

[132] A. Kumar, P. K. Shah, J.S.Dubey, R.S. Shriwastaw, M.P. Dhotre, A. Bhandekar, K.M.Pandit, V.D. Alur, B.N. Rath, P. Mishra, and S. Kumar. Evaluation of Integrity of PHWR Coolant Tubes after Reactor Operation. In *Proceedings of First Structural Integrity Conference and Exhibition (SICE-2016)*, Bangalore, July 2016.

[133] Delayed Hydride Cracking in Zirconium Alloys in Pressure Tube Nuclear Reactors. IAEA TECDOC-1410, 2004.

[134] A. Grybenas, R. Levinskas, and V. Makarevicius. Investigation of Delayed Hydride Cracking in the Zr-2.5% Nb Alloy. *Hydrogen Materials Science and Chemistry of Carbon Nanomaterials*, pages 467–470, 2007.

[135] Y. Gou, Y. Li, Y. Liu, H. Chen, and S. Ying. Evaluation of A Delayed Hydride Cracking in Zr-2.5Nb CANDU and RBMK Pressure Tubes. *Materials and Design*, 30 Issue 4:1231–1235, 2009.

[136] J.I. Mieza, G.L. Vigna, and G. Domizzi. Evaluation of Variables Affecting Crack Propagation By Delayed Hydride Cracking in Zr-2.5Nb With Different Heat Treatments. *Journal of Nuclear Materials*, 411 Issue 1-3:150–159, 2011.

[137] G. K. Shek, M. T. Jovanovic, H. Seahra, Y. Ma, D. Li, and R. L. Eadie. Hydride Morphology and Striation Formation During Delayed Hydride Cracking in Zr-2.5Nb. *Journal of Nuclear Materials*, 231(3):221–30, 1996.

[138] Y. S. Kim. Temperature Dependency of Delayed Hydride Cracking Velocity in Zr-2.5Nb Tubes. *Materials Science and Engineering A*, 468-470:281–287, 2007.

[139] R. K. Sundaramoorthy. *Initiation of Delayed Hydride Cracking in Zr-2.5Nb Micro Pressure Tubes*. PhD thesis, Queens University, Canada, 2009.

[140] P. K. Shah, H. K. Sriharsha, A. P. Kulkarni, K. Pandit, S. Chatterjee, M. P.

Dhotre, and S. Kumar. Delayed Hydride Crack Growth Velocity Measurement in Zircaloy-2 Pressure Tube. In *Proc. Of the Symposium Zirconium-2002, ZIRC-2002*, pages 487–491, BARC, India, 2002.

[141] C. E. Coleman and J. F. R. Ambler. Susceptability of Zirconium Alloys to Delayed Hydride Cracking. *ASTM STP 633*, pages 589–607, 1977.

PUBLICATIONS

Publications in peer reviewed journals

1. "Fracture Toughness of Irradiated Zr–2.5Nb Pressure Tube from Indian PHWR", Priti Kotak Shah, J.S. Dubey, R.S. Shriwastaw, M.P. Dhotre, A. Bhandekar, K.M. Pandit, S. Anantharaman, R.N. Singh, J.K. Chakravartty, Journal of Nuclear Materials 458 (2015) 319–325.

2. "Tensile Strength of Zr-2.5Nb Pressure Tubes: A statistical Study", Priti Kotak Shah, J.S. Dubey, D. Datta, R.S. Shriwastaw, B.N. Rath, R.N. Singh and S. Anantharaman, Nuclear Engineering & Design, 295 (2015) 789-796.

3. "Delayed Hydride Crack Growth Study on Irradiated Zr-2.5Nb Pressure Tube", Priti Kotak Shah, J. S. Dubey, Ashwini Kumar, R.S. Shriwastaw, B.N. Rath, K. M. Pandit, M.P. Dhotre, P. Mishra, V.D. Alur and S. Anantharaman, Journal of Nuclear Materials 460 (2015) 1–4.

4. "Anisotropy in Impact Behavior of Zr-2.5Nb Pressure Tube Alloy", Priti Kotak Shah, P.M. Satheesh, R.N. Singh, J.S. Dubey, R.S. Shriwastaw, K.S. Balakrishnan, A.P. Kulkarni, Prerna Mishra, V.P. Jathar, S. Majumdar, V.D. Alur, S. Anantharaman and J.K. Chakravartty, Transactions of The Indian Institute of Metals Vol. 64, Issue 1-2, (2011) 67-70

International conferences

1. "Characterisation of Zr-2.5Nb Pressure Tube Off-cuts", Priti K. Shah, J.S. Dubey, R. S. Shriwastaw, K.S. Balakrishnan, B.N. Rath, S. Banerjee, S. Kumar, S. Anantharaman, J. K. Chakravartty, NMD-ATM-2010 held at IISc Bangalore

2. "Fracture Toughness Evaluation of RAPS-2 & KAPS-2 Pressure Tube Off-cuts", Priti K. Shah, J.S. Dubey, R. S. Shriwastaw, K.S. Balakrishnan, S. Anantharaman, J. K. Chakravartty1, ANM-2011 held at Mumbai

Thank You